Spin Space Groups: Full Classification and Applications

Zhenyu Xiao,[1,*] Jianzhou Zhao[2,*] Yanqi Li,[1] Ryuichi Shindou,[1] and Zhi-Da Song[1,3,4,†]

[1]*International Center for Quantum Materials, School of Physics, Peking University, Beijing 100871, China*
[2]*Co-Innovation Center for New Energetic Materials, Southwest University of Science and Technology,*
Mianyang 621010, China
[3]*Hefei National Laboratory, Hefei 230088, China*
[4]*Collaborative Innovation Center of Quantum Matter, Beijing 100871, China*

In this work, we exhaust all the spin space symmetries, which fully characterize collinear, noncollinear, and commensurate spiral as well as incommensurate spiral magnetism, etc., and investigate enriched features of electronic bands that respect these symmetries. We achieve this by systematically classifying the so-called spin space groups (SSGs)—joint symmetry groups of spatial and spin operations that leave the magnetic structure unchanged. Generally speaking, they are accurate (approximate) symmetries in systems where spin-orbit coupling (SOC) is negligible (finite but weaker than the energy scale of interest), but we also show that specific SSGs could remain valid even in the presence of strong SOC. In recent years, SSGs have played increasingly pivotal roles in various fields such as altermagnetism, topological electronic states, and topological magnon, etc. However, due to its complexity, a complete SSG classification has not been completed up to now. By representing the SSGs as $O(N)$ representations, we—for the first time— obtain the complete classifications of 1421, 9542, and 56 512 distinct SSGs for collinear ($N = 1$), coplanar ($N = 2$), and noncoplanar ($N = 3$) magnetism, respectively. SSG not only fully characterizes the symmetry of spin degrees of freedom, but also gives rise to exotic electronic states, which, in general, form projective representations of magnetic space groups (MSGs). Surprisingly, electronic bands in SSGs exhibit features never seen in MSGs, such as (i) nonsymmorphic SSG Brillouin zone, where SSG operations behave as a glide or screw when acting on momentum, (ii) effective π flux, where translation operators anticommute with each other and yield duplicate bands, (iii) higher-dimensional representations unexplained by MSGs, and (iv) unconventional spin texture on a Fermi surface, which is completely determined by SSGs, independent of Hamiltonian details. To apply our theory, we identify the SSG for each of the 1595 published magnetic structures in the MAGNDATA database on the Bilbao Crystallographic Server. Material examples exhibiting the novel features (i)–(iv) are discussed with emphasis. We also investigate new types of SSG-protected topological electronic states that are unprecedented in MSGs. In particular, we propose a 3D $\mathbb{Z}_2$ topological insulator state with a fourfold degenerate Dirac point on the surface and a new scenario of anomalous $\mathbb{Z}_2$ helical states that appear on magnetic domain walls.

I. INTRODUCTION

Symmetry is one of the central concepts in modern physics. In condensed matter, symmetry plays determining roles in phase transitions, low-energy excitations, transport in disordered systems, etc., allowing physicists to qualitatively understand a realistic system without knowing microscopic details. One cannot overemphasize the importance of symmetry in physics. For more than one hundred years, the 230 space groups have been the standard mathematical description of symmetries in solid material crystallography. For magnetic materials, the complete symmetry theory was generally believed to be the 1651 magnetic space groups (MSGs), where a symmetry operation could be a pure spatial operation or a combination of the time-reversal symmetry (TRS) and a spatial operation. In the 1960s, people realized that Heisenberg models with negligible spin-orbit coupling (SOC) enjoy higher symmetries, namely, spin space groups (SSGs) [1]. In an SSG, an operation can be a combination of a spatial operation and an arbitrary spin rotation that is compatible with the group structure. Such symmetries are found crucial to describe the spin waves correctly. Later, the

spin point groups, where the spatial operations are limited to point group operations, were fully classified by Litvin [2,3]. However, due to the complexity of joining spatial and spin operations, a full classification of SSGs has not been completed up to now.

In recent years, SSGs have drawn growing attention because of their applications in magnetic materials with negligible or weak SOC, such as magnetic topological electronic states [4–7], topological magnon bands [8–14], unconventional spin-momentum locking without SOC [15–18], which was later realized as a common feature of the altermagnetism [19–26], etc. To be specific, SSGs can protect (i) exotic nodal-line or -point semimetals, e.g., twelvefold degenerate fermion in three dimensions [5] and eightfold degenerate fermion in two dimensions [6], that are disallowed by conventional symmetries [27]; (ii) exotic topological insulators (TIs), e.g., SOC-free and TRS-free two-dimensional $\mathbb{Z}_2$ TIs [4], that are disallowed by conventional symmetries [28–32]; and (iii) exotic nodal magnon bands, e.g., Dirac points with $\mathbb{Z}$-valued monopole charges [12], which evolve into nodal lines with $\mathbb{Z}_2$-monopole charges [33,34] if weak SOC is considered, as confirmed by the experiment [13]. SSGs are also crucial for understanding the so-called altermagnetism [19,26], where antiparallel spin momenta at two sublattices compensate each other exactly (as in antiferromagnetism) but the two sublattices are not related by inversion or translation. Altermagnetism can exhibit unconventional, e.g., d-, g-, and i-wave-like, spin-momentum locking [15,25], which can lead to a surprisingly large anomalous Hall conductivity when a weak SOC is introduced [16,17], as confirmed by experiments [21–24]. Unconventional momentum-dependent spin polarization also exists in noncollinear magnetism without SOC [18,35]. Therefore, SSGs not only give rise to theoretically exotic states, but also have a strong relevance in realistic magnetic materials. It provides a precise description of magnetic materials with negligible SOC and a good starting point to understand magnetic materials with weak SOC. However, due to lacking a complete classification of SSGs, most discussions are limited to spin point groups or several simple SSGs.

In this work, by reducing the group classification problem to a representation problem, we obtain the full classification of SSGs and find that there exist 67 475 inequivalent SSGs in total (see Sec. F in Supplemental Material [36]). These SSGs fully characterize collinear magnetism (including ferro-, ferri-, antiferro-, and alter-magnetism), coplanar magnetism, noncoplanar magnetism, and spiral magnetism (including commensurate and incommensurate structures).

The complete classification reveals additional novel features of magnetic states beyond those found in previous works. To investigate electron bands using SSGs, we generalize crystal momentum to SSG momentum $\tilde{k}$ and introduce a concept of the SSG Brillouin zone (SBZ)—the reciprocal space formed by SSG momenta. Because of enriched symmetry algebra, the action of SSG translations on electronic states may exhibit anticommutation. An SBZ is said to be noncommuting if the SSG translations have this property and commuting otherwise. Commuting SBZs can be further classified into symmorphic SBZs and non-symmorphic SBZs, wherein the latter exhibits nontrivial transformations of SSG momentum. In a symmorphic SBZ, the momentum transforms normally under an SSG operation g, i.e., $\tilde{k} \to \tilde{k}' = s_g R_g \tilde{k}$, with R_g being the point group part of g and s_g being 1 (−1) for unitary (antiunitary) g. In a nonsymmorphic SBZ, $\tilde{k}$ transforms to $s_g(R_g\tilde{k} + \tilde{q}_g)$, where $\tilde{q}_g$ is *not* a reciprocal lattice vector of SBZ but a "fractional translation" in momentum space. In Secs. III C and IV B, we discuss the noncommuting and nonsymmorphic SBZ in more detail and present several theoretical and material examples. We identify whether the SBZ is noncommuting, nonsymmorphic for each of the 67 475 SSGs (see Tables S1–S690 in Supplemental Material [36]). We note that, while anticommuting translations and nonsymmorphic transformation of momentum [41] can arise in systems subjected to external magnetic flux, these exotic behaviors studied in this work are intrinsically derived from the magnetic structures.

Another advancement from the SSG classification is a systematic classification of spin textures of SSG Bloch states in the momentum space. Spin expectation of SSG Bloch states is transformed under SSG operations, and the transformation realizes a representation of the SSG. If the realized representation is nontrivial, the spin polarization on the Fermi surface must be momentum dependent and generally cannot be described by MSGs. This description fully characterizes the spin textures not only in altermagnetism [15,25], but also in noncollinear magnetism [35], which can be p-, d-, f-…-wavelike. We explicitly derive the representations formed by spin textures in *all* SSGs that have symmorphic SBZs (see Tables S1–S690 in Supplemental Material [36]).

To apply our theory, we identify the SSGs for the 1595 published experimental magnetic structures in the MAGNDATA database [42,43] on the Bilbao Crystallographic Server and tabulate the results in Sec. G in Supplemental Material [36]. For every material, we further determine whether it has a noncommuting, non-symmorphic, or symmorphic SBZ and whether it possesses a nontrivial spin texture. Remarkably, these materials exhibit all the aforementioned exotic features of SSG. Among them, 33 materials have noncommuting SBZs; 153 materials have nonsymmorphic SBZs; 460 of 1409 remaining materials with symmorphic SBZs possess nontrivial spin textures in the momentum space. Within this group of 460 materials, 139 are collinear and fall into the category of altermagnetism. We believe that this useful information will lead to further research for new physics and potential

applications in fields like spintronics. To illustrate these concepts, we perform first-principle calculations on representative examples of materials.

SSGs also protect novel electron topological states that are absent in conventional space groups [44–46] and MSGs [47–52]. In Sec. V, we present three examples of SSG-protected topological states. The first example is a physical realization of a two-dimensional SOC-free and TRS-free $\mathbb{Z}_2$ TI. The hopping Hamiltonian of this model is real, and the topology is introduced by a noncollinear magnetic order. The second example is a three-dimensional SOC-free and TRS-free $\mathbb{Z}_2$ TI possessing a fourfold Dirac point on surfaces. The third example is a two-dimensional system with a protected helical mode along the domain wall between two magnetic domains with the same topological invariant. To our knowledge, the latter two states have never been discussed in conventional symmetry groups or SSGs.

In particular, the third example demonstrates a new scenario of topological states—topological gapless domain wall—that is unseen in previously known free-fermion states (in the absence of chiral and particle-hole symmetries). These examples should be the tip of the iceberg of the unexplored fruitful topological states in SSGs.

We summarize the main results of this work in Fig. 1, and the rest of this paper is organized as follows. In Sec. II, we explain why O(N) representations of space groups can classify all SSGs (see Sec. II A). We also describe a method of constructing all O(N) representations (Sec. II B) and criteria for determining whether two representations yield physically distinct SSGs (Sec. II D). We use O(3) representations of the space group $P3$ as an example of the classification (Sec. II C). We summarize basic information of SSGs in Sec. II E and tabulate all the SSGs in Sec. F in Supplemental Material [36]. In Sec. III, we investigate
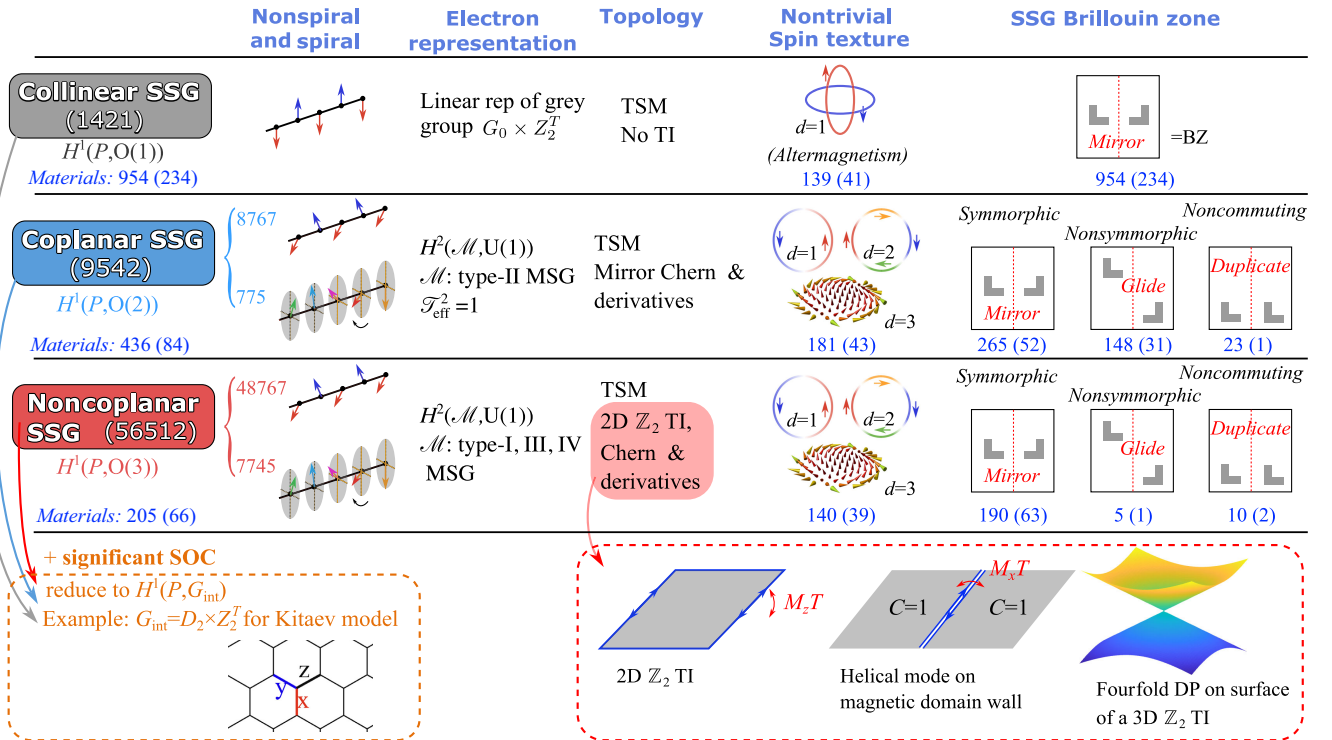

FIG. 1. Summary of results. We obtain all 1421, 9542, and 56 512 distinct SSGs for collinear ($N = 1$), coplanar ($N = 2$), and noncoplanar ($N = 3$) magnetic structures by enumerating O(N) representations. Nonspiral and spiral: All the collinear SSGs describe commensurate magnetic structures, whereas 775 (7745) of the coplanar (noncoplanar) SSGs describe spiral magnetic structures with either commensurate or incommensurate spiral angles. Electron representation: In collinear magnetism, electronic Bloch states form a linear representation of a MSG of type II (gray group). In coplanar (noncoplanar) magnetism, they form projective representations of MSGs $\mathcal{M}$ of type II (I, III, and IV), classified by group cohomology $H^2[\mathcal{M}, U(1)]$. Topology: We show possible electronic topological states for different SSGs, where TSM denotes topological semimetal. We provide concrete models of topological states, e.g., a fourfold degenerate surface Dirac fermion, in noncoplanar magnetism. Spin texture: SSGs determine the dimension d of the span of spin expectations on Fermi surfaces and, if $d > 0$, whether the spin textures are nontrivial. SBZ: The action of SSG translations on SSG Bloch states might anticommute, resulting in a noncommuting SBZ with a duplicated band structure. When the SSG translations commute, the SBZ can be symmorphic or nonsymmorphic, and SSG momentum in the latter is transformed nonsymmorphically under SSG symmetries. We also identify the SSGs of experimental materials. We list the (blue and italic) number of magnetic materials that are subject to the category at the bottom of each cell, and in the parentheses is the number of materials constituent of light elements from the first four periods. Finally, it is notable that some SSGs can be applied to systems with significant SOC, such as symmetry-breaking phases in the Kitaev model.

the representation theory of SSGs and its application in electronic states. We demonstrate that SSGs acting as SSG Bloch states lead to enriched symmetry algebra, necessitating the introduction of concepts of SSG momentum, SBZ, and noncommuting and nonsymmorphic SBZs. In addition, we utilize SSGs to determine the spin texture in the momentum space (see Sec. III D). Section IV focuses on experimental magnetic materials. We identify the SSGs of 1595 magnetic materials in the MAGNDATA database. The statistics are present in Sec. IV A, while the complete information is provided in Sec. G in Supplemental Material [36]. We perform first-principle calculations on material examples exhibiting nonsymmorphic SBZ, extra degeneracies, and unconventional spin texture in the momentum space. In Sec. V, we discuss possible electronic states protected by SSGs and construct three models of topological phases that are protected by symmetries unique in SSGs. Section VI is devoted to discussion and summary, where we also compare our representation-based approach of classifying SSGs with Litvin's approach [2,3].

II. CLASSIFICATION OF SPIN SPACE GROUPS

A. General considerations

Without SOC, the many-body electronic Hamiltonian of a material exhibits an SU(2) spin-rotation symmetry, a spinful time-reversal symmetry Z_2^T, and a space group G_{latt} symmetry of the lattice, where the spatial operations do not act on the spin. The group SU(2) is a double cover of SO(3), and two SU(2) operations corresponding to the same SO(3) rotation differ only by a phase of -1 when acting on the electronic states. In this work, we use the SO(3) group to describe the spin-rotation symmetry of magnetic structures. Additionally, the electron's spin-1/2 nature manifests itself in the projective representation theory (Sec. III). The elements in G_{latt}, the SO(3) rotation group, and Z_2^T mutually commute. Thus, the full symmetry group is $G_{\text{latt}} \times \text{SO}(3) \times Z_2^T$. A generic magnetic structure may individually break G_{latt}, SO(3), Z_2^T but preserve some joint operations. An SSG, denoted as $\mathcal{G}$ hereafter, is defined as the symmetry group of the magnetic structure, which is a continuous or discrete subgroup of $G_{\text{latt}} \times \text{SO}(3) \times Z_2^T$, depending on the magnetic order.

To proceed, we consider a magnetic structure, characterized by local spin magnetic moments $\mathbf{S}(\mathbf{r}_i)$'s, where $\mathbf{r}_i$'s are the position of magnetic atoms. The spin rotations act on the magnetic structure as SO(3) matrices. Hence, for $\mathbf{S}(\mathbf{r}_i)$, a generic symmetry operation consists of a spatial operation $\{R|\mathbf{v}\} \in G_{\text{latt}}$, a spin rotation $U \in \text{SO}(3)$, and a possible time-reversal operation T. It can be written as $\{XU|R|\mathbf{v}\}$ with X being identity I or T, and it transforms the magnetic structure $\mathbf{S}(\mathbf{r}_i)$ to

$$\mathbf{S}'(\mathbf{r}_i) = s(X)U\mathbf{S}(\{R|\mathbf{v}\}^{-1}\mathbf{r}_i), \tag{1}$$

where $s(X) = 1$ and -1 for $X = I$ and T, respectively. The SSG consists of all such composite operations that leave the magnetic structure unchanged, i.e.,

$$\mathcal{G} = \{\{XU|R|\mathbf{v}\}|\{XU|R|\mathbf{v}\}\mathbf{S} = \mathbf{S}\}, \tag{2}$$

where $\{XU|R|\mathbf{v}\}\mathbf{S}$ is the transformed magnetic structure defined in Eq. (1).

The spatial operations $\{R|\mathbf{v}\}$ in $\mathcal{G}$ form a space group:

$$P = \{\{R|\mathbf{v}\}|\{XU|R|\mathbf{v}\} \in \mathcal{G}\}, \tag{3}$$

which is named the parent space group. It is worth mentioning that, in general, P is a subgroup of the full space group G_{latt} of the lattice. A homomorphism exists from the SSG $\mathcal{G}$ to its parent space group P, and the kernel of the homomorphism is the pure-spin-operation group $\mathcal{S}$, where operations are in the form $\{XU|1|\mathbf{0}\}$. $\mathcal{S}$ is uniquely determined by whether the magnetic structure is collinear, coplanar, or noncoplanar [2–4]. Without loss of generality, we always assume that the magnetic moments are confined to the x, y plane for the coplanar structures and are oriented along the z direction for the collinear structure. Before investigating $\mathcal{S}$, let us consider the restrictions of the spin-operation part XU of a general operation in $\mathcal{G}$ for different arrangements. Noncoplanar structures have no specific restrictions on XU. However, for coplanar (collinear) structures, the spin-operation part XU of any operation in $\mathcal{G}$ must preserve the spin moments within the xy plane (along the z direction). Thus, for these two kinds of structures, $s(X)U$ takes a block diagonal form $\text{diag}(O_{xy}, O_z)$, where O_{xy} is an O(2) matrix acting on the x, y components of the spin moments and O_z is an O(1) matrix acting on the z components.

For noncoplanar structures, operations in $\mathcal{S}$ must leave all components of spin moments invariant, and

$$\mathcal{S} = \{\{I|1|\mathbf{0}\}\}; \tag{4}$$

i.e., there is no nontrivial on-site spin symmetry, or TRS, left. For coplanar structures, since $S_z = 0$, only O_{xy} in the $s(X)U = \text{diag}(O_{xy}, O_z)$ affects the transformation of spin moments, while O_z has no impact. $\mathcal{S}$ is given by

$$\mathcal{S} = \{\{\{I|1|\mathbf{0}\}, \{TU_z(\pi)|1|\mathbf{0}\}\}, \tag{5}$$

where $U_{\mathbf{n}}(\theta)$ represents a θ rotation along the direction $\mathbf{n}$ ($\mathbf{n} = \mathbf{z}$) and the operation $TU_z(\pi)$ transforms a spin moment (S_x, S_y, S_z) to $(S_x, S_y, -S_z)$. In this work, sometimes we also denote the above $\mathcal{S}$ as $\mathcal{S}_{Z_2^T}$. For the collinear structure, only O_z affects the transformation, and

$$\mathcal{S} = \{\{U_z(\theta)|1|\mathbf{0}\}|\theta \in [0, 2\pi)\} \cup \{\{TU_{\mathbf{n}_\theta}(\pi)|1|\mathbf{0}\}|\theta \in [0, \pi)\},$$

$$\tag{6}$$

where the first term is a θ rotation along the z direction and the second term is a π rotation along an in-plane direction $\boldsymbol{n}_\theta = (\cos\theta, \sin\theta, 0)$ followed by a TRS. The two types of operations leave $\boldsymbol{S}$ unchanged if $S_x = S_y = 0$. We can equivalently write the collinear $\mathcal{S}$ as

$$\mathcal{S} = \mathcal{S}_{Z_2^T} \ltimes \mathcal{S}_{U(1)}, \tag{7}$$

where $\mathcal{S}_{U(1)}$ contains the continuous rotation of $\mathcal{S}$ [the first term of Eq. (6)] and is a normal subgroup of $\mathcal{S}$ and $\mathcal{S}_{Z_2^T} = \{1, TU_x(\pi)\}$.

An SSG can be decomposed to cosets with respect to the pure-spin-operation group $\mathcal{S}$:

$$\mathcal{G} = \mathcal{S}g_1 + \mathcal{S}g_2 + \cdots. \tag{8}$$

As shown in the following paragraphs, we can properly choose the coset representatives such that they commute with every element in $\mathcal{S}$ and form a discrete normal subgroup G, which is isomorphic to the quotient group $\mathcal{G}/\mathcal{S}$, of $\mathcal{G}$. Therefore, a generic SSG has the structure

$$\mathcal{G} = \mathcal{S} \times G. \tag{9}$$

We name G the quotient SSG (qSSG). For given $\mathcal{S}$, the classification problem of SSGs is now reduced to the classification problem of qSSGs.

For noncoplanar magnetic structures, $\mathcal{S}$ is trivial, and the homomorphism from $\mathcal{G} = G$ to P is an isomorphism. In G, each spatial operation $\{R|\boldsymbol{v}\}$ is equipped with a unique spin operation XU. [Suppose both $\{XU|R|\boldsymbol{v}\}$ and $\{X'U'|R|\boldsymbol{v}\}$ belong to the SSG and $X'U' \neq XU$; then, $\{XU|R|\boldsymbol{v}\}^{-1}\{X'U'|R|\boldsymbol{v}\} = \{X^{-1}X'U^{-1}U'|1|\boldsymbol{0}\}$ is a nontrivial pure-spin operation, contradicting Eq. (4).] Therefore, G realizes a mapping from P to $XU \in Z_2^T \times$ SO(3) $\simeq$ O(3), i.e., a linear O(3) representation of P. Let ρ and σ be O(3) representations of P realized by two SSGs. If ρ and σ are equivalent, an orthogonal matrix O exists such that $D_\rho(p) = O^T D_\sigma(p) O$ for any $p \in P$, which means that differences between the two representations can be eliminated by a change of the spin axes. These two SSGs are considered to be the same. All possible noncoplanar SSGs can be obtained from the set of inequivalent O(3) representations, classified by the group cohomology $H^1[P, \mathrm{O}(3)]$.

There are various possible choices of coset representatives of $\mathcal{G}/\mathcal{S}$ for coplanar and collinear structures. To provide a concrete scheme, we adopt the following approach. For coplanar (collinear) structures, only O_{xy} (O_z) in a spin operation influences the transformation of spin moments. Therefore, we can choose the $O_z = \det(O_{xy})$ (for coplanar) or $O_{xy} = O_z 1_{2\times 2}$ (for collinear) in the spin operations of the coset representatives. For a coplanar structure, the only nontrivial spin operation in $\mathcal{S}$ [Eq. (5)] is $TU_z(\pi)$, containing time-reversal T. Consequently, each spatial operation in a coplanar SSG corresponds to two spin operations: one with the time-reversal operator T (antiunitary) and another without it (unitary). The choice $O_z = \det(O_{xy})$ implies that $\det[s(X)U] = 1$, leading to all coset representatives being unitary and forming the unitary subgroup G of the SSG $\mathcal{G}$. As the corresponding O(3) matrix of $TU_z(\pi)$ is $\mathrm{diag}(1_{2\times 2}, -1)$, the spin operations $\mathrm{diag}(O_{xy}, O_z)$ of the SSG representatives commute with $\mathcal{S}$. For a collinear structure, the choice $O_{xy} = O_z 1_{2\times 2}$ implies that the spin operations of coset representatives are either I or T. These spin operations constitute a group and commute with all spin operations. Thus, the coset representatives form a group G and commute all operations in $\mathcal{S}$. We also note that qSSG G for a collinear SSG is the same as a magnetic space group of type I, III, or IV, where each spatial operation is uniquely accompanied by I or T. Following the same derivation as in the noncoplanar case, the qSSG G realizes a linear O(2) [O(1)] representation of P and is classified by $H^1[P, \mathrm{O}(2)]$ (for coplanar) or $H^1[P, \mathrm{O}(1)]$ (for collinear).

In summary, the SSGs for noncoplanar, coplanar, and collinear magnetic structures can be classified by the O(3), O(2), and O(1) representations of their parent space group, respectively. Before presenting our classification scheme of SSGs based on the representation theory of space groups in detail, we utilize a flow chart to depict this process (Fig. 2). In the subsequent section, we outline the initial steps of the flow chart, which involve obtaining all distinct O(3) representations of a given space group and obtaining all O(2) and O(1) representations as by-products.

B. O(3), O(2), and O(1) representations

A generic O(3) representation consists of a nontrivial O(n) ($n = 0, 1, 2, 3$) representation and $(3 - n)$ identity representations. Here, $n = 0$ means that the O(3)
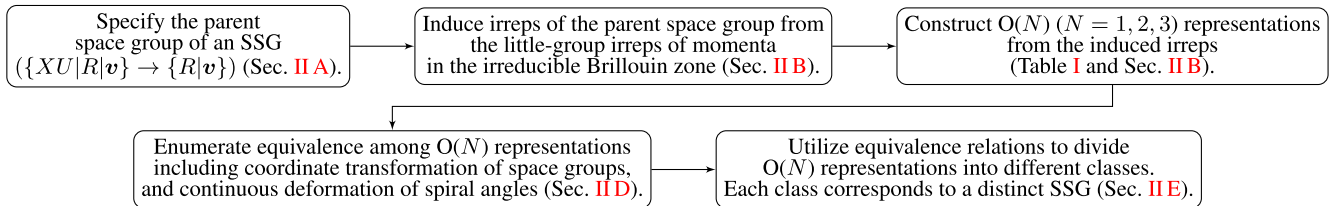

FIG. 2. Flowchart of obtaining all distinct SSGs based on the representation theory of space groups. Here, irrep stands for irreducible representations.

representation is an identity representation. The nontrivial $O(n)$ representation is equivalent to an n-dimensional real representation that is decomposed into a direct sum of nonidentity real irreducible representation (irrep), conjugate pairs of complex irreps (see Sec. A in Supplemental Material [36] for more details). Therefore, in order to enumerate all the distinct $O(3)$ representations, we need only to find all possible combinations of the irreps of the parent space group P. All irreps of P can be induced from allowable irreps of the little groups $P^{\boldsymbol{k}}$ of $\boldsymbol{k}$ vectors in the irreducible BZ [53]. An irrep $\rho_{\boldsymbol{k}}$ of $P^{\boldsymbol{k}}$ at $\boldsymbol{k}$ is considered "allowable" if the momentum of the irrep's basis is $\boldsymbol{k}$, requiring that $D_{\rho_{\boldsymbol{k}}}(\{I|\boldsymbol{t}\}) = e^{i\boldsymbol{k}\cdot\boldsymbol{t}}1_{r\times r}$, where $D_{\rho_{\boldsymbol{k}}}(\cdot)$ is the representation matrix and r is the dimension of $\rho_{\boldsymbol{k}}$. Hereafter, the notation $\rho_{\boldsymbol{k}}$ always refers to an allowable irrep of $P^{\boldsymbol{k}}$. The construction of $\rho_{\boldsymbol{k}}$ is detailed in Sec. A in Supplemental Material [36], and explicit forms of all irreps of all space groups can be obtained from the Representations DSG program [54] on the Bilbao Crystallographic Server. The induced irrep of P, $\rho_{\boldsymbol{k}}\uparrow P$, is supported by the basis of $\rho_{\boldsymbol{k}}$ and the rotated bases at the star of $\boldsymbol{k}$, $\{R_g\boldsymbol{k}|g\in P/P^{\boldsymbol{k}}\}$, implying that its dimension is $|P|/|P^{\boldsymbol{k}}|$ times the dimension of $\rho_{\boldsymbol{k}}$, where $|\cdot|$ denotes the order of a group. If $\boldsymbol{k}$ is not TRS invariant, $\rho_{\boldsymbol{k}}\uparrow P$ must be a complex irrep, and its complex conjugation $\rho_{\boldsymbol{k}}^*\uparrow P$ is induced from an irrep $\rho_{\boldsymbol{k}}^*$ of $P^{-\boldsymbol{k}}$. If $\boldsymbol{k}$ is a TRS-invariant momentum, $\rho_{\boldsymbol{k}}\uparrow P$ can be a real, complex, or pseudoreal irrep of P. As $O(3)$ representations are constructed from irreps with dimensions smaller than or equal to three, we need only to consider TRS-invariant $\boldsymbol{k}$'s with $|P^{\boldsymbol{k}}| = |P|, \frac{1}{2}|P|, \frac{1}{3}|P|$ and non-TRS-invariant $\boldsymbol{k}$'s with $P^{\boldsymbol{k}} = P$. Notably, the dimension of a pseudoreal irrep must be even (see Sec. A in Supplemental Material [36]), and, hence, a pair of pseudoreal irreps has a minimum dimension of four, and it is unnecessary to consider them when studying $O(3)$ representations.

A space group has a finite number of high-symmetry points (HSPs) $\boldsymbol{k}$ in the BZ. Here, $\boldsymbol{k}$ being an HSP means that $\boldsymbol{k}$ is TRS invariant or the little group of $\boldsymbol{k}$'s neighborhood is smaller than $P^{\boldsymbol{k}}$. Hence, it is direct to enumerate the finite number of irreps induced from these $\boldsymbol{k}$'s. On the other hand, a space group also has high-symmetry lines and planes of momenta and generic momenta in the irreducible BZ. Different $\boldsymbol{k}$ in these regions induce different irreps of the space group. To handle the infinite number of irreps induced by $\boldsymbol{k}$ in these regions, we regard that an irrep induced by $\boldsymbol{k}_1$ and that by $\boldsymbol{k}_2$ belong to the same class, if $P^{\boldsymbol{k}_1} = P^{\boldsymbol{k}_2} \equiv P^{\boldsymbol{k}}$, $\boldsymbol{k}_1$ and $\boldsymbol{k}_2$ are within the fixed-point manifold of $P^{\boldsymbol{k}}$, and if the two irreps can be continuously deformed to each other as $\boldsymbol{k}_{1,2}$ move continuously within the manifold. SSGs described by $O(3)$ representations induced from the irreps in the same class are treated as the same. With these in mind, we need only to consider a finite number of irreps for each space group. It is worth

noting that this scheme can include the SSGs describing incommensurate magnetic structures. If an $O(3)$ representation consists of irreps induced from $\boldsymbol{k}$'s at high-symmetry lines, planes, or generic momenta, the corresponding SSG describes both commensurate and incommensurate magnetic structures, depending on whether $\boldsymbol{k}$'s are rational or not.

We classify the $O(3)$ representations into 16 different types, as summarized in Table I. The $n = 0, 1, 2, 3$ blocks in Table I correspond to the nontrivial $O(n)$ representations, respectively. The nontrivial $O(n)$ representations in each block are further classified into different types based on the little group irreps $\rho_{\boldsymbol{k}}$ from which they are induced. In the following, we use the notation $[\rho_{\boldsymbol{k}}\uparrow P]_d^s$ to represent a d-dimensional real $(s = r)$ or complex $(s = c)$ irrep of the space group P. First, we have the 3D identity representation:

  (i) Type I: a 3D identity representation.

Second, we have only one type of the $n = 1$ $O(3)$ representations:

  (i) Type II: a direct sum of two trivial irreps and a 1D nontrivial real irrep, $[\rho_{\boldsymbol{k}}\uparrow P]_1^r$, where $P^{\boldsymbol{k}} = P$

TABLE I. Sixteen types of nontrivial $O(n)$ ($n = 0, 1, 2, 3$) representations, which decompose into nonidentity real irreps and pairs of complex irreps. $n = 0$ corresponds to the identity representation. The classification is based on the nature of constituent irreps. A nontrivial d-dimensional real $(s = r)$ or complex $(s = c)$ irrep induced from $\rho_{\boldsymbol{k}}$ of the little group $P^{\boldsymbol{k}}$ is written as $[\rho_{\boldsymbol{k}}\uparrow P]_d^s$. $[\rho_{\boldsymbol{k}}^*\uparrow P]_d^c$ represents the complex conjugate of $[\rho_{\boldsymbol{k}}\uparrow P]_d^c$. A generic $O(N)$ ($N = 1, 2, 3$) representation consists of a nontrivial $O(n)$ ($n = 1\dots N$) representation and ($N - n$) number of identity representations. The column "$|P|/|P^{\boldsymbol{k}}|$" specifies the order of $\boldsymbol{k}$-star. The columns "TRS" and "HSP" specify whether $\boldsymbol{k}$ is a TRS-invariant momentum and an HSP, respectively. $\boldsymbol{k}$ being an HSP means that $\boldsymbol{k}$ is TRS invariant or the fixed-point manifold of $P^{\boldsymbol{k}}$ is pointlike. The third row indicates that a type-III nontrivial $O(2)$ representation consists of two independent type-II nontrivial $O(1)$ representations. The ninth row indicates that a type-A ($A = $ IX$-$XIV) nontrivial $O(3)$ representation consists of a type-II nontrivial $O(1)$ representation and a type-($A - 6$) nontrivial $O(2)$ representation.

n	Type	Irreps	$|P|/|P^{\boldsymbol{k}}|$	TRS	HSP
0	I	1	1	✓	✓
1	II	$[\rho_{\boldsymbol{k}}\uparrow P]_1^r$	1	✓	✓
2	III	II $\oplus$ II	$\cdots$	$\cdots$	$\cdots$
	IV	$[\rho_{\boldsymbol{k}}\uparrow P]_1^c \oplus [\rho_{\boldsymbol{k}}^*\uparrow P]_1^c$	1	✓ or ✗	✓
	V	$[\rho_{\boldsymbol{k}}\uparrow P]_1^c \oplus [\rho_{\boldsymbol{k}}^*\uparrow P]_1^c$	1	✗	✗
	VI	$[\rho_{\boldsymbol{k}}\uparrow P]_2^r$	1	✓	✓
	VII	$[\rho_{\boldsymbol{k}}\uparrow P]_2^r$	2	✓ or ✗	✓
	VIII	$[\rho_{\boldsymbol{k}}\uparrow P]_2^r$	2	✗	✗
3	IX$-$XIV	II $\oplus$ (III$-$VIII)	$\cdots$	$\cdots$	$\cdots$
	XV	$[\rho_{\boldsymbol{k}}\uparrow P]_3^r$	1	✓	✓
	XVI	$[\rho_{\boldsymbol{k}}\uparrow P]_3^r$	3	✓	✓

(otherwise, the dimension is larger than one) and k must be TRS invariant (otherwise, the irrep cannot be real).

Third, the $n = 2$ O(3) representations are divided into six types:

(i) Type III: a direct sum of one trivial irrep and two nontrivial 1D real irreps, $[\rho_k \uparrow P]_1^r \oplus [\rho'_{k'} \uparrow P]_1^r$, where both k and k' are TRS invariant and $P^k = P^{k'} = P$.

(ii) Types IV and V: a direct sum of one trivial irrep and a pair of 1D complex irreps, $[\rho_k \uparrow P]_1^c \oplus [\rho_k^* \uparrow P]_1^c$, where k is not necessarily TRS invariant and $P^k = P$. The O(3) representation is type IV if k is an HSP and is type V otherwise. We distinguish the two types, because the former SSGs describe only commensurate magnetic structures, whereas the latter describes both incommensurate and commensurate structures. In the latter case, the fixed-point manifold of P^k can be high-symmetry lines, planes, or generic momenta in the BZ. SSGs given by the O(3) representations from irrational (rational) k in the fixed-point manifold describe incommensurate (commensurate) magnetic structures [see Figs. 4(f)–4(h) for examples for type-V SSGs].

(iii) Type VI: a direct sum of one trivial irrep and a 2D real irrep, $[\rho_k \uparrow P]_2^r$, where $P^k = P$, k is TRS invariant, and ρ_k is a 2D real irrep.

(iv) Type VII: a direct sum of one trivial irrep and a 2D real irrep, $[\rho_k \uparrow P]_2^r$, where $|P^k| = |P|/2$ and k is an HSP. k is not necessarily TRS invariant. However, if it is not, the star of k must include $-k$. Otherwise, the induced irrep cannot be real. We distinguish type VII from type VI, because it involves two propagating wave vectors.

(v) Type VIII: a direct sum of one trivial irrep and a 2D real irrep, $[\rho_k \uparrow P]_2^r$, where $|P^k| = |P|/2$ and k is not an HSP. The star of k must include its TRS partner $-k$. As the wave vector k can move in the fixed-point manifold of P^k, type VIII can describe both incommensurate and commensurate magnetic structures.

The $n = 3$ O(3) representations can be divided into eight types, where the first six are direct sums of 1D irrep and 2D representations, and the latter two are 3D irreps:

(i) Types IX–XIV: direct sums of a 1D real irrep, $[\rho_k \uparrow P]_1^r$, and a 2D real representation. The 1D real irrep has the same form as in type II, and the 2D real representations in types IX–XIV are the same as the nontrivial parts in types III–VIII, respectively (see Table I).

(ii) Type XV: a 3D real irrep, $[\rho_k \uparrow P]_3^r$, with $|P^k| = |P|$. k must be TRS invariant; otherwise, the induced irrep cannot be real.

(iii) Type XVI: a 3D real irrep, $[\rho_k \uparrow P]_3^r$, with $|P^k| = |P|/3$. k must be TRS invariant; otherwise, the induced irrep cannot be real.

Dividing the O(3) representations into the 16 types allows us to enumerate all the representations efficiently. Additionally, it also automatically yields all the O(2) representations (types I–VIII) and O(1) representations (types I and II), which, according to Sec. II A, classify the SSGs with coplanar and collinear magnetic structures, respectively.

Note that two different complex irreps may induce the same real representation. Consider a complex irrep ρ_k at k; its complex conjugation ρ_k^* must be an irrep at $-k$, denoted as ρ'_{-k}. Hence, there must be $[\rho_k \uparrow P]_1^c \oplus [\rho_k^* \uparrow P]_1^c = [\rho'_{-k} \uparrow P]_1^c \oplus [\rho'^*_{-k} \uparrow P]_1^c$. To avoid this redundancy, we limit k of ρ_k, from which the O(N) representations are induced, in the irreducible BZ.

C. Example: SSGs in the parent space group P3

To demonstrate how we obtain all O(N) (N = 1, 2, 3) representations of a space group and how they classify all the collinear, coplanar, and noncoplanar SSGs, we use magnetic structures with the parent space group P3 (No. 143) as examples. After obtaining these SSGs, we clarify the SSG and magnetic unit cells in SSGs and their relationship with the momenta of O(N) representations. The group P3 is generated by a threefold rotation $C_{3z} = \{3_{001}|\mathbf{0}\}$ and lattice translations. It possesses a hexagonal prism BZ. As explained at the beginning of the last subsection, to obtain all O(N) (N ≤ 3) representations, we need only to consider TRS-invariant k's with $|P^k| = |P|, |P|/2, |P|/3$ and non-TRS-invariant k's with $P^k = P$. Such momenta in the irreducible BZ include Γ $(0, 0, 0)$, A $(0, 0, \pi)$, M $(\pi, 0, 0)$, L $(\pi, 0, \pi)$, DT $(0, 0, u\pi)$, and P $(2\pi/3, 2\pi/3, v\pi)$, where the component forms are given on the basis of the reciprocal lattice vectors of P3. DT and P are high-symmetry lines parametrized by the continuous variables u and v, respectively [55].

The little groups of Γ, A, DT, and P equal the space group, since they are invariant under the C_{3z} rotation. There are three inequivalent 1D little group irreps on each of them, labeled by $S1$, $S2$, and $S3$ (S = GM, A, DT, P; hereafter, GM means Γ). The explicit representation matrices are given as

$$D_{S1}(C_{3z}) = 1, \ \ D_{S2}(C_{3z}) = e^{i(2\pi/3)}, \ \ D_{S3}(C_{3z}) = e^{-i(2\pi/3)}.$$
$$\tag{10}$$

For all the irreps $S1$, $S2$, and $S3$, the representation matrix for translation $\{1|m_1, m_2, m_3\}$ is $e^{i(k_1 m_1 + k_2 m_2 + k_3 m_3)}$, where (k_1, k_2, k_3) is the momentum of the irrep written on the basis of the reciprocal lattice and (m_1, m_2, m_3) is an integer-valued vector written on the basis of lattice vectors. The little group of M or L is the translation subgroup of P3. Therefore, $|P^{M,L}| = |P|/3$. $P^{M,L}$ has only one 1D irrep

(M1, L1) on each of them, where the translation $\{1|m_1, m_2, m_3\}$ is represented by $e^{i(k_1 m_1 + k_2 m_2 + k_3 m_3)}$.

1. O(1) representations and collinear SSGs

We construct O(1) representations to classify collinear SSGs. As discussed in Sec. II B, collinear SSGs are categorized under the first two of the total 16 SSG types. The type-I collinear SSG is described by the 1D identity representation (GM1). Hence, the collinear magnetic moments $S(r_i)$'s are invariant under any spatial operation without spin operations, as exampled in Fig. 3(a). This SSG is named L143.1.1 GM1, where "L" stands for collinear, "143" is the parent space group index, the first "1" represents type I, the second "1" is the index of SSG for a given parent space group and type, and "GM1" represents the little group irrep from which the O(1) representation is induced (refer to Sec. II F for the detailed naming convention of SSGs). Notably, although

magnetic moments in Fig. 3(a) align collinearly along the x axis, rotating them simultaneously to a different direction n does not alter the SSG symmetry. On the contrary, the MSG of a structure depends on the specific orientation of $S(r_i)$'s. In an MSG, a C_{3z} rotation necessitates $2\pi/3$-spin rotation $U_z(2\pi/3)$ along the z direction or its combination with time reversal T. The latter implies the existence of $(C_{3z}T)^3 = T$, which is impossible in the presence of nonzero magnetic moments; and the former also does not preserve the magnetic structure invariant [Fig. 3(b2)]. The type-II SSGs are described by a nontrivial real irrep $[\rho_k \uparrow P]_1^r$, where k is TRS invariant and $P^k = P$. The space group $P3$ has only one nontrivial 1D real irrep—$[A1 \uparrow P]_1^r$. Therefore, only one type-II SSG, named L143.2.1 A1, exists for the space group [Fig. 3(c)]. The 1D real irrep implies that collinear magnetic moments $S(r_i)$'s change sign under the translation $\{I|0, 0, 1\}$.
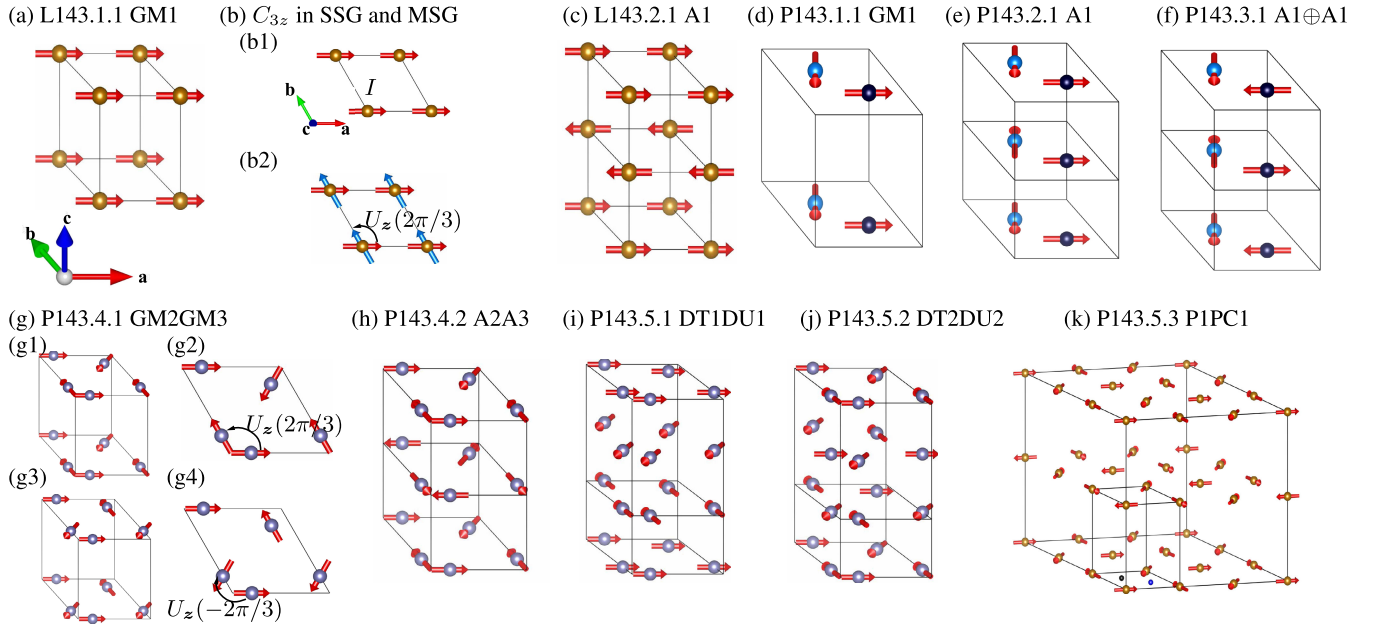

FIG. 3. (a),(c) Collinear and (d)–(k) coplanar magnetic structures for all distinct SSGs whose parent space group is $P3$ (No. 143). The notations of SSGs, which consist of one prefix letter, three indices, and O(3) representations of the space group (see Sec. II F), are labeled at the top of each subfigure. Atoms in different Wyckoff positions are depicted with different colors. The golden atoms occupy Wyckoff position 1a [$(0, 0, z)$ with $z = 0$]; the light-blue atoms occupy Wyckoff position 1b [$(1/3, 2/3, z)$ with $z = 0$]; the dark-purple atoms occupy Wyckoff position 1c [$(2/3, 1/3, z)$ with $z = 0$]; the gray atoms occupy Wyckoff position 3d [$(x, y, z), (-y, x - y, z), (-x + y, -x, z)$ with $y = z = 0$]. (b) The comparison between $2\pi/3$ rotation in SSG and MSG. (a) Collinear magnetic moments $S(r_i)$'s remain invariant under all spatial operations. (c) Collinear $S(r_i)$'s change sign under $\{1|001\}$. (d) Coplanar $S(r_i)$'s remain invariant under all spatial operations. (e) The SSG 143.2.1 A1 is given by the O(2) representation $[GM1 \uparrow P]_1^r \oplus [A1 \uparrow P]_1^r$, while the trivial irrep $[GM1 \uparrow P]_1^r$ is omitted in its notation. Irrep $[GM1 \uparrow P]_1^r$ implies that one component (e.g., x) of coplanar $S(r_i)$'s is invariant under all operations. Irrep $[A1 \uparrow P]_1^r$ implies that the other component (e.g., y) changes sign under $\{I|001\}$. (f) Two irreps $[A1 \uparrow P]_1^r$'s imply that both components of coplanar $S(r_i)$'s change sign under $\{1|001\}$. (g) Coplanar $S(r_i)$'s are rotated by $2\pi/3$ [(g1) and (g2)] or $-2\pi/3$ [(g3) and (g4)] under C_{3z} rotation. (h) Coplanar $S(r_i)$'s are rotated by $2\pi/3$ under C_{3z} and change sign under $\{1|001\}$. (i)–(k) Spiral magnetic structures. (i) Coplanar $S(r_i)$'s are invariant under C_{3z} and are rotated by $u\pi$ ($u = 2/3$) under $\{1|001\}$. (j) Coplanar $S(r_i)$'s are rotated by $2\pi/3$ under C_{3z} and are rotated by $u\pi$ ($u = 2/3$) under $\{1|001\}$. (k) Coplanar $S(r_i)$'s are invariant under C_{3z} and are rotated by $2\pi/3$, $2\pi/3$, and $v\pi$ ($v = 1$) under the translations $\{1|100\}$, $\{1|010\}$, and $\{1|001\}$, respectively. These crystal structures and subsequent structures are illustrated by using the VESTA software [56].

2. O(2) representations and coplanar SSGs

We consider O(2) representations and coplanar SSGs. These SSGs are categorized within the first eight types in Table I. The type-I and type-II O(2) representations are given by the direct sum of an identity irrep combined with type-I and type-II O(1) representations, respectively. Thus, $P3$ has one type-I coplanar SSG, P143.1.1 GM1 [Fig. 3(d)], and one type-II coplanar SSG, P143.2.1 A1 [Fig. 3(e)]. Here, "P" represents coplanar, with the rest of the naming convention similar to that of collinear SSGs. Note that the O(2) representation A1 $\oplus$ 1 characterizes the SSG P143.2.1, but the trivial irrep 1 is omitted in the notation (also refer to Sec. II F). Type-III SSGs are given by $[\rho_k \uparrow P]_1^r \oplus [\rho'_{k'} \uparrow P]_1^r$. Given that $P3$ possesses only a single 1D nontrivial real irrep, there is only one type-III SSG— N143.3.1 A1 $\oplus$ A1 [Fig. 3(f)]—given by the direct sum of two A1's. Refer to the caption of Fig. 3 for the descriptions of these SSG symmetries that are determined by the corresponding representations.

Type-IV SSGs are described by a direct sum of a complex irrep $[\rho_k \uparrow P]_1^c$ and its complex conjugation $[\rho_k^* \uparrow P]_1^c$, where $P^k = P$ and k is TRS invariant. Only GM and A satisfy the requirements of type IV. Irreps GM2 and GM3 form a complex conjugate pair, giving the SSG P143.4.1 GM2GM3. Irreps A2 and A3 form another complex conjugation pair, giving another SSG P143.4.2 A2A3. Let us first look at P143.4.1 GM2GM3. The representation matrix of C_{3z} given by GM2 $\oplus$ GM3 is equivalent to the real rotation matrix

$$\begin{pmatrix} \cos(\frac{2\pi}{3}) & -\zeta \sin(\frac{2\pi}{3}) \\ \zeta \sin(\frac{2\pi}{3}) & \cos(\frac{2\pi}{3}) \end{pmatrix}, \qquad (11)$$

where ζ being either 1 or -1 indicates that the coplanar magnetic moments are rotated by $2\pi/3$ [Fig. 3(g1)] and $-2\pi/3$ [Fig. 3(g3)] under the C_{3z} rotation, respectively. A magnetic structure satisfying the rotation matrix with $\zeta = 1$ is also (equivalently) described by the conventional magnetic space group [Fig. 3(g2)], whereas a magnetic structure satisfying the rotation matrix with $\zeta = -1$ can be described only by the SSG [Fig. 3(g4)]. The $\zeta = \pm 1$ configurations belong to the same SSG, because, in the absence of SOC, we can adopt different spin coordinates irrespective of the real space coordinate, and the two configurations are continuously connected to each other under a spin coordinate transformation. For example, consider a continuous rotation around the x axis $e^{-i\theta\hat{S}_x}$ as the spin coordinate transformation. When θ changes continuously and reaches π, the anticlockwise structure in the x, y spin plane ($\zeta = -1$) will be transformed into a clockwise structure ($\zeta = +1$). Notably, besides the $\pm 2\pi/3$ rotation around the z axis, this SSG can describe cases with the $\pm 2\pi/3$ rotation around a generic axis n. Figure 3(h) shows the other type-IV SSG N143.4.2 A2A3 and describes its symmetry.

The type-V SSGs are also constructed from $[\rho_k \uparrow P]_1^c \oplus [\rho_k^* \uparrow P]_1^c$ as in type IV, except that k is now not an HSP. $P^k = P$ is satisfied by those k's on DT and P. Let us consider $k = (0, 0, u\pi)$ on the line DT and its irrep DTi ($i = 1, 2, 3$). The complex conjugate of DTi is a complex irrep with momentum at the other point $(0, 0, -u\pi)$ on the line DT. To emphasize that these two irreps have different momenta on the same line, we follow the convention in Bilbao Crystallographic Server [54] and denote the complex conjugate of DTi as DUi and the real representation constructed from DTi and DUi as DTiDUi. Although DTiDUi from different momenta (different u) on the line DT represent inequivalent representations, we classify them as the same SSG, as they describe the same kind of magnetic structures (see the discussion in Sec. II B). Similarly, the complex conjugate of irrep Pi ($i = 1, 2, 3$) on the P line is denoted as PCi, and their direct sum is referred to as PiPCi. In the following, we will explain DTiDUi ($i = 1, 2, 3$) and PiPCi ($i = 1, 2, 3$) and demonstrate that some of these six describe the same SSG; some are transformed into one another under a change of the coordinate system. First, let us examine the representations DTiDUi on the line DT. If the momentum of DTi ($i = 1, 2, 3$) is $(0, 0, u\pi)$ ($|u| \leq 1$), the representation matrices of translation $\{I|0, 0, 1\}$ for DTiDU$i(u)$ are the same for different i and equivalent to the rotation matrix

$$D_{\text{DT}i\text{DU}i(u)}(\{I|0,0,1\}) = \begin{pmatrix} \cos(u\pi) & -\zeta \sin(u\pi) \\ \zeta \sin(u\pi) & \cos(u\pi) \end{pmatrix}, \qquad (12)$$

where $\zeta = \pm 1$. The representation matrices of C_{3z} for DTiDU$i(u)$ with different i are given by

$$D_{\text{DT1DU1}(u)}(C_{3z}) = \begin{pmatrix} 1 & 0 \\ 0 & 1 \end{pmatrix},$$

$$D_{\text{DT2DU2}(u)}(C_{3z}) = \begin{pmatrix} \cos(\frac{2\pi}{3}) & -\zeta \sin(\frac{2\pi}{3}) \\ \zeta \sin(\frac{2\pi}{3}) & \cos(\frac{2\pi}{3}) \end{pmatrix},$$

$$D_{\text{DT3DU3}(u)}(C_{3z}) = \begin{pmatrix} \cos(\frac{2\pi}{3}) & \zeta \sin(\frac{2\pi}{3}) \\ -\zeta \sin(\frac{2\pi}{3}) & \cos(\frac{2\pi}{3}) \end{pmatrix}, \qquad (13)$$

respectively. Notice that, for a given DTiDUi representation, the ζ's in Eqs. (12) and (13) must be the same, because the representation matrices of translation and rotation are transformed from the two 1D complex irreps by the same unitary matrix. The first type-V SSG is N143.5.1 DT1DU1 [see the structure and symmetry in Fig. 3(i)]. As discussed in the type-IV SSG, the two configurations from $\zeta = \pm 1$ should belong to the same SSG. Additionally, it is worth noting that different u gives only a different spiral angle in the magnetic structure in Fig. 3(i), and the other features of the structure are exactly the same for different u. This let us regard that different u's on the line DT give the same SSG.

Next, let us consider DT2DU2 and DT3DU3. For DT2 at $\mathbf{k} = (0, 0, u\pi)$ and $\zeta = \pm 1$ in Eqs. (12) and (13), DT2DU2 describes a magnetic structure where two components (e.g., x, y) of the magnetic moments are rotated by $\pm 2\pi/3$ under C_{3z} and rotated by $\pm u\pi$ under $\{1|0, 0, 1\}$, respectively [see Fig. 3(j)]. Meanwhile, for DT3 at $\mathbf{k} = (0, 0, -u\pi)$ and $\zeta = \mp 1$ in Eqs. (12) and (13), DT3DU3 give the same representation matrices. It seems that DT2DU2 and DT3DU3 are the same representation. However, given that we consider only $\rho_{\mathbf{k}}$ in the irreducible BZ, DT2DU2 and DT3DU3 are still inequivalent representations, because DT2DU2 induced from $u \in (0, 1)$ (within the irreducible BZ) is equivalent only to DT3DU3 induced from $u \in (-1, 0)$ (outside the irreducible BZ). Nevertheless, the two representations are continuously connected as u approaches zero. Physically, if the spin axes are properly chosen, DT2DU2 ($\zeta = 1$) and DT3DU3 ($\zeta = -1$) describe similar magnetic structures with spiral angles $u\pi \in (0, \pi)$ and $u\pi \in (\pi, 2\pi)$, respectively. In this work, we identify them as in the same class, as the spiral angles can continuously change. Such equivalences are systematically addressed in Sec. II D. We name the SSG as P143.5.2 DT2DU2.

Lastly, we consider irreps Pi ($i = 1, 2, 3$) from the momentum $\mathbf{k} = (2\pi/3, 2\pi/3, v\pi)$ and their complex conjugations PCi. For each PiPCi representation, the coplanar magnetic moments are rotated by $2\pi/3$, $2\pi/3$, and $v\pi$ under the translations $\{1|1, 0, 0\}$, $\{1|0, 1, 0\}$, and $\{1|0, 0, 1\}$, respectively. Note that the choice of rotating $\mathbf{S}(\mathbf{r}_i)$'s in either an anticlockwise or clockwise direction is arbitrary, as discussed around Eqs. (11) and (12). Here, we choose to rotate them in the anticlockwise direction without loss of generality. PiPCi ($i = 1, 2, 3$) also requires that $\mathbf{S}(\mathbf{r}_i)$'s are rotated by $(i-1)2\pi/3$ under the C_{3z} rotation around the origin. Although the rotation angles are different for different i, magnetic structures for PiPCi ($i = 1, 2, 3$) are indeed equivalent; they are transformed to each other by shifts of the origin. To be concrete, let us begin with a magnetic structure for P1PC1 [Fig. 3(k)], where the magnetic moments are invariant under C_{3z} around the golden point in Fig. 3(k). By shifting the origin to the blue (black) point in Fig. 3(k), one can see that the magnetic moments in the same magnetic structure are rotated by $2\pi/3$ ($-2\pi/3$) under C_{3z} around the new origin. Therefore, all PiPCi representations ($i = 1, 2, 3$) describe the same SSG, and we name it N143.5.3 P1PC1. The equivalence among PiPCi representations can be shown by transformations of representations associated with the lattice coordinate transformation, which are systematically discussed in Sec. II D. For P3, the type-VI SSG does not exist; $P^{\mathbf{k}} = P$ at TRS-invariant $\mathbf{k}$ requires that k must be Γ or A, while these two points do not have 2D irreps. Type-VII and -VIII SSGs do not exist for the parent space group P3 either, because there is no $\mathbf{k}$ with $|P^{\mathbf{k}}| = |P|/2$.

3. O(3) representations and noncoplanar SSGs

We construct O(3) representations that classify noncoplanar SSGs. An O(3) representation of types I–VIII consists of an O(2) representation in the same type and a trivial irrep. Figures 4(a)–4(h) show magnetic structures conforming to these SSGs, sharing the same number of coplanar SSGs. The O(2) representation indicates that two components (e.g., x and y) of the magnetic moments transform as those in coplanar SSGs, while the trivial irrep indicates that the remaining component (e.g., z) is invariant under all spatial operations. Type IX–XIV SSGs are described by direct sums of a nontrivial 1D real irrep and a 2D nontrivial real representation. Here, the 1D real irreps are the same as those in type II, and the 2D real representations are the same as those in types III–VIII, respectively. Having only type III–V SSGs, P3 has only type IX, X, and XI SSGs. Since P3 possesses only one nontrivial 1D real irrep A1, there exists a one-to-one correspondence between SSGs of types IX–XI [Figs. 4(i)–4(n)] and SSGs of types III–V [Figs. 4(c)–4(h)]. The additional A1 representation in type IX–XI SSGs makes one component (e.g., z) of the magnetic moments change sign under a lattice translation along the z axis, whereas the other two components (e.g., x and y) transform identically as those in type III–V SSGs discussed so far.

Type-XV SSGs, characterized by $[\rho_{\mathbf{k}} \uparrow P]_3^r$ with $|P^{\mathbf{k}}| = |P|$ and $\mathbf{k}$ being TRS invariant, do not exist for P3. Two TRS-invariant $\mathbf{k}$ points, A and Γ, satisfy $|P^{\mathbf{k}}| = |P|$, but neither of them possesses a 3D irrep.

Type-XVI SSGs are characterized by a 3D real irrep $[\rho_{\mathbf{k}} \uparrow P]_3^r$ with $|P^{\mathbf{k}}| = |P|/3$ and TRS-invariant $\mathbf{k}$. M and L satisfy the requirements, and each possesses only one irrep. Hence, P3 has only two type-XVI SSGs, namely, N143.16.1 M1 [Fig. 4(o)] and N143.16.2 L1 [Fig. 4(p)]. For the SSGs N143.16.1 M1 and N143.16.2 L1, the O(3) representation matrices of the lattice translation $\{1|m_1, m_2, m_3\}$ are given by

$$\text{diag}((-1)^{m_1}, (-1)^{m_2}, (-1)^{m_1+m_2}) \tag{14}$$

and

$$\text{diag}((-1)^{m_1+m_3}, (-1)^{m_2+m_3}, (-1)^{m_1+m_2+m_3}), \tag{15}$$

respectively. Here, the basis of the O(3) matrices is composed of three inequivalent TRS-invariant points. For N143.16.1 M1, the points are $(\pi, 0, 0)$, $(0, \pi, 0)$, and $(\pi, \pi, 0)$, while for N143.16.2 L1, they are $(\pi, 0, \pi)$, $(0, \pi, \pi)$, and (π, π, π). The O(3) representation matrix of the C_{3z} rotation is given by the same matrix for N143.16.1 M1 and N143.16.2 L1:

$$\begin{pmatrix} 0 & 1 & 0 \\ 0 & 0 & 1 \\ 1 & 0 & 0 \end{pmatrix}. \tag{16}$$
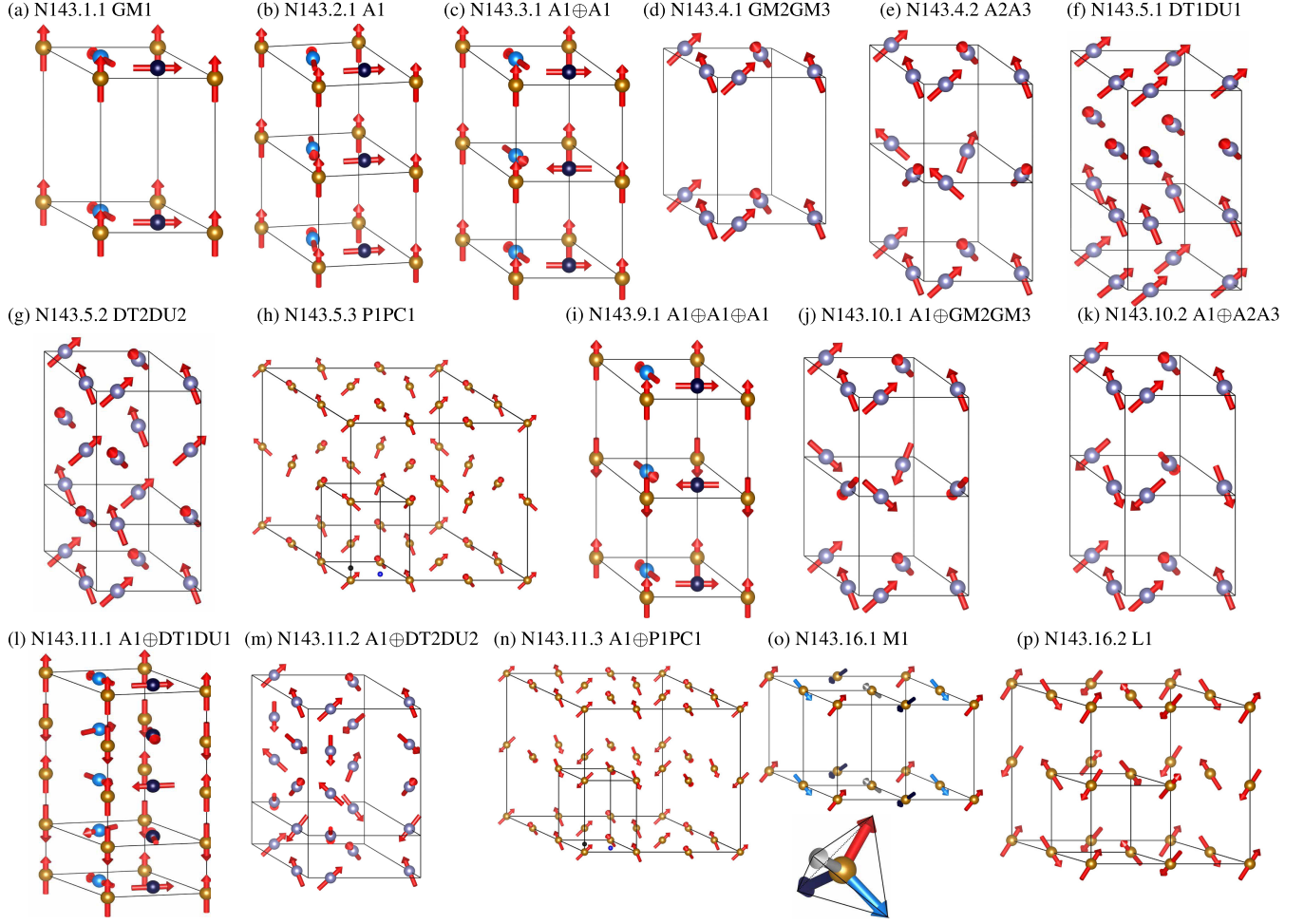
FIG. 4.   Noncoplanar magnetic structures for all distinct SSGs whose parent space group is $P3$ (No. 143). The notations of SSGs, which consist of one prefix letter, three indices, and O(3) representations of the space group (see Sec. II F), are labeled at the top of each subfigure. Atoms in different Wyckoff positions are depicted with different colors, with the same rule as Fig. 3. (f)–(h) and (l)–(n) display spiral magnetic structures, with (f) and (g) having $\boldsymbol{k}$ on line DT chosen as $(0, 0, 2\pi/3)$, (l) and (m) having $\boldsymbol{k}$ on line DT chosen as $(0, 0, \pi/2)$, and (h) and (n) having $\boldsymbol{k}$ on line P chosen as $(2\pi/3, 2\pi/3, \pi)$. (h),(n) The coordinates of the black and blue points are $(2/3, 1/3, 0)$ and $(1/3, 2/3, 0)$, respectively.

For the magnetic structure with SSG N143.16.1 M1, the magnetic moments are rotated by $2\pi/3$ along the 111 direction [Eq. (16)] under the C_{3z} rotation and are rotated by π along the y and x directions [Eq. (14)] under $\{1|1, 0, 0\}$ and $\{1|0, 1, 0\}$, respectively. Therefore, the spin operations in this SSG constitute the chiral tetrahedral group T. Required by the symmetries, the magnetic moment at the C_{3z}-invariant origin aligns with the rotation axes of $2\pi/3$-spin rotation (i.e., 111 direction). Under $\{1|1, 0, 0\}$, $\{1|0, 1, 0\}$, and $\{1|1, 1, 0\}$, this magnetic moment is transformed into different directions. Thus, in the magnetic unit cell, four distinct magnetic moments exist, presented by different colors in Fig. 4(o). Notably, the magnetic moments point to the four vertexes of a tetrahedron [Fig. 4(o)], manifesting the tetrahedral group structure of spin operations. For SSG N143.16.2 L1, the magnetic structure on the $z = 0$ plane is identical to those for SSG

N143.16.1 M1 [Fig. 4(p)]. However, these magnetic moments are reversed under $\{1|0, 0, 1\}$. Thus, the spin operations in this SSG constitute the achiral tetrahedral group T$_d$. We also note that SSG N143.16.1 M1 possesses an interesting property: There exist two anticommuting translation operations for the electronic Hamiltonian described by this SSG (see Sec. III C).

Magnetic structures presented in Figs. 3 and 4 are merely examples illustrating the SSGs. For collinear magnetic structures [Figs. 3(a) and 3(c)], we choose magnetic moments $S(r_i)$'s aligned along the x direction. For coplanar magnetic structures [Figs. 3(d)–3(k)], we choose $S(r_i)$'s aligned within the x, y plane. For noncoplanar magnetic structures in Figs. 4(a)–4(h), we choose the z component of $S(r_i)$'s to be transformed according to the 1D identity irrep; for those in Figs. 4(i)–4(n), we choose the z component to be transformed according to the 1D nontrivial real irrep.

The particular choice of the spin orientation and the spin coordinate system is only for the sake of clarity in the illustration. The same SSGs still apply if all the magnetic moments are simultaneously rotated by an arbitrary O(3) matrix O, as we discuss for the SSG N143.4.1 GM2GM3.

4. SSG unit cell and magnetic unit cell

The SSG unit cell of an SSG $\mathcal{G}$ refers to the unit cell of its parent space group P and is associated with the translation subgroup $T = \{\{1|\boldsymbol{v}_g\}|R_g = 1, g \in \mathcal{G}\}$ of P. In Figs. 3 and 4, the smaller cells enclosed by the solid black line are the SSG unit cells. The magnetic unit cell, also known as magnetic supercell, is associated with the pure translation subgroup T_M, given as

$$T_M = \{\{I|1|\boldsymbol{v}\}|\{I|1|\boldsymbol{v}\} \in \mathcal{G}\}. \tag{17}$$

Here, the subscript "M" denotes MSG, because T_M is also a subgroup of an MSG.

The magnetic unit cell and T_M are uniquely determined by the momenta of the O(N) representation. For a noncoplanar SSG, the O(3) representation matrix of the translation $\{1|\boldsymbol{v}\} \in T$ is equivalent to the matrix $O_{\boldsymbol{v}} = \text{diag}(e^{i\boldsymbol{k}_1 \cdot \boldsymbol{v}}, e^{i\boldsymbol{k}_2 \cdot \boldsymbol{v}}, e^{i\boldsymbol{k}_3 \cdot \boldsymbol{v}})$ up to a unitary transformation, where $\boldsymbol{k}_i$'s ($i = 1, 2, 3$) are the momenta of the O(3) representation. Note that $e^{i\boldsymbol{k}_i \cdot \boldsymbol{v}}$'s either are all real or consist of a conjugate pair and a real number, required by $O_{\boldsymbol{v}}$ being equivalent to an O(3) matrix. All $\{1|\boldsymbol{v}\} \in T$ such that $O_{\boldsymbol{v}} = I$ constitute T_M.

Let us consider the SSG N143.5.1 DT1DU1 [see Fig. 4(f)] as an example. The SSG is given by the direct sum of a complex irrep DT1, its complex conjugate DU1, and an identity irrep, the momenta of which are $(0, 0, u\pi)$ with $u \notin \mathbb{Z}$, $(0, 0, -u\pi)$, and $\boldsymbol{0}$, respectively. Thus, the representation matrix $O_{\boldsymbol{v}}$ for $\{1|\boldsymbol{v}\}$ with $\boldsymbol{v} = \sum_{i=1}^{3} m_i \boldsymbol{a}_i$ ($m_i \in \mathbb{Z}$) is equivalent to $\text{diag}(e^{iu\pi m_3}, e^{-iu\pi m_3}, 1)$. The condition $O_{\boldsymbol{v}} = I$ requires that $\frac{1}{2}um_3 \in \mathbb{Z}$ and have no constraints on m_1 and m_2. For the structure in Fig. 4(f), $u = 2/3$, and, hence, m_3 is required to be a multiple of 3. The lattice vectors of the magnetic unit cell are $\boldsymbol{a}_1$, $\boldsymbol{a}_2$, and $3\boldsymbol{a}_2$, which is 3 times as large as the SSG unit cell. For more generic u, if $\frac{1}{2}u$ is a rational number p/q with p and q coprime integers, the magnetic unit cell is q times as large as the SSG unit cell. If $\frac{1}{2}u$ is irrational, only $m_3 = 0$ satisfy the requirement. An irrational u corresponds to the incommensurate magnetic structure, where the size of the magnetic unit cell is infinite. As also discussed earlier in this section, although the size of a magnetic unit cell depends on u, DT1DU1 with different u corresponds to the same SSG in our classification. The magnetic unit cell in generic noncoplanar SSGs can be determined similarly, and, for coplanar and collinear SSGs, $O_{\boldsymbol{v}}$ should be a 2×2 or 1×1 identity matrix, respectively.

The magnetic moments in the equivalent positions of two different SSG unit cells are not necessarily identical. The magnetic moment $\boldsymbol{S}(\boldsymbol{r}_i + \boldsymbol{v})$ at position $\boldsymbol{r}_i + \boldsymbol{v}$ ($\{1|\boldsymbol{v}\} \in T_M$) satisfies that $\boldsymbol{S}(\boldsymbol{r}_i + \boldsymbol{v}) = \mathcal{U}O_{\boldsymbol{v}}\mathcal{U}^{-1}\boldsymbol{S}(\boldsymbol{r}_i)$, where $\mathcal{U}$ is a unitary matrix transforming the diagonal matrix $O_{\boldsymbol{v}}$ to an O(3) matrix. Thus, the momenta of O(N) representations give the magnetic propagation vectors. The O(N) representations with multiple nonzero momenta correspond to SSGs describing the multiple-Q structure. For example, the SSG N143.5.1 DT1DU1 has two opposite propagation vectors $(0, 0, \pm u\pi)$. Besides these two vectors, the third propagation vector of the SSG N143.11.1 A1 $\oplus$ DT1DU1 is $(0, 0, \pi)$.

D. Equivalence in spin space groups

In the last subsection, we have often seen that some inequivalent O(N) ($N = 3, 2, 1$) representations correspond to the physically same SSG. In this subsection, we introduce the concept of O(N) representation *class*, which defines the physically distinct SSGs uniquely and in a mutually exclusive way. Two O(N) representations are categorized into the same class if and only if they satisfy one of the following three conditions: (i) They are equivalent representations; (ii) they change into each other upon a coordinate transformation in real space; (iii) they are induced from momenta that share the same little group, and they are continuously connected. In the following, we explain these conditions in detail.

(i) *Coordinate transformation in spin space.*—Equivalent O(N) representations are in the same class. This equivalence arises from the freedom of the spin coordinates; in the SSG, spin rotation and rotation in real space are decoupled. To be more specific, two O(N) representations, ρ and σ, of the parent space group P are equivalent, if the representation matrices of ρ and σ, $D_\rho(p)$ and $D_\sigma(p)$, are transformed to each other by an orthogonal matrix O for any elements p in the parent space group; $D_\sigma(p) = O^T D_\rho(p)O$, $\forall\ p \in P$. This means that ρ and σ correspond to the same spin operations in different coordination of the spin axes.

(ii) *Coordinate transformation in real space.*—If an O(N) representation ρ is transformed into another σ upon allowable coordinate transformation in real space, ρ and σ belong to the same O(N) representation class. A coordinate transformation $\{V|\boldsymbol{t}\}$ for a space group P involves a change of the axes by a matrix V and a shift of the origin by a vector $\boldsymbol{t}$. An allowable $\{V|\boldsymbol{t}\}$ generates an automorphism in the space group P:

$$\{R|\boldsymbol{v}\} \rightarrow \{V|\boldsymbol{t}\}^{-1}\{R|\boldsymbol{v}\}\{V|\boldsymbol{t}\} \in P, \quad \forall\ \{R|\boldsymbol{v}\} \in P. \tag{18}$$

The group structure is invariant under the allowable transformation $\{V|t\}$. Especially, for $R = 1$, $\{V|t\}^{-1}\{1|v\}\{V|t\} = \{1|V^{-1}v\} \in P$ requires that the Bravais lattice is invariant by $\{V|t\}$. The invariance implies that, for lattice basis a_i ($i = 1, 2, 3$), Va_i can be expanded in terms of the lattice basis with integer coefficients, $Va_i = \sum_{j=1}^{3} a_j M_{ji}$ with a unimodular integer matrix M ($M_{ij} \in \mathbb{Z}$ and $\det M = \pm 1$). Here, M is the representation matrix of V on the basis a_i. We require that the chirality of the unit cell is preserved by $\{V|t\}$, resulting in $\det V = 1$. Thanks to the automorphism, an allowable $\{V|t\}$ transforms an irrep ρ into another irrep σ according to

$$D_\sigma(\{R|v\}) = D_\rho(\{V|t\}\{R|v\}\{V|t\}^{-1}). \quad (19)$$

The transformation of an O(N) representation under $\{V|t\}$ is fully determined by the transformations of each irrep that constitutes the O(N) representation. Notably, the type of an O(N) representation listed in Sec. II B is invariant under an allowable transformation $\{V|t\}$. This is because the type of the O(N) representation is determined only by the order and fixed points of P^k and the TRS invariance of k, all of which remain invariant under an allowable transformation. Under the transformation $\{V|t\}$, the original little group P^k is transformed into $P^{V^{-1}k} = \{V|t\}^{-1}P^k\{V|t\}$, which is isomorphic to P^k, and, hence, it has the same order and same type of fixed-point region (pointlike, linelike, etc.). Note also that if k is TRS invariant, $V^{-1}k$ must also be TRS invariant. This is because V is represented by a unimodular integer matrix on the basis of the reciprocal lattice vectors as well as the lattice vectors. Therefore, the transformed O(N) representation must have the same type as the original one.

Every space group generally has an infinite number of allowable transformations, and the allowable transformations form a group. Therefore, we have only to consider the transformations of the constituent irreps under the generators of the group. For example, consider the parent space group $P3$. To keep the hexagonal lattice of $P3$ unchanged, V must be an element of the point group of the hexagonal lattice, D_{6h}. Given that V must be a proper operation ($\det M = 1$), allowable V's form the point group D_6. The shift vector t is also subject to symmetry constraints. For $P3$, the shifted origin must be C_{3z} invariant; allowable t must have the form of (m_1, m_2, z), $(m_1 + 1/3, m_2 + 2/3, z)$, or $(m_1 + 2/3, m_2 + 1/3, z)$ with $m_1, m_2 \in \mathbb{Z}$ and $z \in \mathbb{R}$. In summary, the group formed by the allowable transformations for $P3$ is generated by $\{6_{001}|0\}$, $\{2_{100}|0\}$,

$\{1|1/3, 2/3, 0\}$, $\{1|2/3, 1/3, 0\}$, and $\{1|0, 0, z\}$, where rotations 6_{001} and 2_{100} are the generators of the D_6 group.

Let us next explain how all type-V O(3) representations of $P3$, DTiDUi and PiPCi for $i = 1, 2, 3$, are transformed under the generators of allowable coordinate transformations for $P3$. According to Eq. (19), the momentum k of an irrep is transformed to $V^{-1}k$ under $\{V|t\}$, while any V in the group cannot transform the line DT to P or vice versa. This shows that DTiDUi and PjPCj lead to distinct representation classes, respectively. Section B in Supplemental Material [36] shows that all coordinate transformations leave DT1 invariant; $\{2_{100}|0\}$ transforms C_{3z} to C_{3z}^{-1} and, hence, transforms irrep DT2 into DT3 [Eq. (13)]. The transformation between DT2 and DT3 is consistent with the previous discussion in Sec. II C; DT2DU2 and DT3DU3 represent the same magnetic structure under a coordinate transformation and, hence, belong to the same class (Sec. II C). (One should notice that DT2DU2 and DT3DU3 are also subject to the equivalence (iii), as explained in the second paragraph below.) Section B in Supplemental Material [36] also demonstrates that, under the action of $\{1|2/3, 1/3, 0\}$ ($\{1|1/3, 2/3, 0\}$), the irrep P1 is transformed into P2 ($P3$). The transformation suggests that P1PC1, P2PC2, and P3PC3 all lead to the same SSG N143.5.3 P1PC1. In fact, the equivalence among P1, P2, and P3 is also consistent with the observation in the real space (Sec. II C).

(iii) *Continuously connected wave vector.*—The third equivalence relation for the O(N) representation classification applies to representations induced from non-HSP k's. Such O(N) representations include type-V O(3) and O(2) ($[\rho_k\uparrow P]_1^c \oplus [\rho_k^*\uparrow P]_1^c$), type-VIII O(3) and O(2) ($[\rho_k\uparrow G]_2^r$), type-XI O(3) ($[\rho_k\uparrow P]_1^c \oplus [\rho_k^*\uparrow P]_1^c \oplus [\rho_p'\uparrow P]_1^r$), and type-XIV O(3) ($[\rho_k\uparrow G]_2^r \oplus [\rho_p'\uparrow P]_1^r$) representations. As k is not an HSP, the fixed-point manifold of P^k has a dimension larger than 0, and k is not TRS invariant. Consider another momentum k' within the same fixed-point manifold and compare two O(N) representations induced from k and k'. The third equivalence claims that the two representations belong to the same representation class if they can be continuously deformed to each other by a continuous change of the momentum between k and k' in the manifold. Notice that any O(1) representation is free from this equivalence relation, because an O(1) representation must always be induced from a TRS-invariant momentum (an HSP). Without this equivalence relation, the number of distinct SSGs (representation classes) would be infinite; different momenta in the BZ could define different SSGs. The equivalence

relation is crucial for a complete classification of SSGs.

We have seen two examples of the third equivalence relation in Sec. II C, N143.5.1 DT1DU1 and N143.5.2 DT2DU2. Thereby, we considered that DT1DU1 induced from different momenta on the line DT belong to the same class and showed that all of them describe the same magnetic spiral structure with different spiral angles. For N143.5.2 DT2DU2, we found two different 2D real representations—i.e., DT2DU2 and DT3DU3 defined after Eq. (13)—and showed that they can be continuously connected to each other, describing the same kind of magnetic structure. (One should notice that DT2DU2 and DT3DU3 are also subject to the equivalence (ii), as explained in the second paragraph above.) These observations justify the third equivalence relation.

The third equivalence becomes more intricate when the parent space group is nonsymmorphic. To illustrate this point, let us consider the parent space group $P2_1$ (No. 4), which is generated by lattice translations $\{1|1,0,0\}$, $\{1|0,1,0\}$, $\{1|0,0,1\}$, and the screw rotation $\{2_{010}|0,1/2,0\}$. We consider irreps on the high-symmetry line LD $(0, u\pi, 0)$ $(u \notin \mathbb{Z})$. At every $\mathbf{k} = (0, u\pi, 0)$, there exist two complex irreps $\text{LD1}(u)$ and $\text{LD2}(u)$. The representation matrices of translations and the screw are $D_{\text{LD1}(u)}(\{1|\mathbf{v}\}) = D_{\text{LD2}(u)}(\{I|\mathbf{v}\}) = e^{i\pi u m_2}$ and

$$D_{\text{LD1}(u)}(\{2_{010}|0,1/2,0\}) = e^{i(\pi/2)u},$$
$$D_{\text{LD2}(u)}(\{2_{010}|0,1/2,0\}) = e^{i(\pi/2)(u+2)}, \qquad (20)$$

respectively. Here, $\mathbf{v} = (m_1, m_2, m_3) \in \mathbb{Z}^3$ is the translation vector. Note that $\text{LD1}(u)$ and $\text{LD2}(u)$ are deformed to each other as u increases by 2, so they are in the same representation class according to the third equivalence relation. Physically, this equivalence means that two magnetic structures described by the two irreps (plus their complex conjugations) can be deformed to each other by a continuous change of the spiral wave vector. Section B in Supplemental Material [36] provides more technical details regarding the application of the third equivalence relation.

E. Summary of the full classification

As detailed in Sec. II B, for each parent space group, we can construct all the O(N) (N = 3, 2, 1) representations from the irreps $\rho_{\mathbf{k}}$, where the irreps $\rho_{\mathbf{k}}$ have been exhaustively tabulated on the Bilbao Crystallographic Server [54]. Thanks to the third equivalence relation in Sec. II D, each connected region in the BZ that shares the same little group $P^{\mathbf{k}}$, e.g., high-symmetry lines, planes, or the asymmetric unit, is represented by one $\mathbf{k}$ in the region. Under the modulo of the three types of equivalence relations in Sec. II D, we obtain all the distinct SSGs. As summarized in Table II, for N = 3 (noncoplanar), 2 (coplanar), and 1 (collinear), we obtain 56 512, 9542, and 1421 SSGs,

TABLE II. The numbers of SSGs for collinear, coplanar, and noncoplanar magnetic structures. The table also shows the statistics of SSGs according to the type of momenta $\mathbf{k}$ whose irreps $\rho_{\mathbf{k}}$ constitute the O(N) representations (N = 1, 2, 3). "(0, 0, 0)" means that the representations are induced from irreps at the origin of the BZ. In the corresponding SSGs, translation operations are always accompanied with the identity spin operation. "HSP" means that the representations are induced by high-symmetry points (HSPs), some of which are not the origin of the BZ. The corresponding SSGs describe commensurate magnetic structures. "Non-HSP" means that the representations consist of irreps induced by non-HSP momenta. The corresponding SSGs can describe incommensurate magnetic structures.

Type of momenta $\mathbf{k}$	Collinear	Coplanar	Noncoplanar
(0, 0, 0)	904	3019	8505
HSP	517	5748	40262
Non-HSP	$\cdots$	775	7745
Total	1421	9542	56512

respectively. We explicitly tabulate all the SSGs in Sec. F in Supplemental Material [36].

It is worth noting that the number of collinear SSGs (1421) equals the number of MSGs of types I, III, and IV. As established in Sec. II A, we require the spin operations in a qSSG G to be either time-reversal (T) or identity (I), and, hence, G is exactly the same as a magnetic space group of type I, III, or IV. The consistency in the number of groups confirms the validity of our method based on the representation theory.

F. Nomenclature of SSGs

We label an SSG with one letter and three indices: $\alpha\mathcal{I}.\mathcal{J}.\mathcal{K}$. The prefix letter $\alpha = $ L, P, N refers to collinear, coplanar, and noncoplanar magnetic structures, respectively, for the SSG. The SSG with these three kinds of magnetic structures are defined by O(1), O(2), and O(3) representations, respectively. The first index $\mathcal{I}$, ranging from 1 to 230, specifies the parent space group. The second index $\mathcal{J}$ specifies the type of O(N) representations (Table I). For N = 1, 2, 3, $\mathcal{J}$ ranges from 1 to 2, 8, and 16, respectively. For a given parent space group and a given O(N) type, the third index $\mathcal{K}$ specifies distinct O(N) representation classes. For clarity, we always indicate the constituent irreps of the O(N) representation after the third index $\mathcal{K}$. For examples, the type-I noncoplanar SSG given by the identity representation [Fig. 4(a)] with the parent space group $P3$ (No. 143) is named N143.1.1 GM1, where GM1 refers to the identity representation; the type-III noncoplanar SSG given by the O(3) representation A1 $\oplus$ A1 $\oplus$ 1 [Fig. 4(c)] is named N143.3.1 A1 $\oplus$ A1, where the identity irrep ($\oplus$ 1) is omitted for simplicity. In the nomenclature, the identity irrep is always omitted except for the type-I SSGs. To avoid ambiguity, if several inequivalent O(N) representations correspond to the same

SSG, we consistently choose one of them, where the explicit choice for each SSG can be found in Sec. F in Supplemental Material [36]. For example, the type-V SSG shown in Fig. 4(h) is always named as N143.5.3 P1PC1 but not N143.5.3 PiPCi ($i = 2, 3$), though these representations can be transformed into each other under a coordinate transformation in real space.

It should be emphasized that SSGs with the same indices $\mathcal{I}.\mathcal{J}.\mathcal{K}$ but different prefixes α are different. For instance, the SSG N143.2.1 A1 characterizes noncoplanar magnetic structures [Fig. 4(b)], where the spin rotations assigned to the spatial operations are given by the O(3) representation A1 $\oplus$ 1 $\oplus$ 1. On the contrary, the SSG P143.2.1 A1, referred to as $\mathcal{G}$, characterizes coplanar magnetic structures [Fig. 3(e)] and has a nontrivial pure-spin-operation subgroup $\mathcal{S}$ [Eq. (5)]. In its qSSG $G \simeq \mathcal{G}/\mathcal{S}$ [Eq. (9)], spin rotations assigned to the spatial operations are given by the O(2) representation A1 $\oplus$ 1 that acts only in the x, y subspace of the spin space.

III. ELECTRONIC BAND THEORY IN SSGs

In this section, we explore SSG applications to electronic Hamiltonians. We demonstrate how symmetry algebra, characterized by projective representations, impacts the Bloch states. A generic mean-field electronic Hamiltonian in a magnetic material with negligible SOC is given by

$$\mathcal{H} = \frac{\hat{\mathbf{p}}^2}{2m} \sigma_0 + V(\mathbf{r})\sigma_0 + J\mathbf{S}(\mathbf{r}) \cdot \boldsymbol{\sigma}, \qquad (21)$$

where $\mathbf{S}(\mathbf{r})$ is the magnetic moment density at $\mathbf{r}$; $\boldsymbol{\sigma} = (\sigma_x, \sigma_y, \sigma_z)$ is the Pauli matrices for the spin-1/2 operator; J is the coupling strength between them. The Hamiltonian $\mathcal{H}$ respects the symmetry of the SSG $\mathcal{G}$, if $V(\mathbf{r})$ and $\mathbf{S}(\mathbf{r})$ are invariant under the SSG operations, i.e.,

$$V(\mathbf{r}) = V(\{R|\mathbf{v}\}^{-1}\mathbf{r}), \quad \mathbf{S}(\mathbf{r}) = s(X)U\mathbf{S}(\{R|\mathbf{v}\}^{-1}\mathbf{r}), \quad (22)$$

for any $\{XU|R|\mathbf{v}\} \in \mathcal{G}$.

A. Projective representation

The symmetry operators acting on electronic states form a *projective* representation of SSG. The adjoint representation of SU(2) group are given by SO(3) matrices: $\hat{U}(\mathbf{d} \cdot \boldsymbol{\sigma})\hat{U}^{-1} = (U\mathbf{d}) \cdot \boldsymbol{\sigma}$, where $\hat{U}$ is the SU(2) matrix corresponding to U. For a θ-rotation U along a direction $\mathbf{n}$, $\hat{U}$ can be given by either $e^{-i(\theta/2)\mathbf{n}\cdot\boldsymbol{\sigma}}$ or $-e^{-i(\theta/2)\mathbf{n}\cdot\boldsymbol{\sigma}}$. This can be regarded as a one-to-two mapping between U and $\hat{U}$. Similarly, one also has a mapping for the time-reversal operation, $\hat{X}\boldsymbol{\sigma}\hat{X}^{-1} = s(X)\boldsymbol{\sigma}$. Here, $\hat{X} = i\sigma_y\mathcal{K}$ with $\mathcal{K}$ being complex conjugate if $X = T$ and $\hat{X} = \sigma_0$ if $X = I$. In terms of $\hat{U}$ and $\hat{X}$ thus defined, a two-component fermion wave function $\psi(\mathbf{r}) = [\psi_\uparrow(\mathbf{r}), \psi_\downarrow(\mathbf{r})]^T$ is transformed under generic $g = \{X_g U_g | R_g | \mathbf{t}_g\} \in \mathcal{G}$ as

$$(\hat{g}\psi)(\mathbf{r}) \equiv \hat{X}_g \hat{U}_g \psi(\mathbf{r}'), \qquad (23)$$

where $\mathbf{r}' = R_g^{-1}(\mathbf{r} - \mathbf{t}_g)$ and $\hat{X}_g$ and $\hat{U}_g$ are obtained from X_g and U_g by the mapping, respectively. This action on the wave functions verifies that $\hat{g}\mathcal{H}\hat{g}^{-1}$ is transformed according to the right-hand sides of Eq. (22). As the mapping from U to $\hat{U}$ is one to two, we should specify an (arbitrarily chosen) sign of $\hat{g} \equiv \hat{X}_g \hat{U}_g$ for every g. One can verify that, for $g_1 g_2 = g_3$, we have

$$\hat{g}_1 \hat{g}_2 = \omega_2(g_1, g_2)\hat{g}_3, \qquad (24)$$

where $\omega_2(g_1, g_2)$ is referred to as the *factor system* of the projective representation. For example, if we choose $\hat{U}_{g_i} = e^{-i(\theta_i/2)\mathbf{n}_i \cdot \boldsymbol{\sigma}}$ for all $g_{1,2,3}$, where $\mathbf{n}_i$ and θ_i are the rotation axis and angle of U_{g_i}, respectively, then $\omega_2(g_1, g_2)$ can be determined as $e^{-i(\theta_3/2)\mathbf{n}_3 \cdot \boldsymbol{\sigma}}e^{i(\theta_2/2)\mathbf{n}_2 \cdot \boldsymbol{\sigma}}e^{i(\theta_1/2)\mathbf{n}_1 \cdot \boldsymbol{\sigma}}\hat{X}_{g_3}\hat{X}_{g_2}^{-1}\hat{X}_{g_1}^{-1} = \pm 1$.

A different choice of the signs of $\hat{U}_g$ yields an equivalent factor system. In general, we can further assign an additional U(1) factor for each $\hat{g}$ without changing the algebra of the symmetry group. By a change of $\hat{g}_i$ in Eq. (24) into $e^{i\alpha_i}\hat{g}_i$, the factor system transforms to

$$\omega_2(g_1, g_2) \rightarrow e^{i(\alpha_1 + \zeta\alpha_2 - \alpha_3)}\omega_2(g_1, g_2), \qquad (25)$$

where $\zeta = 1$ (-1) if g_1 is unitary (antiunitary). Two factor systems related by such a U(1) gauge transformation are considered to be equivalent. For each SSG, we can determine its unique factor system based on the spin operations $\hat{g} \equiv \hat{X}_g \hat{U}_g$ and study the electronic band theory under the determined factor system. On the other hand, noncollinear SSGs are isomorphic to MSGs (see Sec. III C), and two distinct SSGs isomorphic to the same MSG $\mathcal{M}$ might realize its inequivalent factor systems.

In a conventional MSG, the SOC term being invariant requires that $U_g \equiv \det(R_g)R_g$. Thus, $\hat{g}$'s also form a projective representation of the parent space group, which is usually referred to as the double magnetic space group. A crucial feature of SSG is that the factor system can be inequivalent to those of MSGs, because, in the absence of SOC, U_g can be different from $\det(R_g)R_g$ and, hence, give different signs to ω_2. In the following, we present an example of ω_2 that cannot be realized in MSGs.

Let us consider the SSG N143.16.1 M1 [Fig. 4(o)]. The transformation of the magnetic moments under lattice translation $\{1|m_1, m_2, m_3\}$ is given by Eq. (14). Specifically, the lattice translation $t_3 = \{1|0, 0, 1\}$ is associated with an identity spin operation, while $t_1 = \{1|1, 0, 0\}$, $t_2 = \{1|0, 1, 0\}$, and $t_{12} = \{1|1, 1, 0\}$ should be accompanied by π spin rotation along the y, x, and z directions, respectively. We can choose the corresponding SU(2) spin rotation matrices of t_1, t_2, and t_{12} as $\hat{U}_{t_1} = i\sigma_y$,

$\hat{U}_{t_2} = i\sigma_x$, and $\hat{U}_{t_{12}} = i\sigma_z$, respectively. Then, it is direct to verify that

$$\hat{t}_1\hat{t}_2 = -\hat{t}_2\hat{t}_1 = \hat{t}_{12}. \tag{26}$$

The translation operators $\hat{t}_{1,2}$ anticommute with each other as if they were magnetic translations encompassing a plaquette with π flux. As discussed in the next subsection, such translation operators lead to a noncommuting BZ. This feature is unique to SSG and can never be realized in conventional space groups or MSGs.

B. Collinear SSGs

The representation theory of Bloch states in collinear SSGs is simpler than that in generic noncollinear SSGs. We show in this subsection that they are effectively described by *single-valued gray* space groups. In our construction, the spin operations in a collinear qSSG G are either I or T, and operations with identity spin operation (I) form a subgroup G_0. For type-I SSGs that are described by the identity representation of the parent space group P, $G = G_0$, and a collinear SSG $\mathcal{G}$ satisfies that [Eq. (7)]

$$\mathcal{G} = G_0 \times [\mathcal{S}_{Z_2^T} \ltimes \mathcal{S}_{U(1)}]. \tag{27}$$

For type-II SSGs that are described by nontrivial O(1) representations of P, $|G_0| = 1/2|G|$, and $\mathcal{G}$ can be decomposed as [Eq. (7)]

$$\mathcal{G} = (G_0 + hG_0) \times [\mathcal{S}_{Z_2^T} \ltimes \mathcal{S}_{U(1)}], \tag{28}$$

where $h \in (G - G_0)$ is a spatial operation accompanied by T; $\mathcal{S}_{Z_2^T}$ is a Z_2 group generated by $TU_x(\pi)$; and $\mathcal{S}_{U(1)}$ is the continuous spin-rotation (along the z direction) group. $\mathcal{S}_{U(1)}$ allows the block diagonalization of the electronic Hamiltonian $\mathcal{H}$ into spin-up ($\mathcal{H}_\uparrow$) and spin-down ($\mathcal{H}_\downarrow$) sectors. In both types of collinear SSGs, the little group of both $\mathcal{H}_\uparrow$ and $\mathcal{H}_\downarrow$ is $G_0 \times [\mathcal{S}_{Z_2^T} \ltimes \mathcal{S}_{U(1)}]$. The band structure of $\mathcal{H}_\uparrow$ or $\mathcal{H}_\downarrow$ is fully characterized by the discrete subgroup $G_0 \times \mathcal{S}_{Z_2^T}$, because the action of $\mathcal{S}_{U(1)}$ on different states in a given spin sector is the same and proportional to an identity matrix. As G_0 consists of only spatial operations with identity spin operation, the factor system of G_0 is trivial, i.e., $\omega_2(g_1, g_2) = 1$ ($\forall\ g_{1,2} \in G_0$). $\mathcal{S}_{Z_2^T}$ is generated by $-i\sigma_x i\sigma_y \mathcal{K} = i\sigma_z \mathcal{K}$—a time-reversal operator (acting on fermions) that squares to 1, and operations in G_0 and $\mathcal{S}_{Z_2^T}$ commute. These imply that electronic bands in each spin sector respect a single-valued gray group $G_0 \times \mathcal{S}_{Z_2^T}$ as if $\mathcal{H}_\uparrow$ and $\mathcal{H}_\downarrow$ were in a nonmagnetic material belonging to the space group G_0.

The SSG of a material uniquely determines whether its electronic bands are spin split. In a type-I collinear SSG [Eq. (27)], net spin polarization is allowed, and the spin splitting is generally nonzero. In a type-II collinear SSG [Eq. (28)], operations in $hG_0 \times \mathcal{S}_{Z_2^T}$ flip the spin. If hG_0 contains an inversion operation combined with time reversal ($\mathcal{PT}$ operation), this spin-flipping and momentum-preserving operation implies $E_{n\uparrow}(\mathbf{k}) = E_{n\downarrow}(\mathbf{k})$. Here, $E_{ns}(\mathbf{k})$ is the nth energy band in the s-spin sector. If hG_0 contains a translation followed by time reversal, this spin-flipping and momentum-flipping operation implies $E_{n\uparrow}(\mathbf{k}) = E_{n\downarrow}(-\mathbf{k}) = E_{n\downarrow}(\mathbf{k})$, where the second equation is due to the $\mathcal{S}_{Z_2^T}$ symmetry. Therefore, spin splitting is forbidden at every momentum for materials where the spin-up and spin-down atoms are related by inversion or translation [25]. Other types of spin-flipping operations—i.e., rotation, mirror, screw, and glide—allow spin splittings at a generic momentum. In Sec. III D, we discuss the symmetry of the spin texture of electronic bands in more detail.

C. Noncollinear SSGs

Coplanar or noncoplanar SSGs do not have spin U(1) symmetry, and, hence, it is necessary to analyze the symmetries of the total Hamiltonian $\mathcal{H}$. A coplanar SSG $\mathcal{G} = G \times \mathcal{S}_{Z_2^T}$ [Eq. (9)] is a discrete group. Here, G is the unitary qSSG that is isomorphic to a space group, and $\mathcal{S}_{Z_2^T}$ [Eq. (5)] is a Z_2 group generated by $TU_z(\pi)$. Thus, it is isomorphic to a gray space group (or type-II MSG). In a noncoplanar SSG, each spatial operation corresponds to a unique spin operation. Consequently, a noncoplanar SSG is a discrete group and is isomorphic to a type-I, -III, or -IV MSG, where antiunitary (unitary) operations in an SSG are mapped to antiunitary (unitary) ones in the MSG. As explained in Sec. III A, when the symmetry operations $g \in \mathcal{G}$ act on the fermionic degrees of freedom, they form a projective representation of $\mathcal{G}$ or, isomorphically, a projective representation of $\mathcal{M}$. Thus, the algebra of the symmetry operators $\hat{g}$ in a noncollinear SSG is fully characterized by the factor system ω_2 that belongs to the second cohomology group

$$\omega_2 \in H^2[\mathcal{M}, \text{U}(1)]. \tag{29}$$

Enumerating all irreps of $\mathcal{M}$ with inequivalent ω_2's that can be realized by SSGs completes the representation theory of SSGs, which is beyond the scope of the current work, and we leave it for future studies.

In the following, we investigate a generalization of Bloch states in noncollinear SSGs. Let us consider the unitary translation subgroup T_U of the SSG $\mathcal{G}$:

$$T_U = \{\{U|1|\mathbf{v}\}|\{U|1|\mathbf{v}\} \in \mathcal{G}, \det U = 1\}. \tag{30}$$

The generators of T_U are joint operations of spin rotations and translations:

$$t_i = \{U_{t_i}|1|\mathbf{a}_i\} \quad (i = 1, 2, 3), \tag{31}$$

where $\boldsymbol{a}_i$ are primitive lattice vectors and $U_i \in SO(3)$. It is noteworthy that $U_{t_i} U_{t_j} = U_{t_j} U_{t_i}$, since both must equal the spin rotation associated with the spatial translation $\{1|\boldsymbol{a}_i + \boldsymbol{a}_j\}$, which is unique by definition. The corresponding translation operators acting on fermion wave functions can be written as

$$\hat{t}_i = \{\hat{U}_{t_i}|1|\boldsymbol{a}_i\} \quad (i = 1, 2, 3) \tag{32}$$

with $\hat{U}_{t_i}$ being the SU(2) representation matrix (with an arbitrarily chosen sign as explained in Sec. III A) of the SO(3) rotation U_i. As SU(2) is a double covering of SO(3), even though $\hat{U}_{t_i} \hat{U}_{t_j}$ and $\hat{U}_{t_j} \hat{U}_{t_i}$ correspond to the same SO(3) rotation, they may differ by a minus sign, i.e., $\hat{U}_{t_i} \hat{U}_{t_j} = \zeta \hat{U}_{t_j} \hat{U}_{t_i}$ with $\zeta = \pm 1$. Therefore, in contrast to ordinary MSGs, the translation generators $\hat{t}_i$ in a noncollinear SSG—when acting on fermions—do not necessarily commute with each other. In general, there is $\hat{t}_i \hat{t}_j = \zeta \hat{t}_j \hat{t}_i$, with $\zeta = \hat{U}_{t_i} \hat{U}_{t_j} \hat{U}_{t_i}^\dagger \hat{U}_{t_j}^\dagger$.

1. Symmorphic and nonsymmorphic SBZ

When $[\hat{t}_i, \hat{t}_j] = 0$ $(i, j = 1, 2, 3)$, eigenstates of $\mathcal{H}$ follow the Bloch theorem—they are common eigenstates of $\mathcal{H}$ and $\hat{t}_{1,2,3}$. To be specific, a common eigenstate $|\psi(\tilde{\boldsymbol{k}})\rangle$ with wave vector $\tilde{\boldsymbol{k}}$ satisfies

$$\hat{t}_i|\psi(\tilde{\boldsymbol{k}})\rangle = e^{i\tilde{k}_i}|\psi(\tilde{\boldsymbol{k}})\rangle \quad (i = 1, 2, 3), \tag{33}$$

where $\tilde{\boldsymbol{k}} = (1/2\pi)\sum_i \tilde{k}_i \boldsymbol{b}_i$, $\tilde{k}_i = \tilde{\boldsymbol{k}} \cdot \boldsymbol{a}_i \in [0, 2\pi)$, and $\boldsymbol{b}_i$'s are the reciprocal lattice vectors, with $\boldsymbol{a}_i \cdot \boldsymbol{b}_j = 2\pi\delta_{ij}$. Hereafter, we refer to $\tilde{\boldsymbol{k}}$ as the *SSG momentum* and refer to $|\psi(\tilde{\boldsymbol{k}})\rangle$ as the *SSG Bloch state*. The SSG momentum $\tilde{\boldsymbol{k}}$ and SSG Bloch state $|\psi(\tilde{\boldsymbol{k}})\rangle$ are different from crystal momentum $\boldsymbol{k}$ and traditional Bloch state $|\psi(\boldsymbol{k})\rangle$. The latter pair is defined as the common eigenstate and eigenvalues of pure spatial translations [Eq. (17)]. Note that, to distinguish SSG momentum $\tilde{\boldsymbol{k}}$ from crystal momentum $\boldsymbol{k}$, we adopt different notations. If all $\hat{t}_i$'s are pure translations, SSG and crystal momenta coincide; we use $\boldsymbol{k}$ to denote both. We refer to the reciprocal space formed by the SSG momenta as the SSG Brillouin zone (SBZ) to distinguish it from the magnetic BZ formed by the crystal momenta. SBZ is expanded by $\boldsymbol{b}_i$ $(i = 1, 2, 3)$, while the magnetic BZ is a fraction of SBZ (see an example in the last of this subsection) unless all $\hat{t}_i$'s are pure translations.

An SSG momentum $\tilde{\boldsymbol{k}}$ may transform *nonsymmorphically* under SSG symmetry operations, i.e., $\nexists \tilde{\boldsymbol{k}} \in$ SBZ that is invariant under all the SSG symmetries, which is crucially different from a crystal momentum $\boldsymbol{k}$. To see this, we consider the conjugate operation of $\hat{t}_i = \{\hat{U}_{t_i}|1|\boldsymbol{a}_i\}$ under a generic SSG operation $\hat{g} = \{\hat{X}_g \hat{U}_g | R_g | \boldsymbol{v}_g\}$:

$$\hat{g}^{-1}\hat{t}_i\hat{g} = e^{i2\pi\tilde{q}_i(g)}\widehat{g^{-1}t_i g}, \tag{34}$$

where $\tilde{q}_i(g)$ is determined by

$$\hat{U}_g^{-1}\hat{X}_g^{-1}\hat{U}_{t_i}\hat{X}_g\hat{U}_g = e^{i2\pi\tilde{q}_i(g)}\hat{U}_{R_g^{-1}\boldsymbol{a}_i}. \tag{35}$$

Here, $\hat{U}_{R_g^{-1}\boldsymbol{a}_i}$ denotes the SU(2) spin rotation matrix for $\{1|R_g^{-1}\boldsymbol{a}_i\}$ and should be chosen consistently with $\hat{U}_{t_i}$: $\hat{U}_{R_g^{-1}\boldsymbol{a}_i} = \prod_{i=1}^3 \hat{U}_{t_i}^{m_i}$ if $R_g^{-1}\boldsymbol{a}_i = \sum_i^3 m_i\boldsymbol{a}_i$. One can directly verify that $\hat{g}|\psi(\tilde{\boldsymbol{k}})\rangle$ is an eigenstate of $\hat{t}_i$ with the eigenvalue $e^{is_g[R_g\tilde{\boldsymbol{k}}\cdot\boldsymbol{a}_i + \tilde{q}_i(g)]}$, where $s_g = 1$ (-1) for unitary (antiunitary) g. Hence, the SSG momentum $\tilde{\boldsymbol{k}}$ is transformed into $s_g(R_g\tilde{\boldsymbol{k}} + \tilde{\boldsymbol{q}}_g)$ by $\hat{g}$, with $\tilde{\boldsymbol{q}}_g = \sum_i \tilde{q}_i(g)\boldsymbol{b}_i$. In a generic SSG with a nontrivial factor system, $\tilde{\boldsymbol{q}}_g$ is *not* necessarily a reciprocal lattice vector, where $\hat{g}$ acts as a screw or glide on the SSG momentum. On the other hand, $2\tilde{\boldsymbol{q}}$ must be a reciprocal lattice vector, because $\hat{U}_g$ are SU(2) matrices, requiring $e^{i2\pi\tilde{q}_i(g)} = \pm 1$.

Because of an arbitrary choice of the origin of the SBZ, a fractional $\tilde{\boldsymbol{q}}_g$ does not necessarily mean the nonsymmorphic action of g in the SBZ. Some fractional $\tilde{\boldsymbol{q}}_g$'s can be made to zero or the reciprocal lattice vectors by a gauge transformation of $\hat{t}_i$. Let us consider the gauge transformation $\hat{t}_i \to e^{i2\pi\theta_i}\hat{t}_i$ that shifts the SSG momentum $\tilde{\boldsymbol{k}}$ to $\tilde{\boldsymbol{k}}' = \tilde{\boldsymbol{k}} + \boldsymbol{\theta}$, where $\boldsymbol{\theta} = \sum_{i=1}^3 \theta_i\boldsymbol{b}_i$. Owing to the flexibility in selecting the origin, $e^{i2\pi\theta_i}$ is not limited to ± 1 but can be a generic U(1)-valued complex number. This extension also facilitates the transformation process between SSG momentum and crystal momentum (see the discussions in the context of the band of $CoSO_4$ in Sec. IV B). The shifted SSG momentum $\tilde{\boldsymbol{k}}'$ is transformed by $\hat{g}$ into $s_gR_g(\tilde{\boldsymbol{k}}' - \boldsymbol{\theta}) + s_g\tilde{\boldsymbol{q}}_g + \boldsymbol{\theta}$. Hence, the fractional momentum transfer $\tilde{\boldsymbol{q}}_g$ becomes $\tilde{\boldsymbol{q}}_g + s_g\boldsymbol{\theta} - R_g\boldsymbol{\theta}$ in the shifted SBZ. If there exists such a gauge $\boldsymbol{\theta}$ satisfying

$$-s_g\boldsymbol{\theta} + R_g\boldsymbol{\theta} \equiv \tilde{\boldsymbol{q}}_g \quad \forall\, g \in \mathcal{G}, \tag{36}$$

for all $g \in \mathcal{G}$, all the transfer $\tilde{\boldsymbol{q}}_g$ can be eliminated by the gauge transformation. Here, the symbol "$\equiv$" means that SSG momenta on the left-hand and right-hand sides differ only by a reciprocal lattice vector. If there exists no such $\boldsymbol{\theta}$ that satisfies Eq. (36) for all g, the SBZ is nonsymmorphic. For each SSG listed in Tables S1–S690 in Supplemental Material [36], we identify whether its SBZ is symmorphic or nonsymmorphic, using an automatic algorithm detailed in Sec. C in Supplemental Material [36].

Here, we use two SSGs with the same parent space group $P\bar{1}$ (No. 2) to illustrate the symmorphic and nonsymmorphic SBZs, respectively. $P\bar{1}$ is generated by translations $\{1|\boldsymbol{a}_i\}$ $(i = 1, 2, 3)$, with a_i being lattice vectors, and the inversion $\{\bar{1}|0\}$. Let us first consider a coplanar SSG, P2.3.4 R1$^+$ $\oplus$ R1$^-$, which is induced from the even (R1$^+$) and odd (R1$^-$) irreps at the TRS-invariant momentum R (π, π, π). Following the argument in Sec. II C, we can

obtain the generators of this SSG: translations $t_i = \{U_z(\pi)|1|\boldsymbol{a}_i\}$, the inversion $\mathcal{P} = \{U_y(\pi)|\bar{1}|\boldsymbol{0}\}$, and an effective time reversal $\mathcal{T} = \{TU_z(\pi)|I|\boldsymbol{0}\}$, which is the generator of the pure-spin-operation group $\mathcal{S}_{Z_2^T}$ for coplanar structures [Eq. (5)]. We can choose $\hat{U}_{t_i} = i\sigma_z$, $\hat{X}_{\mathcal{T}}\hat{U}_{\mathcal{T}} = i\sigma_x\mathcal{K}$, and $\hat{U}_{\mathcal{P}} = i\sigma_y$. Using Eq. (35), we find that $\tilde{\boldsymbol{q}}_{\mathcal{T}} = \tilde{\boldsymbol{q}}_{\mathcal{P}} = \tilde{\boldsymbol{q}}_{\mathcal{PT}} = \boldsymbol{0}$, and, hence, its SBZ is symmorphic. On the other hand, another coplanar SSG with $P\bar{1}$, P2.3.2GM1$^-$ ⊕ R1$^+$, gives an example of nonsymmorphic SBZ. It is generated by $t_i = \{U_x(\pi)|1|\boldsymbol{a}_i\}$, and the same $\mathcal{P}$ and $\mathcal{T}$ as in P2.3.4 R1$^+$ ⊕ R1$^-$. We choose $\hat{U}_{t_i} = i\sigma_x$, $\hat{X}_{\mathcal{T}}\hat{U}_{\mathcal{T}} = i\sigma_x\mathcal{K}$, and $\hat{U}_{\mathcal{P}} = i\sigma_y$ and find that $\tilde{\boldsymbol{q}}_{\mathcal{P}} = \boldsymbol{0}$ and $\tilde{\boldsymbol{q}}_{\mathcal{T}} = \tilde{\boldsymbol{q}}_{\mathcal{PT}} = \frac{1}{2}(\boldsymbol{b}_1 + \boldsymbol{b}_2 + \boldsymbol{b}_3)$ in P2.3.2 GM1$^-$ ⊕ R1$^+$. Although we can gauge eliminate $\tilde{\boldsymbol{q}}_{\mathcal{T}}$ by shifting the origin of SBZ, the action of $\hat{\mathcal{P}}\hat{\mathcal{T}}$ on SSG momenta always induces the fractional translation, irrespective of the choice of origin. The SBZ of P2.3.2 GM1$^-$ ⊕ R1$^+$ is, hence, nonsymmorphic. We compare the SBZs of the two SSGs in Figs. 5(a) and 5(b). As shown in Fig. 5(b), in the nonsymmorphic SBZ, TRS-invariant and inversion-invariant momenta do not coincide, and no momenta have the $\hat{\mathcal{P}}\hat{\mathcal{T}}$ symmetry.

A nonsymmorphic SBZ generally leads to extra degeneracy of energy bands in the magnetic BZ. In the following, we compare a description of electron bands by the SSG
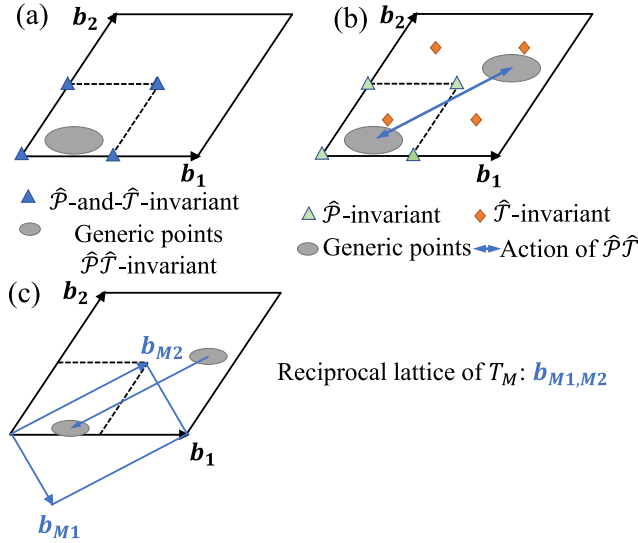

(a) $\boldsymbol{b}_2$ (b) $\boldsymbol{b}_2$

$\boldsymbol{b}_1$ $\boldsymbol{b}_1$

▲ $\hat{\mathcal{P}}$-and-$\hat{\mathcal{T}}$-invariant   △ $\hat{\mathcal{P}}$-invariant   ◆ $\hat{\mathcal{T}}$-invariant
⬭ Generic points   ⬭ Generic points ◄► Action of $\hat{\mathcal{P}}\hat{\mathcal{T}}$
   $\hat{\mathcal{P}}\hat{\mathcal{T}}$-invariant

(c) $\boldsymbol{b}_2$

$\boldsymbol{b}_{M2}$ Reciprocal lattice of T_M: $\boldsymbol{b}_{M1,M2}$

$\boldsymbol{b}_1$

$\boldsymbol{b}_{M1}$

FIG. 5. SSG Brillouin zone (SBZ) subtended by the reciprocal basis $\boldsymbol{b}_i$ ($i = 1, 2, 3$). For the clarity of demonstration, the 3D SBZ is projected into $\boldsymbol{b}_1, \boldsymbol{b}_2$ plane. (a) SBZ of SSG P2.3.3 R1$^+$ ⊕ R1$^+$ is symmorphic, and (b) SBZ P2.3.2GM1$^-$ ⊕ R1$^+$ is nonsymmorphic. Symmetries of SSG momenta are demonstrated by $\mathcal{P}$- and $\mathcal{T}$-invariant SSG momentum points in the SBZs. (c) The SBZ (region enclosed by black vectors) and magnetic BZ (region enclosed by blue vectors) of SSG P2.3.2GM1$^-$ ⊕ R1$^+$. Two grey regions that are related by $\hat{\mathcal{P}}\hat{\mathcal{T}}$ symmetry are inequivalent in the SBZ but are equivalent in the magnetic BZ.

momentum with the traditional description by the crystal momentum. Crystal momentum is related to the pure-translation subgroup T_M of the SSG $\mathcal{G}$ [Eq. (17)]. T_M is an invariant subgroup of the SSG $\mathcal{G}$ and a subgroup of T_U [Eq. (30)]. Therefore, an SSG Bloch state defined in Eq. (33) is also a common eigenstate of operations in T_M. In SSGs with nonsymmorphic SBZ, $|T_M|$ is a fraction of $|T_U|$. This implies that the first BZ for the crystal momentum is smaller than that for the SSG momentum (SBZ). The energy bands in the first BZ can be obtained by folding those in the SBZ. To be concrete, let us consider the example of P2.3.2GM1$^-$ ⊕ R1$^+$. T_M of this SSG can be generated by $\{I|1|\boldsymbol{a}_{Mi}\}$ ($i = 1, 2, 3$) with $\boldsymbol{a}_{M1} = \boldsymbol{a}_1 - \boldsymbol{a}_2$, $\boldsymbol{a}_{M2} = \boldsymbol{a}_1 + \boldsymbol{a}_2$, and $\boldsymbol{a}_{M3} = \boldsymbol{a}_2 + \boldsymbol{a}_3$, because $[U_x(\pi)]^2 = 1$. Their reciprocal lattice vectors are given as $\boldsymbol{b}_{M1} = \frac{1}{2}(\boldsymbol{b}_1 - \boldsymbol{b}_2 + \boldsymbol{b}_3)$, $\boldsymbol{b}_{M2} = \frac{1}{2}(\boldsymbol{b}_1 + \boldsymbol{b}_2 - \boldsymbol{b}_3)$, and $\boldsymbol{b}_{M3} = \boldsymbol{b}_3$. The volume enclosed by $\boldsymbol{b}_{Mi}$'s is half of that enclosed by $\boldsymbol{b}_i$'s. As shown before, $\hat{\mathcal{P}}\hat{\mathcal{T}}$ in this SSG transforms an SSG momentum $\tilde{\boldsymbol{k}}$ to $\tilde{\boldsymbol{k}} + \tilde{\boldsymbol{q}}_{\mathcal{PT}}$, indicating that the two corresponding SSG Bloch states share the same energy. Meanwhile, $\tilde{\boldsymbol{q}}_{\mathcal{PT}} = \boldsymbol{b}_{M2} + \boldsymbol{b}_{M3}$. Thus, if we fold the SBZ to the first BZ, these two SSG momenta are considered equivalent [Fig. 5(c)], and the energy bands shown in the magnetic BZ are at least double degenerate at every momentum. A similar analysis can be successfully applied to explanations of extra degeneracy in the energy bands of CuSO$_4$ obtained from the first-principle calculation (see Sec. IV B).

2. Noncommuting SBZ

Suppose that the electronic Hamiltonian $\mathcal{H}$ respects both $\hat{t}_{1,2}$, while $\hat{t}_1$ and $\hat{t}_2$ anticommute: $\{\hat{t}_1, \hat{t}_2\} = 0$. Then, eigenstates of $\mathcal{H}$ cannot be labeled by eigenvalues of $\hat{t}_{1,2}$ simultaneously, because $\hat{t}_1$ and $\hat{t}_2$ do not share a common set of eigenstates. In this case, the SBZ possesses a *noncommuting* nature (noncommuting SBZ). In this section, we use SSG N143.16.1 M1 [Fig. 4(o)] as an example to demonstrate several exotic features of the noncommuting SBZ.

As discussed in Sec. III A, in SSG N143.16.1 M1, $\{\hat{t}_1, \hat{t}_2\} = 0$ and $[\hat{t}_{1,2}, \hat{t}_3] = 0$. We can define SSG Bloch states in terms of the eigenvalues of the commuting operators $\hat{t}_1, \hat{t}_2^2$, and $\hat{t}_3$ and introduce a folded SBZ spanned by $\boldsymbol{b}_1, \frac{1}{2}\boldsymbol{b}_2$, and $\boldsymbol{b}_3$. The SSG Bloch state satisfies

$$\hat{t}_{1,3}|\psi(\tilde{\boldsymbol{k}})\rangle = e^{i\tilde{k}_{1,3}}|\psi(\tilde{\boldsymbol{k}})\rangle, \qquad \hat{t}_2^2|\psi(\tilde{\boldsymbol{k}})\rangle = e^{i\tilde{k}_2}|\psi(\tilde{\boldsymbol{k}})\rangle, \quad (37)$$

where $\tilde{\boldsymbol{k}} = \frac{1}{2\pi}(\tilde{k}_1\boldsymbol{b}_1 + \tilde{k}_2\frac{1}{2}\boldsymbol{b}_2 + \tilde{k}_3\boldsymbol{b}_3)$, with $\tilde{k}_{1,3} = \tilde{\boldsymbol{k}} \cdot \boldsymbol{a}_{1,3} \in [0, 2\pi)$ and $\tilde{k}_2 = 2\tilde{\boldsymbol{k}} \cdot \boldsymbol{a}_2 \in [0, 2\pi)$. The anticommutation $\{\hat{t}_1, \hat{t}_2\} = 0$ implies extra degeneracy in the folded SBZ. Suppose $|\psi(\tilde{\boldsymbol{k}})\rangle$ is an eigenstate with an energy $E(\tilde{\boldsymbol{k}})$. We construct the state $\hat{t}_2|\psi(\tilde{\boldsymbol{k}})\rangle$. As $\hat{t}_2$ commutes with $\mathcal{H}$, $\hat{t}_2|\psi(\tilde{\boldsymbol{k}})\rangle$ has the same energy. As $\{\hat{t}_1, \hat{t}_2\} = 0$, there is

$\hat{t}_1 \hat{t}_2 |\psi(\tilde{k})\rangle = -\hat{t}_2 \hat{t}_1 |\psi(\tilde{k})\rangle = e^{i[\tilde{k}+(1/2)b_1]\cdot a_1} \hat{t}_2 |\psi(\tilde{k})\rangle$. In other words, $\hat{t}_2 |\psi(\tilde{k})\rangle$ is an eigenstate with energy $E(\tilde{k})$ and the SSG momentum $\tilde{k} + \frac{1}{2}b_1$. Therefore, the energy bands at $\tilde{k}$ are always identical to those at $\tilde{k} + \frac{1}{2}b_1$. This degeneracy is well known in π-flux models. Unlike the π-flux models, the electron Hamiltonian [Eq. (21)] has no external magnetic field, and the degeneracy emerges from the noncollinear magnetism. Since $\hat{t}_2$ rotates spin along the x direction, the degenerate states at $\tilde{k}$ and $\tilde{k} + \frac{1}{2}b_1$ have opposite spin expectation values in the y, z plane.

The shape of the SBZ is C_{3z} asymmetric: $\frac{1}{2}b_2$ is a reciprocal lattice vector in the reduced SBZ, but $R_z(2\pi/3)\frac{1}{2}b_1 = -\frac{1}{2}(b_1 + b_2)$ is not, where $R_z(2\pi/3)$ denotes $2\pi/3$ rotation along the z axis. However, counterintuitively, the C_{3z} symmetry is preserved, leading to extra degeneracies. We find that while $\hat{C}_{3z}|\psi(\tilde{k})\rangle$ is not an SSG Bloch state, $\hat{C}_{3z}|\phi_+\rangle$ $(\hat{C}_{3z}|\phi_-\rangle)$ is an SSG Bloch state with energy $E(\tilde{k})$ and SSG momentum $R_z(2\pi/3)\tilde{k}$ $(R_z(2\pi/3)\tilde{k} + \frac{1}{2}b_1)$, where $|\phi_\pm\rangle$'s are properly chosen linear combinations of $|\psi(\tilde{k})\rangle$ and $\hat{t}_2 |\psi(\tilde{k})\rangle$. Note that $\hat{C}_{3z}|\phi_\pm\rangle$ are also related by $\hat{t}_2$. The details of derivation can be found in Sec. C in Supplemental Material [36], and a gauge transformation on $\hat{t}_{1,2}$ is applied to simplify the expression of the transformation. Simply speaking, $\hat{C}_{3z}$ does not transform a single SSG momentum to another one but transforms a pair to another, requiring bands at these C_{3z}-related pairs to share the same energy.

D. Spin texture in the momentum space

In this subsection, we study symmetries of spin texture $\tilde{S}(\tilde{k})$ in a certain equal-energy surface (e.g., Fermi surface) in the SBZ. Here, $\tilde{S}(\tilde{k})$ is an expectation value of the spin operator with respect to an SSG Bloch state at $\tilde{k}$. In the presence of energy degeneracy at $\tilde{k}$, $\tilde{S}(\tilde{k})$ is a sum of the spin expectation values of the degenerate SSG Bloch states. SSGs completely determine whether a nonzero spin texture $\tilde{S}(\tilde{k})$ is allowed and how it transforms under symmetries. We first consider $\tilde{S}(\tilde{k})$ in those SSGs where unitary translation generators $\hat{t}_{1,2,3}$ all commute with each other. An SSG momentum $\tilde{k}$ transforms into $s_g(R_g\tilde{k} + \tilde{q}_g)$ under an SSG operation $g = \{X_g U_g | R_g | v_g\}$, where $s_g = 1$ (−1) for $X_g = I$ (T). Meanwhile, the spin expectation transforms according to $X_g U_g$. Hence, $\tilde{S}(\tilde{k})$ satisfies the symmetry constraint

$$\tilde{S}\left(s_g(R_g\tilde{k} + \tilde{q}_g)\right) = s_g U_g \tilde{S}(\tilde{k}). \qquad (38)$$

We use symmetries that leave generic $\tilde{k} \in$ SBZ invariant to determine the dimension d_{SBZ} of the symmetry-allowed span of $\tilde{S}(\tilde{k})$ in the momentum space. d_{SBZ} represents

noncoplanar ($d_{\text{SBZ}} = 3$), coplanar ($d_{\text{SBZ}} = 2$), or collinear ($d_{\text{SBZ}} = 1$) distribution of $\tilde{S}(\tilde{k})$ in the SSG momentum space; $d_{\text{SBZ}} = 0$ means $\tilde{S}(\tilde{k}) \equiv 0$. The relevant symmetries are the spin-U(1) rotation (in collinear SSGs), spin-rotation translations, and space-time inversion ($\mathcal{PT}$) with spin rotation. For collinear SSGs, $d_{\text{SBZ}} \le 1$ due to the spin-U(1) symmetry. As discussed in Sec. III B, $d_{\text{SBZ}} = 0$ if the spin-up and spin-down atoms in real space are related by $\mathcal{PT}$ operation or translation followed by time reversal, and $d_{\text{SBZ}} = 1$ otherwise (ferromagnetism or altermagnetism). For noncollinear SSGs, symmetries leaving each $\tilde{k}$ invariant can be only unitary translations, generated by $\hat{t}_{1,2,3}$, and spin-rotation $\mathcal{PT}$ operation, denoted as $\hat{\mathcal{P}}\hat{\mathcal{T}}$. If $\hat{\mathcal{P}}\hat{\mathcal{T}}$ is present and $\tilde{q}_{\mathcal{PT}} = 0$, d_{SBZ} is given by the dimension of a subspace in the spin space satisfying Eq. (38), i.e., $d_{\text{SBZ}} = \dim[\cap_{i=1}^3 \ker(U_{t_i} - I) \cap \ker(U_{\mathcal{PT}} + I)]$. Otherwise, $d_{\text{SBZ}} = \dim[\cap_{i=1}^3 \ker(U_{t_i} - I)]$.

The group structure of the little group of generic SSG momenta gives certain constraints on the forms of U_{t_i}, $U_{\mathcal{PT}}$, and their relationship, which allows us to obtain d_{SBZ} with a simple rule as summarized in Table III. First, we consider cases without $\mathcal{PT}$ symmetry. If all U_{t_i}'s equal the identity I, no constraint exists and $d_{\text{SBZ}} = 3$. If some of them do not equal I, to satisfy $[\hat{t}_i, \hat{t}_j] = 0$, they must share a same rotation axis, leading to $d_{\text{SBZ}} = 1$, $\tilde{S}(\tilde{k})$ is nonzero along the rotation axis (see Sec. C in Supplemental Material [36]). Next, we consider the case with $\mathcal{PT}$ symmetry and $U_{t_i} = I$ ($i = 1, 2, 3$), implying that $\tilde{q}_{\mathcal{PT}} = 0$. Since the square of $\mathcal{PT}$ operation should be the identity, $U_{\mathcal{PT}}^2 = I$, and $U_{\mathcal{PT}}$ can be either I or a π rotation $U_m(\pi)$, which lead to $d_{\text{SBZ}} = 0$ and 2, respectively. When both $\mathcal{PT}$ symmetry and a nontrivial U_{t_i} are present, d_{SBZ} apparently depends on whether $\tilde{q}_{\mathcal{PT}}$ is zero or not. Interestingly, in Sec. C in Supplemental Material [36], we find that d_{SBZ} is always 1 if there exists a $U_{t_i} \ne I$ independent of the form of $\mathcal{PT}$.

Notably, d_{SBZ} does not necessarily coincide with the dimension N of the span of magnetic moments $S(r)$ in

TABLE III. The dimensions d_{SBZ} (d_{BZ}) of the span of spin texture $\tilde{S}(\tilde{k})$ [$\vec{S}(k)$] in the SBZ (BZ) of noncollinear SSGs. Columns and rows specify spin rotations that accompany translations (t_i) and space-time reversal $\mathcal{PT}$, respectively. $\{U_{t_i}\} = \{U_n(\theta_i)\}$ means that all the translations are accompanied by spin rotations along the same axis n by θ_i ($i = 1, 2, 3$), and at least one θ_i is nonzero.

$U_{\mathcal{PT}}$	$\{U_{t_i}\}$		
	Identity	$\{U_n(\theta_i)\}$	Noncommuting
Absent	3/3	1/1	1/0
Identity	0/0	1/0	1/0
$U_m(\pi)$	2/2	1/1 ($m \perp n$)	1/0
		1/0 ($m \parallel n$)	

the real space. In fact, in either noncoplanar or coplanar SSGs, d_{SBZ} can be 0, 1, 2, or 3. As discussed before, in the absence of $\mathcal{PT}$ operation and with $U_{t_i} = I$ in a coplanar SSG, d_{SBZ} can indeed be 3, due to the lack of local constraints on $\tilde{S}(\tilde{k})$. To substantiate this somewhat counterintuitive scenario, we present an electronic model with SSG P143.1.1 GM1, exhibiting $d_{SBZ} = 3$ in Supplemental Material [36]. In contrast, in some noncoplanar magnetic structures, d_{SBZ} can be 1. For example, in the SSG N143.3.1 A1 $\oplus$ A1 [Fig. 4(c)], the translation along $\boldsymbol{a}_3$ is accompanied by spin rotation $U_{t_3} = U_z(\pi)$. Thus, $\tilde{S}(\tilde{k})$ of an SSG Bloch state at generic $\tilde{k}$, which is an eigenstate of $\hat{t}_3 = \{i\sigma_z|1|\boldsymbol{a}_3\}$, can have a nonzero component only along the z direction, leading to $d_{SBZ} = 1$.

If the SBZ is symmorphic, i.e., $\tilde{\boldsymbol{q}}_g$ in Eq. (38) can be eliminated by a certain gauge [Eq. (36)], the symmetry of $\tilde{S}(\tilde{k})$ can be characterized by a d_{SBZ}-dimensional representation $\tilde{\rho}$ of a point group $\tilde{P} = \{s_g R_g | g \in \mathcal{G}\}$. Nonidentity representation $\tilde{\rho}$ implies the spin texture on the Fermi surface forming a nontrivial pattern, as exampled in Sec. IV. In Sec. G in Supplemental Material [36], we tabulate the $\tilde{\rho}$ and $\tilde{P}$ for all the SSGs.

We define the spin texture $\vec{S}(\boldsymbol{k})$ in the magnetic BZ ($\boldsymbol{k}$ denotes crystal momentum), following the same approach as for $\tilde{S}(\tilde{k})$. Note that we use different notations to distinguish spin textures in the magnetic BZ and SBZ. In cases where BZ is identical to SBZ, we use the notation $\vec{S}(\boldsymbol{k})$. $\vec{S}(\boldsymbol{k})$ is potentially more feasible for experimental measurement and is relevant to first-principle calculations, which are generally performed in the magnetic BZ. We now investigate the dimension d_{BZ} of the span of $\vec{S}(\boldsymbol{k})$. If $\hat{t}_i = \{\sigma_0|1|\boldsymbol{a}_i\}$, the magnetic BZ is identical to SBZ, and $d_{BZ} = d_{SBZ}$. If $\hat{t}_i = \{\hat{U}_{\boldsymbol{n}}(\theta_i)|1|\boldsymbol{a}_i\}$, the magnetic BZ is given by the folded commuting BZ. As $d_{SBZ} = 1$ in this case, d_{BZ} equals 0 if the $\vec{S}(\tilde{k})$'s at momenta folded to the same $\boldsymbol{k}$ always cancel each other and 1 otherwise. The only symmetry that leads to the cancellation at every $\boldsymbol{k}$ is $\mathcal{PT}$. One can verify that $U_{\mathcal{PT}} = I$ or $U_m(\pi)$ with $\boldsymbol{m} \parallel \boldsymbol{n}$ result in the cancellation. We summarize d_{BZ} in Table III. Additionally, it is important to note that crystal momentum $\boldsymbol{k}$ always transforms symmorphically. In SSGs with symmorphic SBZs but some of $U_{t_i} \neq I$, $\vec{S}(\boldsymbol{k})$ does not equal $\tilde{S}(\tilde{k})$. However, SSG operations impose the same forms of constraints [Eq. (38) with $\tilde{\boldsymbol{q}}_g \equiv \boldsymbol{0}$] on them. It implies that $d_{BZ} = d_{SBZ}$, and $\vec{S}(\boldsymbol{k})$ realizes the same representation $\tilde{\rho}$ of the point group $\tilde{P} = \{s_g R_g | g \in \mathcal{G}\}$ as $\tilde{S}(\tilde{k})$.

Finally, we comment on some universal properties of spin textures of SSGs with the noncommuting SBZ. In the reduced SBZ, all translation operations commute with each other, while some of them are still accompanied by nontrivial spin rotations (see Sec. III C 2 for an example). A similar analysis as in the commuting SBZ (see Sec. C in

Supplemental Material [36]) shows that d_{SBZ} is always 1. On the other hand, $d_{BZ} \equiv 0$, because $\{\hat{t}_i, \hat{t}_j\} = 0$ requires that U_{t_i} and U_{t_j} must be π rotation along two perpendicular directions.

IV. MATERIALS WITH SSG SYMMETRIES

A. Identifying SSGs for 1595 magnetic materials

We identify the SSGs for *all* the 1595 published experimental magnetic structures (materials with noninteger site occupation numbers are excluded) in the MAGNDATA database [42,43] on the Bilbao Crystallographic Server. The identification algorithm and the SSGs of all these materials are provided in Secs. D and G in Supplemental Material [36], respectively. Out of the 1595 structures, we find 242 distinct collinear SSGs, 183 distinct coplanar SSGs, and 106 distinct noncoplanar SSGs. Among these SSGs, the most frequently occurring types are type II (815 structures) for collinear structures, type III (211 structures) for coplanar structures, and type IX (69 structures) for noncoplanar structures. A collinear (coplanar) [noncoplanar] SSG of type II (III) [IX] indicates that the transformation of each component of the spin moments is described by an independent real 1D irrep. Table IV shows the statistics of the features of these materials determined by SSGs. Additionally, for reference, we provide statistics limited to materials with light elements (shown in parentheses), where all constituent elements are from the first four periods of the periodic table, and SOC is generally weak. Remarkably, all the exotic features of SSGs that we have studied, such as noncommuting SBZ, nonsymmorphic SBZ, and nontrivial spin textures, occur in these published experimental materials. In the subsequent sections, we present the results from first-principle calculations performed on selected materials as illustrative examples.

B. Material examples

This subsection is devoted to four material examples—i.e., coplanar $CoSO_4$, collinear $FeGe_2$, coplanar Mn_3Ge,

TABLE IV. The statistics of published magnetic materials in the MAGNDATA database. Each cell contains the number of magnetic materials possessing specific features. The number in parentheses is the statistics limited to materials with light elements from the first four periods of the periodic table. The statistics of spin textures are limited to the materials with SSGs processing symmorphic SBZ, and the "nontrivial $\tilde{S}(\tilde{k})$" means that the transformation of $\tilde{S}(\tilde{k})$ realizes a nontrivial representation of the SSG.

	Collinear	Coplanar	Noncoplanar
Total	954 (234)	436 (84)	205 (66)
Noncommuting SBZ	$\cdots$	23 (1)	10 (2)
Nonsymmorphic SBZ	$\cdots$	148 (31)	5 (1)
Symmorphic SBZ	954 (234)	265 (52)	190 (63)
Nontrivial $\tilde{S}(\tilde{k})$	139 (41)	181 (43)	140 (39)

and noncoplanar Mn_3GaN—that exhibit novel electronic states or spin textures protected by SSGs. Three other material examples, including coplanar $InMnO_3$, noncoplanar Mn_3Ge, and coplanar $FePO_4$, are discussed in Sec. D in Supplemental Material [36]. These materials are calculated using the density functional theory (DFT), as implemented in the Vienna *Ab Initio* Simulation Package [57,58]. The projector augmented wave pseudopotentials are adopted in the calculation [59,60]. The generalized gradient approximation with the Perdew-Burke-Ernzerhof realization [61] is used for the exchange correlation functional. The kinetic energy cutoff is fixed to 450 eV, which is larger than the ENMAX in the pseudopotential files of all elements. The energy convergence criteria are set to be 10^{-6} eV. The k-point mesh for the Brillouin zone integration is 10 000/(number of atoms) [62].

We first perform fully noncollinear magnetic structure calculations *without* considering the SOC effect. Remarkably, for three of the four materials—i.e., collinear $FeGe_2$, coplanar Mn_3Ge, and noncoplanar Mn_3GaN—the directions of magnetic moments converge to the experimental results (up to a global spin rotation). The remaining material, coplanar $CoSO_4$, also converges to a magnetic structure that is close to the experimental structure but exhibits a slightly smaller canting angle. To match the experimental data for $CoSO_4$, we introduce a penalty contribution to the total energy (see Sec. D in Supplemental Material [36] for more details). The good agreement between DFT results without SOC and experimental structures suggests that SOC, except for choosing a global spin coordinate, does not play a major role in determining the collinear or noncollinear magnetic structures of these materials.

To demonstrate the perturbative nature of SOC, we compare the band structures with and without SOC of all these materials in Sec. D in Supplemental Material [36]. We observe that SOC leads to small splittings of the band degeneracy predicted by SSG. Specifically, the typical splitting along high-symmetry paths is less than 5 meV, which is considerably smaller than the typical distance between two adjacent nondegenerate energy bands in the absence of SOC. These quasidegeneracies could not be understood without SSGs. We claim that SSGs provide accurate descriptions for these systems when the energy scale of interest is larger than the splittings.

1. Nonsymmorphic SBZ in $CoSO_4$

The compound $CoSO_4$ (No. 1.519 in the MAGNDATA database) has a base-centered orthorhombic lattice structure. The spin moments of $CoSO_4$ in the antiferromagnetic phase are determined from a neutron diffraction study [63]. The moments lie in the y, z plane and have around $\pm25°$ canting angles concerning the y axis, and the body-centered translation relates spin moments with opposite directions [Fig. 6(a)]. This magnetic structure is described by the
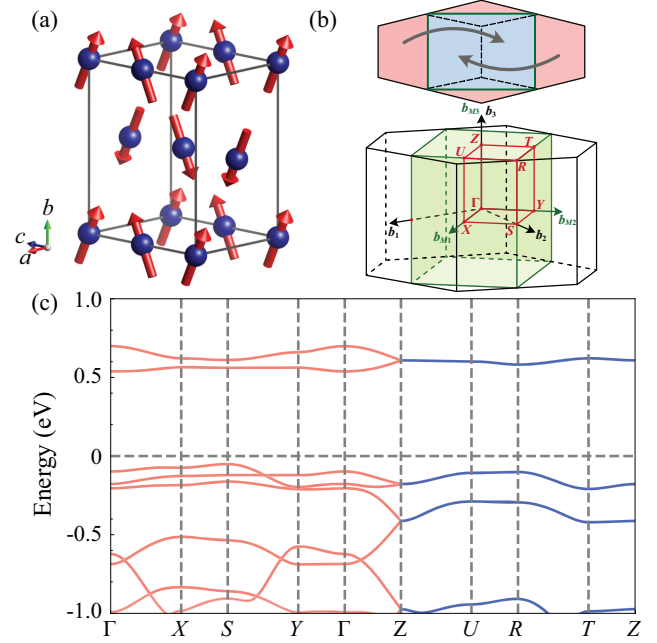

FIG. 6. (a) The magnetic structure of $CoSO_4$ showing only the magnetic atoms (Co). (b) Bottom: the first BZ in the SSG reciprocal lattice b_i's (black lines) and MSG reciprocal lattice b_{Mi}'s (green region). Top: the folding process of the SSG BZ (the large hexagon) into the MSG BZ (the smaller rectangle), viewed from the z-axis perspective. (c) The energy bands obtained from the first-principle calculation. At every k, $E(k)$ is at least twofold degenerate. The light red and blue lines represent the twofold and fourfold degeneracy, respectively.

MSG $C_P m'cm'$ (No. 63.16.526 in the Opechowski-Guccione setting [64]). Figure 6(c) shows the energy bands obtained from the first-principle calculation. These bands are plotted in the BZ of the MSG and exhibit the following two features: (i) The bands are at least twofold degenerate in the whole MSG BZ. This degeneracy is protected by the MSG $\mathcal{PT}$ symmetry $\{i\sigma_y \mathcal{K}|\bar{1}|1/2(a_{M1} + a_{M2})\}$ which squares to -1. Here, a_{Mi}'s ($i = 1, 2, 3$) denote the lattice vectors of the pure translation subgroup given by the conventional lattice vectors of the orthorhombic lattice (see discussion of T_M in Sec. III C 1). (ii) The degree of degeneracy becomes four along Z-U-R-T-Z [the high-symmetry points are denoted in Fig. 6(b)]. And we verify this fourfold degeneracy exists in the whole $k_z = \pi$ plane. MSG explains the fourfold degeneracy along the high-symmetry lines R-T and T-Z, which form a projective representation of the little cogroup $m'mm$. However, MSG can protect only twofold degeneracy and, hence, cannot explain the extra degeneracy at the remaining momenta in the $k_z = \pi$ plane. We find that the hidden SSG symmetry explains the fourfold degeneracy, as discussed below.

The SSG P63.3.89 Y1$^+$ $\oplus$ Y3$^+$ with parent space group $Cmcm$ (No. 63) characterizes this magnetic structure. Table V shows the generators of the SSG, where a_i are lattice vectors of the unitary translation subgroup T_U of

TABLE V. The generators of the SSG P63.3.89 $Y1^+ \oplus Y3^+$ of coplanar magnetic material $CoSO_4$. Here, $a_{1,2}$ are body-centered translation vectors. The last row is for the pure-spin-operation group $\mathcal{S}$. The last column shows how the SSG momentum is transformed under the SSG operations.

SSG operation	Spin operations on electrons	Transformation of SSG momentum $\tilde{k}$
$\{U_x(\pi)\|1\|a_{1,2}\}$	σ_x	$\tilde{k}$
$\{I\|1\|a_3\}$	σ_0	$\tilde{k}$
$\{I\|\bar{1}\|0\}$	σ_0	$-\tilde{k}$
$\{U_y(\pi)\|m_{001}\|1/2a_3\}$	σ_y	$-R_z(\pi)\tilde{k} + 1/2(b_1 + b_2)$
$\{I\|m_{100}\|0\}$	σ_0	$-R_x(\pi)\tilde{k}$
$\{TU_x(\pi)\|1\|0\}$	$\sigma_z\mathcal{K}$	$-\tilde{k} + 1/2(b_1 + b_2)$

SSGs. $a_{1,2}$ are the base-centered translation vectors, and a_i's are

$$a_1 = \frac{1}{2}(a_{M1} + a_{M2}), \quad a_2 = \frac{1}{2}(a_{M1} - a_{M2}), \quad a_3 = a_{M3}. \quad (39)$$

Thus, the size of the SBZ spanned by b_i is twice that of the magnetic BZ spanned by b_{Mi} [see Fig. 6(b)]. With the spin operations acting on electrons given in Table V, we determine the transformation of SSG momentum (see the last column). The SSG operation $\hat{P}\hat{T} = \{\sigma_z\mathcal{K}|\bar{1}|0\}$ acts on SSG momentum $\tilde{k}$ as a fractional translation ($\tilde{k} \rightarrow \tilde{k} + \tilde{q}_{\mathcal{PT}}$) with $\tilde{q}_{\mathcal{PT}} = \frac{1}{2}(b_1 + b_2)$, and the mirror operation $M_z = \{U_y(\pi)|m_{001}|\frac{1}{2}a_3\}$ acts on $\tilde{k}$ as a glide operation with $\tilde{q}_{M_z} = \frac{1}{2}(b_1 + b_2)$, which indicate a non-symmorphic SBZ. We first study the electronic bands in the SBZ. No SSG momentum is invariant under $\hat{P}\hat{T}$ operation, and $\hat{P}\hat{T}$ requires that $E_n(\tilde{k}) = E_n(\tilde{k} + \tilde{q}_{\mathcal{PT}})$ for all $\tilde{k} \in$ SBZ. In addition, the $\tilde{k}_z = \pi$ plane has the symmetry $\hat{C}_{2z}\hat{T} = \{i\sigma_x\mathcal{K}|2_{001}|\frac{1}{2}a_3\}$, and $(\hat{C}_{2z}\hat{T})^2|\psi(\tilde{k}_x, \tilde{k}_y, \pi)\rangle = -|\psi(\tilde{k}_x, \tilde{k}_y, \pi)\rangle$. It results in Kramer's degeneracy on that plane. Then, we fold the SBZ to the magnetic BZ. We introduce a phase factor of i to the spin rotation associated with the translations $\{U_x(\pi)|1|a_{1,2}\}$, altering the accompanying spin rotation from $-i\sigma_x$ to σ_x (see Table V). Under this gauge for SSG, the translations along the lattice vectors of MSG are always accompanied by σ_0 spin rotation without an extra phase. Thus, the crystal momentum k equals the SSG momentum $\tilde{k}$ after modulo reciprocal lattice b_{Mi}'s. On the other hand, $\tilde{q}_{\mathcal{PT}} = b_{M1}$ is a reciprocal lattice vector in the magnetic BZ. Thus, the energy bands at a momentum k in the magnetic BZ consist of $E_n(\tilde{k})$ and $E_n(\tilde{k} + \tilde{q}_{\mathcal{PT}})$ in the SSG BZ. This implies that the degrees of degeneracy at k in the MSG BZ should be twice as $E_n(\tilde{k})$ in the SSG BZ. After folding, every band in the $k_z = \pi$ plane is fourfold degenerate.
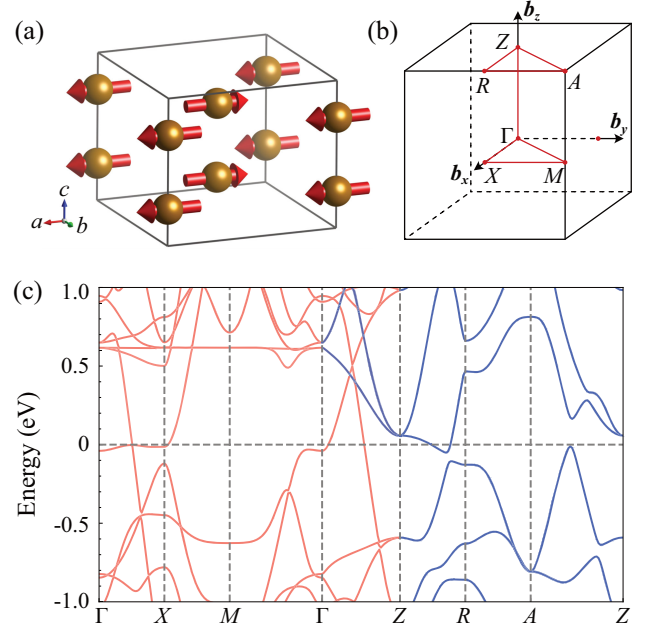

FIG. 7. (a) The magnetic structure of $FeGe_2$ showing only the magnetic atoms (Fe). (b) The first BZ in the SSG reciprocal lattice b_i's, which coincides with MSG reciprocal lattice. (c) The energy bands obtained from the first-principle calculation. Every single line is at least twofold degenerate. The light red and blue lines represent the twofold and fourfold degeneracy, respectively.

2. Extra band degeneracies in $FeGe_2$

The antiferromagnetic material $FeGe_2$ (No. 1.557) has a body-centered orthorhombic lattice structure. A neutron diffraction experiment [65] found that the spin moments are along the x direction, and moments with opposite signs are related by a body-centered translation vector [Fig. 7(a)]. The structure is described by the MSG $I_Pb'am'$ (No. 72.12.641) [66]. Figure 7(c) shows the energy bands from the first-principle calculation. The energy bands are always double degenerate, which can be explained by the MSG's $\mathcal{PT}$ symmetry. However, the fourfold degeneracy at Γ point and path Z-R-A-Z [see their positions in Fig. 7(b)] cannot be explained by the MSG, because the little MSG cogroups on them have only 2D coirreps (see explicit representation matrices in the Corepresentations tools [50,51]). We can use the representation theory of collinear SSG (Sec. III B) to explain these degeneracies.

This antiferromagnetic structure is described by the type-II collinear SSG L140.2.8 $M1^+$ with parent space group $I4/mcm$ (No. 140). Besides the pure-spin-operation group $\mathcal{S} = \mathcal{S}_{U(1)} \times \mathcal{S}_{Z_2^T}$, this SSG $\mathcal{G}$ is generated by $\{I|1|a_i\}$ ($i = 1, 2, 3$), $\{I|4_{001}^+|0\}$, $\{I|2_{010}|0, 0, 1/2\}$, $\{I|\bar{1}|0\}$, and $\{T|1|1/2, 1/2, 1/2\}$. Here, a_i's denote the lattice vectors of the conventional unit cell, and the translation parts of spatial operations are written on the basis of a_i's. Also note that here $\mathcal{S}_{Z_2^T}$ is generated by $\{e^{-i(\pi/2)\sigma_y}i\sigma_y\mathcal{K}|1|0\} = \{\mathcal{K}|1|0\}$, since spins are along the x direction. As discussed

in Sec. III B, the Hamiltonian for the collinear magnetism can be block diagonalized into spin-up and spin-down parts. Because of the existence of a spin-flipping unitary translation $\{-i\sigma_z|1|1/2,1/2,1/2\}$, $E_{n\uparrow}(\boldsymbol{k}) = E_{n\downarrow}(\boldsymbol{k})$. Thus, we need only to study spin-up (or spin-down) energy bands, whose symmetry is effectively described by single-valued gray group $G_0 \times \mathcal{S}_{Z_2^T}$. Here, G_0 is the operations in $\mathcal{G}$ with identity spin operations, and $G_0 \times Z_2^T$ is identical to the gray group $P4/mcc1'$ (No. 124.2.1019). The little cogroup of $P4/mcc1'$ at the Γ point is magnetic point group $4/mmm1'$, which has eight 1D coirreps and two 2D coirreps (refer to Bilbao Crystallographic Server for the character table). Thus, $E_{n\uparrow}(\boldsymbol{k})$ can be either twofold degenerate or nondegenerate at Γ. The Z-R line has a joint symmetry of mirror and time reversal, given as $\hat{M}_z\hat{T} = \{\mathcal{K}|m_{100}|0,0,1/2\}$, and the action $(\hat{M}_z\hat{T})^2$ on $|\psi(k_x,0,\pi)\rangle$ equals -1, leading to Kramer's degeneracy of $E_{n\uparrow}(\boldsymbol{k})$. Similarly, on lines R-A and A-Z, $\{\mathcal{K}|m_{010}|0,0,1/2\}$ and $\{\mathcal{K}|m_{110}|0,0,1/2\}$ lead to Kramer's degeneracy, respectively. The total degrees of the degeneracy of energy bands are twice as $E_{n\uparrow}(\boldsymbol{k})$, which can be either two or four at Γ and always four along Z-R-A-Z.

The specific irreps constituted by the Bloch states at a given momentum, along with their degrees of degeneracy, are contingent upon the symmetry of the local orbitals of the atoms and the representation they form. The Fe atoms of FeGe$_2$ are situated at the coordinates $(0,0,\frac{1}{4})$, $(0,0,\frac{3}{4})$, $(\frac{1}{2},\frac{1}{2},\frac{1}{4})$, and $(\frac{1}{2},\frac{1}{2},\frac{3}{4})$. Let us first consider the site-symmetry group of the spin-up (or spin-down) orbitals at $(0,0,\frac{1}{4})$. In addition to the operations in the group $\mathcal{S}_{Z_2^T}$, the symmetry group is generated by $\{I|4_{001}^+|\boldsymbol{0}\}$, $\{I|2_{010}|0,0,-1/2\}$, isomorphic to the magnetic point group $4221'$. Specifically, the orbitals corresponding to $A_{1,2}$ or $B_{1,2}$, in conjunction with the orbitals at $(0,0,\frac{3}{4})$ linked via SSG symmetry, contribute to the 1D coirreps at Γ (see the details of the induction process, for example, in Ref. [51]). In contrast, the E orbitals contribute to the 2D coirreps at Γ. We note that states $|\uparrow,p_x\rangle$ and $|\uparrow,p_y\rangle$, which remain invariant under the effective time reversal in the $\mathcal{S}_{Z_2^T}$, form the coirrep E of $4221'$. The site-symmetry group in the other positions of Fe atoms is also isomorphic to $4221'$, where the orbitals contribute to the coirreps in the momentum space in a similar manner. For generic collinear magnetic structures, the effective symmetry group of spin-up (or spin-down) energy bands is always isomorphic to a gray group, and the effective site-symmetry group of local spin-up orbitals is isomorphic to a gray point group. Hence, the techniques of band representation of magnetic topological quantum chemistry [44,51] can be directly applied in the context of collinear SSGs.

It is notable that applying a global spin rotation on the magnetic structure does not affect the SSG, as discussed in Sec. II C, but it might enhance the MSG symmetry. For

example, consider rotating all the magnetic moments of FeGe$_2$ [see Fig. 7(a)] by $U_y(\pi/2)$. After this rotation, the magnetic moments align along the c axis, the fourfold rotation axis of the crystal, thereby enhancing the MSG to $I_P4/m'cm$ (No. 140.11.1206). The enhanced MSG shares the same parent space group as the SSG L140.2.8 M1$^+$ but remains smaller than the SSG. The mapping from the parent space group to the enhanced MSG is one to one, whereas that to the SSG is one to many due to the pure-spin-operation group $\mathcal{S}$ [Eq. (9)]. By examining the coirreps of the magnetic little cogroup of the enhanced MSG, we find that it can explain the fourfold degeneracies on the line R-A but fails to explain the degeneracies at Γ or line R-Z-A.

3. E_{2g} spin texture in Mn$_3$Ge

The compound Mn$_3$Ge (No. 0.377) has a hexagonal lattice structure. It has a coplanar $(x, y$ plane) triangular antiferromagnetic structure in the magnetic phase [Fig. 8(a)] [67–70]. Its MSG is $Cm'cm'$ (No. 63.8.518), and its SSG is P194.6.1 GM5$^+$ with parent space group $P6_3/mmc$. Besides $\mathcal{S}_{Z_2^T}$, the SSG is generated by $\mathcal{P} = \{I|\bar{1}|0,0,0\}$, $C_{6z} = \{U_z(2\pi/3)|6_{001}^+|0,0,1/2\}$, $C_{2,1\bar{1}0} = \{U_{1\bar{1}0}(\pi)|2_{1\bar{1}0}|0,0,1/2\}$, and pure translations $\{I|1|\boldsymbol{a}_i\}$ of the hexagon lattice. Here, $1\bar{1}0$ represents the direction of $\boldsymbol{a}_1 - \boldsymbol{a}_2$ equivalent to the direction of $-\sqrt{3}/2\boldsymbol{e}_x + 1/2\boldsymbol{e}_y$. Note that, in this SSG, the sixfold screw rotation in real space is accompanied by the threefold rotation in the spin space. Consequently, the $2\pi/3$ rotation in real space is accompanied by $-2\pi/3$ rotation in spin space, and this symmetry was noticed and studied in a 2D model of Mn$_3$Ge [4].
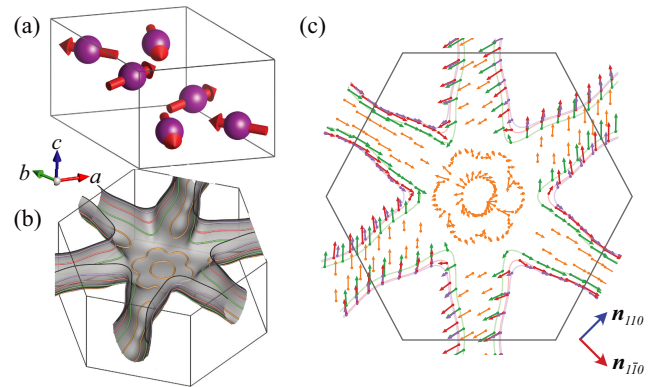

FIG. 8.   (a) The magnetic structure of Mn$_3$Ge showing only the magnetic atoms (Mn). (b) The Fermi surface of Mn$_3$Ge, which is centered at the A $[\boldsymbol{k} = (0,0,\pi)]$ point. Only the lower half is shown, and the full Fermi surface is symmetric with respect to $k_z = \pi$. Different colors represent equal-k_z lines. (c) The spin texture $\vec{S}(\boldsymbol{k})$ on equal-k_z lines labeled in (b). Arrows represent directions of $\vec{S}(\boldsymbol{k})$.

The SSG completely determines the symmetry of $\vec{S}(\boldsymbol{k})$. The $\mathcal{PT}$ operation $\{TU_z(\pi)|\bar{1}|\mathbf{0}\}$ ($\mathcal{T}$ is from $\mathcal{S}_{Z_2^T}$) requires that $\vec{S}(\boldsymbol{k})$ lies in the x, y plane, as the spin moments in real space. The operations $\mathcal{P}$, C_{6z}, and $C_{2,1\bar{1}0}$ lead to a $6/mmm$ point group symmetry in the momentum space. Because of the $U_z(2\pi/3)$ spin rotation in C_{6z}, $\vec{S}(\boldsymbol{k})$ is rotated by $2\pi/3$ rather than $\pi/3$ under C_{6z}. Because of $\{I|m_{001}|0,0,1/2\}$, which is generated by $C_{6z}^3\mathcal{P}$ up to a lattice translation, $\vec{S}(\boldsymbol{k})$ is invariant under the mirror with respect to the $k_z = 0$ plane. Because of $C_{2,1\bar{1}0}$, which is also a MSG symmetry, $\vec{S}(\boldsymbol{k})$ is rotated by $U_{1\bar{1}0}(\pi)$ under $2_{1\bar{1}0}$. $\vec{S}(\boldsymbol{k})$ subject to these constraints form the 2D real irrep E_{2g} of $6/mmm$.

Mn$_3$Ge with the coplanar magnetic structure has three Fermi surfaces. Here, we focus on the Fermi surface around $k_z = \pi$ and leave discussions on the other two to Sec. D in Supplemental Material [36]. First, we verify that $S_z(\boldsymbol{k})$ vanishes at every $\boldsymbol{k}$ and $\vec{S}(\boldsymbol{k})$ is symmetric with respect to $k_z = 0$. Figure 8(c) shows the spin texture on the Fermi surface viewed from the z axis, where different colors represent equal energy contours in different k_z planes. One can verify that $\vec{S}(\boldsymbol{k})$ satisfies all the symmetry constraints derived in the last paragraph. The two-component vector $\vec{S}(\boldsymbol{k})$ has a nontrivial vortex configuration: As $\boldsymbol{k}$ completes an anticlockwise path that circles the z axis, $\vec{S}(\boldsymbol{k})$ is rotated by 4π. This implies the existence of a single vortex with charge $S_V = 2$ on the north pole of the Fermi surface, as indicated by the yellow arrows on the small circle around $k_x = k_y = 0$. The nontrivial S_V arises from $\vec{S}(\boldsymbol{k})$ forming the E_{2g} representation of $6/mmm$. Let us consider a closed path in the $\boldsymbol{k}$ space, e.g., $[k_0\cos(\theta), k_0\sin(\theta), k_{z0}]$ with $k_0 > 0$ and $\theta \in [0, 2\pi)$. The vortex charge is defined as $S_V = (1/2\pi)\int_0^{2\pi} d\theta(d/d\theta)$ $\arctan[S_y(\theta)/S_x(\theta)]$, where $S_\mu(\theta) \equiv S_\mu(k_0\cos(\theta), k_0\sin(\theta), k_{z0})$ ($\mu = x$, y). The expression can be decomposed as $S_V = \sum_{i=1}^6 S_{Vi}$, with each S_{Vi} representing the integral's contribution over the interval $\theta \in [2\pi(i-1)/6, 2\pi i/6)$. The SSG operation C_{6z} requires that $S_{Vi} = S_{Vj}$ for any $i, j = 1, \ldots, 6$. Given the spin operation in C_{6z} as $U_z(2\pi/3)$, $\arctan[S_y(\pi/3)/S_x(\pi/3)] = \arctan[S_y(0)/S_x(0)] + 2\pi/3$, which is also equivalently required by the E_{2g} representation. Consequently, $S_{V1} = (2\pi/3 + 2n\pi)/2\pi(n \in \mathbb{Z})$, leading to $S_V = 6S_{V1} = 6n + 2$. Note that this vortex differs from previously studied ones in systems where SOC plays a major role in band splitting, such as the Rashba model [71], because the charge S_V of the latter one generally can be only 1. We also verify this vortex is stable under SOC (see Fig. S.8 in Supplemental Material [36]). The stability of the vortex originates from its topological nature, which is characterized by the homotopy group $\pi_1(S_1)$ and remains immune under generic weak perturbation including SOC.

4. E_g spin texture in Mn$_3$GaN

The compound Mn$_3$GaN (No. 0.177) has an antiperovskite crystal structure with crystalline symmetry $Pm\bar{3}m$ (No. 221). In the magnetic phase, the magnetic moments (Mn atoms) lie in the 111 plane, forming a triangular antiferromagnetic structure in each 111 cross section [72]. This structure's MSG $R\bar{3}m$ (No. 166.1.1327) is much lower than the crystalline symmetry, but its SSG P221.6.1 GM3$^+$ still enjoys the full crystalline symmetry. This coplanar SSG is generated by $\{I|1|\boldsymbol{a}_i\}$ ($i = 1, 2, 3$), $\mathcal{P} = \{I|\bar{1}|\mathbf{0}\}$, $C_{3,111} = \{U_{111}(2\pi/3)|3_{111}^+|\mathbf{0}\}$, $C_{4z} = \{U_{1\bar{1}0}(\pi)|4_{001}^+|\mathbf{0}\}$, and $\mathcal{T} = \{TU_{111}(\pi)|1|\mathbf{0}\}$ (the generator for $\mathcal{S}_{Z_2^T}$). One can derive $C_{2x} = \{I|2_{100}|\mathbf{0}\}$ and $C_{2,1\bar{1}0} = \{U_{1\bar{1}0}|2_{1\bar{1}0}|\mathbf{0}\}$ from the generators. Here, 111 and $1\bar{1}0$ correspond to the directions $\boldsymbol{e}_x + \boldsymbol{e}_y + \boldsymbol{e}_z$ and $\boldsymbol{e}_x - \boldsymbol{e}_y$, respectively. Because of the $\mathcal{PT}$ symmetry, $\vec{S}(\boldsymbol{k})$ is within the 111 plane. Following a similar analysis as in the previous sections, we find that the $\vec{S}(\boldsymbol{k})$ lying in the 111 plane forms the E_g representation of the point group O_h: It is parity even, is rotated by $2\pi/3$ under $C_{3,111}$, and undergoes a 2D reflection $U_{1\bar{1}0}(\pi)$ under C_{4z}.

Figure 9(b) shows the Fermi surfaces of Mn$_3$GaN obtained by the first-principle calculation. We verify that the 111 component of $\vec{S}(\boldsymbol{k})$ at any $\boldsymbol{k}$ is always zero, consistent with the $\mathcal{PT}$ symmetry constraint. For the clarity
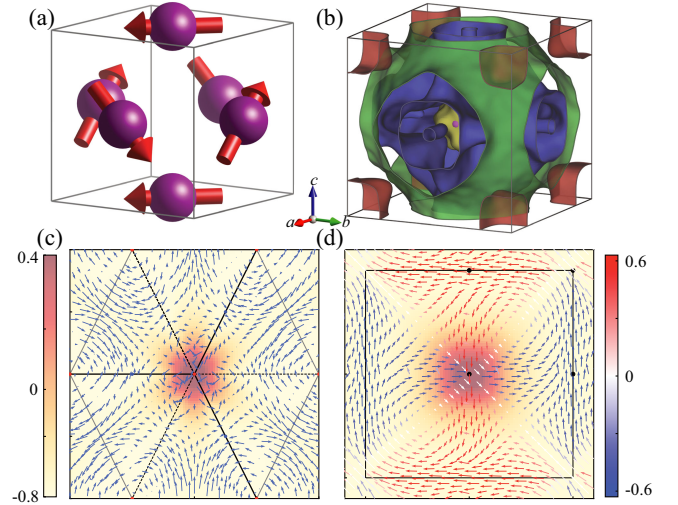

FIG. 9. (a) Magnetic structure of Mn$_3$GaN showing only the magnetic atoms (Mn). (b) The Fermi surfaces of Mn$_3$GaN. (c), (d) The spin texture $\vec{S}(\boldsymbol{k})$ on the 111 plane ($k_x + k_y + k_z = 0$) and 001 plane ($k_z = 0$) in the momentum space. The background colors denote the values of $E(\boldsymbol{k})$ (see the left color bar). The outer hexagon in (c) and the square in (d) denoted the boundary of the first BZ projected to these planes. In (c), $\vec{S}(\boldsymbol{k})$'s are coplanar on the 111 plane. In (d), $\vec{S}(\boldsymbol{k})$'s are not confined to the 001 plane, and the red or blue color (the right color bar) represents the value of $S_z(\boldsymbol{k})$.

of demonstration, we do not show $\vec{S}(\boldsymbol{k})$ on the complicated 3D Fermi surfaces but plot $\vec{S}(\boldsymbol{k})$ of the band, which contributes to the second innermost Fermi surface shown in Fig. 9(b), on the high-symmetry planes containing the Γ point. The 111 plane has the symmetry of D_{3d} generated by $\mathcal{P}$, $C_{3,111}$, and $\{R_{1\bar{1}0}(\pi)|2_{1\bar{1}0}|\mathbf{0}\}$. Thus, $\vec{S}(\boldsymbol{k})$ on this plane form the reduced representation $E_g{\downarrow}D_{3d} = E_g$, which is even parity, is rotated by $2\pi/3$ under $C_{3,111}$, and undergoes a 2D reflection under $2_{1\bar{1}0}$ [$1\bar{1}0$ is the vertical direction in Fig. 9(c)]. The spin texture on the 111 plane can also be explained by the MSG $R\bar{3}m$, since, in these aforementioned operations, spin rotations equal the spatial rotations. On the other hand, the pattern of $\vec{S}(\boldsymbol{k})$ on the 001 plane can be understood only using SSG. The 001 plane has the symmetry of D_{4h}, and, hence, $\vec{S}(\boldsymbol{k})$ on the 001 plane forms the reduced representation $E_g{\downarrow}D_{4h} = A_{1g} + B_{1g}$. As (S_x, S_y, S_z) transforms into $(-S_y, -S_x, -S_z)$ under C_{4z} and is invariant under $\mathcal{P}$ and C_{2x}, one can show that $S_x - S_y$ forms the A_{1g} representation of D_{4h} and $S_x + S_y$, S_z from the B_{1g} representation. The spin texture from first-principle calculation shown in Fig. 9(d) demonstrates this unconventional feature, where the $S_x(\boldsymbol{k}), S_y(\boldsymbol{k})$ are represented by vectors and $S_z(\boldsymbol{k})$ is represented by the colors of the vectors.

V. TOPOLOGICAL PHASES PROTECTED BY SSG

As spatial operations in SSGs are associated with spin rotations, the algebras of SSG symmetry operations, described by projective representation (Sec. III), can be different from those in the MSGs. The enriched symmetry algebra enables novel topological states in the absence of SOC and TRS. Here, we comment on possible topological states in SSGs. For collinear SSGs, as the symmetry operators form a linear representation of gray groups, no stable TI state could be stabilized [44,45]. However, various topological semimetals can be protected as in space groups in class AI. For coplanar SSGs, the effective TRS $\hat{\mathcal{T}}_{\text{eff}} = \hat{U}_{\hat{x}}(\pi)\hat{\mathcal{T}}$, which squares to 1, forbids Chern insulators. Mirror Chern insulators can appear in coplanar SSGs where a mirror operator $\hat{M}$ satisfies $\hat{M}^2 = 1$ and $\{\hat{M}, \hat{\mathcal{T}}\} = 0$. Chern numbers in the mirror-even and mirror-odd sectors must be opposite due to $\hat{\mathcal{T}}_{\text{eff}}$. 3D derivatives of the mirror Chern insulator can be constructed using the topological crystal approach [73,74]. In noncoplanar SSGs, both Chern insulator [75] and $\mathbb{Z}_2$ TI [4], which is protected by $\hat{\mathcal{T}}_{\text{eff}} = \hat{M}\hat{\mathcal{T}}$ ($\hat{\mathcal{T}}_{\text{eff}}^2 = -1$), as well as their 3D derivatives [73,74], can be stabilized. We present three examples of topological states in noncoplanar SSGs in the following subsections.

A. 2D $\mathbb{Z}_2$ TI in the absence of SOC and TRS

It is widely known that the $\mathbb{Z}_2$ TI is protected by the spinful TRS whose square equals -1, which exists only in

nonmagnetic materials with SOC. However, in 2D systems with noncollinear magnetism and negligible SOC, which seem to completely violate the conditions of the existence of TI, the SSG operation $\hat{M}_z\hat{\mathcal{T}} = \{i\sigma_y\mathcal{K}|m_{001}|\mathbf{0}\}$ can serve as an effective TRS that squares to -1 and can give rise to a 2D magnetic $\mathbb{Z}_2$ TI [4]. Note that its counterpart $\{i\sigma_y\mathcal{K}e^{i\pi\sigma_z}|m_{001}|\mathbf{0}\}$ in MSG, which contains π-spin rotation along the z direction, squares to 1 and cannot protect a TI.

Here, we provide a concrete model with real hoppings and noncoplanar magnetism to realize the 2D magnetic $\mathbb{Z}_2$ TI. We consider an A-A stacked bilayer kagome lattice [Figs. 10(a) and 10(b)]. The 2D crystal structure can be described by the space group $P6/mmm$ (No. 191) with lattice constant $c \to \infty$. In each layer, local magnetic moments $\boldsymbol{S}(\boldsymbol{r}_i)$ have a canting angle θ ($\cos\theta = |S_z|/|\boldsymbol{S}|$), and in-plane components form an all-in–all-out spin-ice structure. The magnetic structure on a single-layer kagome lattice has nonzero spin chirality and is identical to the one studied in previous work on metallic pyrochlore ferromagnets [75], in which a Chern insulator phase without SOC can occur. The mirror operation m_{001} transforms two layers into each other, and the moments of two neighboring sites in two layers are opposite to each other. The SSG of this magnetic structure, named $N191.12.2GM1^- \oplus GM5^-$, is generated by the symmetry operators (acting on fermions) $\hat{C}_{3z} = \{e^{-i(\pi/3)\sigma_z}|3_{001}^+|\mathbf{0}\}$, $\hat{C}_{2z} = \{\sigma_0|2_{001}|\mathbf{0}\}$, $\hat{M}_z\hat{\mathcal{T}} = \{i\sigma_y\mathcal{K}|m_{001}|\mathbf{0}\}$, $\hat{C}_{2x} = \{-i\sigma_x|2_{100}|\mathbf{0}\}$, and lattice translations without spin operations.
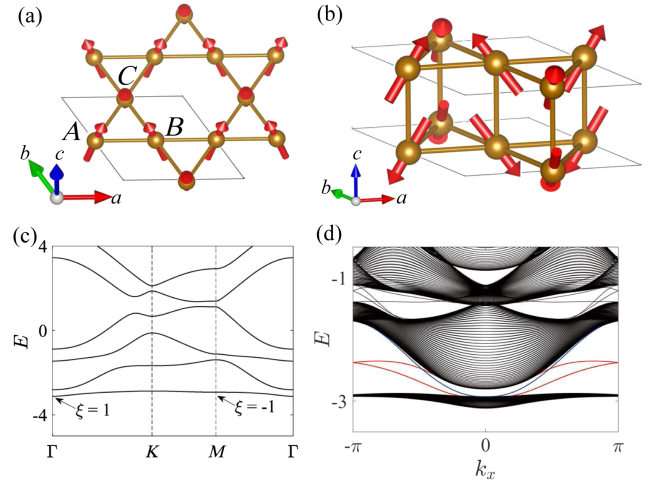

FIG. 10. Noncoplanar magnetic structure on the (a) upper layer and (b) bilayer of the kagome lattice. (c) Energy band of Hamiltonian $\mathcal{H}_{\mathbb{Z}_2}$ [Eq. (40)] in the periodic boundary condition (PBC). Energy is double degenerate in the whole Brillouin zone. (d) Energy band of $\mathcal{H}_{\mathbb{Z}_2}$ under PBC along the x direction and open boundary condition (OBC) along the y direction with $N_y = 50$. The blue (red) line represents the helical edge mode around $y = 0$ ($y = N_y$).

We consider the electronic Hamiltonian with such a magnetic structure:

$$\mathcal{H}_{Z_2} = \sum_{i=1,2}\left[t_\parallel \sum_{\langle R,\alpha;R',\alpha'\rangle}(c^\dagger_{R,\alpha,i}\sigma_0 c_{R',\alpha',i}) + J\sum_{R,\alpha}\mathbf{S}_{R,\alpha,i}\cdot\mathbf{s}_{R,\alpha,i}\right]$$
$$+ t_\perp\sum_{R,\alpha}(c^\dagger_{R,\alpha,1}\sigma_0 c_{R,\alpha,2}+\text{H.c.}),\qquad(40)$$

with

$$s^\mu_{R,\alpha,i} = \frac{1}{2}c^\dagger_{R,\alpha,i}\sigma_\mu c_{R,\alpha,i}\quad(\mu=x,y,z)$$

being the spin operator of the electrons. Here, $c^\dagger_{R,\alpha,i} = (c^\dagger_{R,\alpha,i,\uparrow}, c^\dagger_{R,\alpha,i,\downarrow})$ ($\alpha = A$, B, C, $i = 1$, 2) is a two-component spin-1/2 electron creation operator in the unit cell R, sublattice α, of the ith layer. The first and third terms of the Hamiltonian are intralayer and interlayer nearest-neighboring hopping, respectively. The hopping matrix is proportional to σ_0, because the SOC is considered negligible. The second term describes the on-site interaction between the conduction electron and localized magnetic moments $\mathbf{S}_{R,\alpha,i}$ [Figs. 10(a) and 10(b)]. In the following, we choose $t_\parallel = 1$, $t_\perp = 0.5$, $J = 2$, and $|\mathbf{S}_{R,\alpha,i}| = 1$ with canting angle $\theta = \pi/3$. The band structure is shown in Fig. 10(c), where every band is double degenerate, as explained in the next paragraph.

We can evaluate the $\mathbb{Z}_2$ topological invariant ν of the model by the Fu-Kane formula [76]. In this system, $\hat{M}_z\hat{\mathcal{T}}$ plays the role of TRS, and $\hat{C}_{2z}$, which does not contain spin rotation, plays the role of inversion symmetry because it squares to 1 and commutes with $\hat{M}_z\hat{\mathcal{T}}$ [77]. The topological invariant ν is then determined by $(-1)^\nu = \prod_i \xi(\mathbf{k}_i)$, where $\mathbf{k}_i$ are TRS-invariant momenta and $\xi(\mathbf{k}_i)$ is the product of the $\hat{C}_{2z}$ eigenvalues of occupied Kramers pairs at $\mathbf{k}_i$. (Notice that the joint symmetry $\hat{C}_{2z}\hat{M}_z\hat{\mathcal{T}}$ preserves momentum and squares to -1; hence, it protects double degeneracy of the energy bands.)

When the filling is 2 per unit cell, only the lowest double-degenerate band is occupied, with $\xi(\mathbf{k}) = 1, -1$ at Γ and (three) M points, respectively, implying that the system is topological. We also observe the topological helical edge states on the open boundary of a cylinder geometry [Fig. 10(d)]. The noncoplanar magnetism is essential in realizing a nontrivial $\mathbb{Z}_2$ topological invariant. In coplanar magnetism, we can align the magnetic moments within the x, z plane through a global spin rotation. In such a case, both the hoppings and on-site terms of the Hamiltonian become real, inevitably leading to a $\mathbb{Z}_2$-trivial state. It is the y component of $\mathbf{S}_{R,\alpha,i}$'s in our model that makes the Hamiltonian pseudoreal (i.e., respecting TRS with sign -1) and allows a possible nontrivial $\mathbb{Z}_2$ index.

B. 3D $\mathbb{Z}_2$ TI with fourfold Dirac point on surface

We show that an unavoidable fourfold Dirac point can be protected on the surface of a 3D $\mathbb{Z}_2$ TI protected by SSG symmetries. It provides an exception to the fermion-doubling theorem of 2D systems [78,79].

As shown in Fig. 11(a), the 3D state is constructed by stacking the 2D $\mathbb{Z}_2$ TI layers protected by $\hat{M}_z\hat{\mathcal{T}} = \{i\sigma_y\mathcal{K}|m_{001}|\mathbf{0}\}$ (Sec. VA). We first decorate the integer planes, $z = 0, \pm 1, \pm 2\ldots$, with the 2D Hamiltonian $\mathcal{H}_{Z_2}(k_x, k_y)$ [Eq. (40)]. Different layers are related by the translation $\hat{t}_3 = \{I|1|0,0,1\}$ along the z direction, and the $\mathbb{Z}_2$ topology of the layer at $z = n$ is protected by $\hat{t}_3^{2n}\hat{M}_z\hat{\mathcal{T}}$. We then decorate the half-integer planes, $z = \pm\frac{1}{2}, \pm\frac{3}{2}\ldots$, with the mirror reflection of $\mathcal{H}_{Z_2}(k_x, k_y)$, i.e., $D^\dagger(m_{100})\mathcal{H}_{Z_2}(-k_x, k_y)D(m_{100})$, where $D_{\alpha is,\alpha'i's'}(m_{100}) = M_{\alpha,\alpha'}\delta_{ii'}\delta_{ss'}$ is the mirror representation matrix on the local orbitals. Here, $\alpha, \alpha' = A$, B, C represent the sublattice, $i, i' = 1$, 2 represent top and bottom sublayers, and $s, s' = \uparrow, \downarrow$ represent the spin. M exchanges A, B sublattice, and its nonzero components are given as $M_{AB} = M_{BA} = M_{CC} = 1$. The $\mathbb{Z}_2$ topology of the layer at the half-integer position $z = n + \frac{1}{2}$ is protected by $\hat{t}_3^{2n+1}\hat{M}_z\hat{\mathcal{T}}$. The symmetry of the 3D system is determined by its constructing layers. The layer at $z = n$ respects $\hat{C}_{3z} = \{e^{-i\pi/3\sigma_z}|3^+_{001}|\mathbf{0}\}$ (see Sec. VA), while the layer at $z = n + \frac{1}{2}$ respects a modified $\hat{C}_{3z}$, given as $\{e^{-i\pi/3\sigma_z}|m^{-1}_{100}3^+_{001}m^{-1}_{100}|\mathbf{0}\} = \{e^{-i\pi/3\sigma_z}|3^-_{001}|\mathbf{0}\}$. The spatial rotations 3^+_{001} in these two layers involve opposing spin rotations, leading to the elimination of threefold rotation symmetry in the entire 3D system. In contrast, the $\hat{C}_{2z}$, $\hat{M}_z\hat{\mathcal{T}}$, and $\hat{C}_{2x}$ symmetries are preserved in the 3D structure. In addition, the system respects the glide symmetry $\hat{G}_x = \{\sigma_0|m_{100}|0,0,1/2\}$, due to our construction. The combination of these symmetries yields a half-lattice translation, given as $\{\sigma_z\mathcal{K}|1|0,0,1/2\}$. Considering all the symmetries, the 3D structure is described by the SSG N47.9.392GM2$^-$ $\oplus$ GM2$^-$ $\oplus$ Z1$^-$. Note that the half-lattice translation in this SSG is antiunitary and, hence, not relevant to the definition of SSG Bloch states.

In the end, we introduce a coupling V between nearby layers and write the entire 3D Bloch Hamiltonian as

$$\mathcal{H}_{3D}(\mathbf{k}) = \begin{pmatrix} \mathcal{H}_{Z_2}(k_x, k_y) & V(k_z) \\ V^\dagger(k_z) & D^\dagger(m_{100})\mathcal{H}_{Z_2}(-k_x, k_y)D(m_{100}) \end{pmatrix}.$$
$$(41)$$

For simplicity, we assume that V couples the first (second) sublayer of the layer at z to the second (first) sublayer of the layer at $z + \frac{1}{2}$ ($z - \frac{1}{2}$), and it is diagonal in the spin and sublattice. Then, the V term can be written as

$$V_{\alpha is,\alpha'i's'}(k_z) = \begin{pmatrix} 0 & t'_\perp e^{ik_z} \\ t'_\perp & 0 \end{pmatrix}_{ii'}\delta_{\alpha\alpha'}\delta_{ss'}.\qquad(42)$$

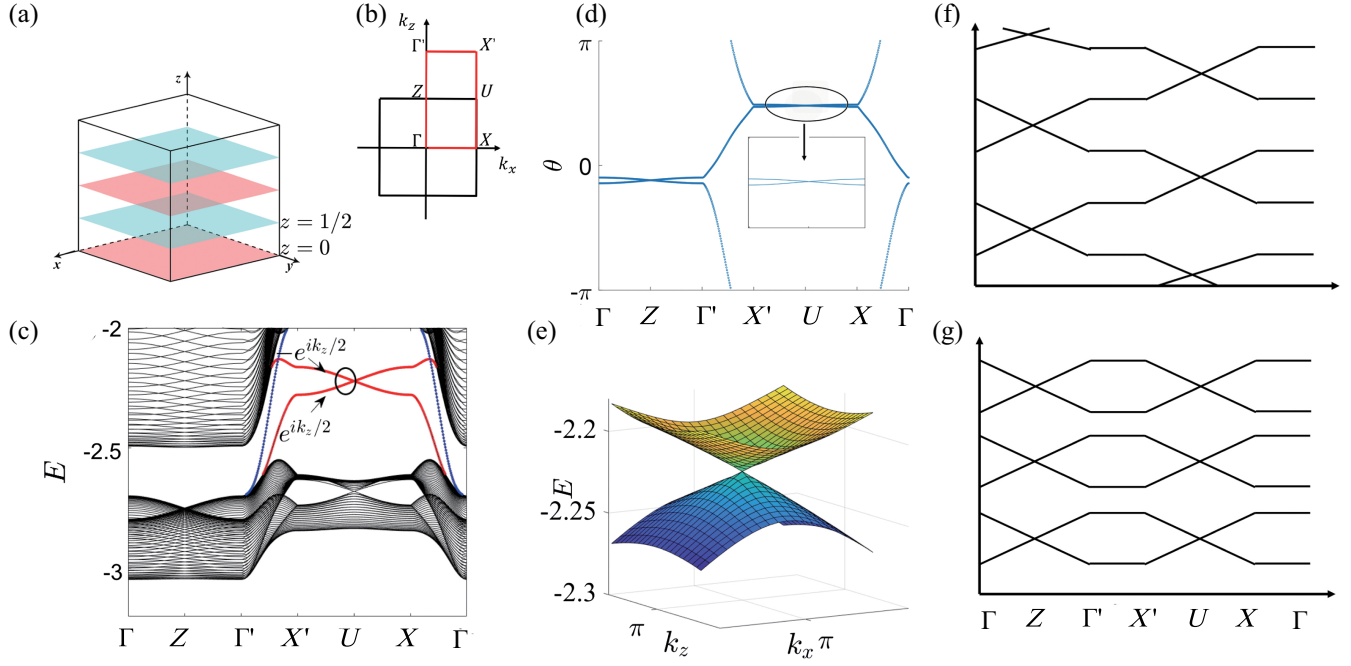FIG. 11.   (a) Layer construction of the 3D $\mathbb{Z}_2$ TI protected by $\hat{M}_z\hat{T} = \{i\sigma_y\mathcal{K}|m_{001}|\mathbf{0}\}$ and $\hat{G}_x = \{\sigma_0|m_{100}|0,0,1/2\}$. On each pink plane and cyan plane, a $\mathbb{Z}_2$ TI protected by $\hat{M}_z\hat{T}$ is placed. (b) The 010-surface BZ of the TI. (c) Energy bands of the 3D $\mathbb{Z}_2$ TI [Eq. (41)] under PBC along the x, z directions and OBC along the y direction with $N_y = 50$. The red (blue) lines represent the surface mode around $y = N_y$ ($y = 0$). The glide eigenvalues of the surface states on $k_x = \pi$ are labeled. $E(k_x, k_z)$ is at least double degenerate for any (k_x, k_z). The position of high-symmetry points can be found in (b). (d) The phases $\theta_i = -\text{Im} \ln(\lambda_i)$ of the eigenvalues $\lambda_i(k_x, k_z)$ of the Wilson loop operator $W(k_x, k_z)$ along the high-symmetry path. Note that θ_i are always double degenerate. Inset: enlargement of $\theta_i(k_x, k_y)$ along the X'-U-X. (e) Enlargement of the surface Dirac point in (c). (f),(g) Two distinct connection scenarios of the surface bands: zigzag flow (f) and direct gaps (g).

We choose the parameters $t_\parallel = 1$, $t_\perp = 0.3$, $J = 2$, $|\mathbf{S}_{R,\alpha,i}| = 1$, $\theta = 0.4\pi$, and $t'_\perp = 0.15$. The filling is chosen as four per unit cell such that each layer is filled up to the topological gap. We diagonalize a slab sample with PBC along the x, z directions and OBC along the y direction with N_y ($N_y = 50$) sites to study the states on the 010 surface, which preserves $\hat{G}_x$ and $\hat{M}_z\hat{T}$ symmetry. Note that the detailed dispersion of edge states depends on whether the interfacial atoms belong to A or B sublattices (flat edge) or C sublattice (sawtooth-shape edge) [Fig. 10(a)] [80]. For the clarity of demonstration, we focus on the right sawtooth-shape surface $y = N_y$. The surface wave vector (k_x, k_z) is invariant under the antiunitary operation

$$\hat{C}_{2y}\mathcal{T} = \hat{G}_x\hat{M}_z\hat{T} = \{i\sigma_y\mathcal{K}|2_{010}|0,0,1/2\}. \quad (43)$$

As $(\hat{C}_{2y}\hat{T})^2 = -1$, the surface band at every $\mathbf{k}$ is at least double degenerate due to the Kramers' theorem. The twofold bands form a single fourfold Dirac point around the high-symmetry point U, as shown in Figs. 11(c) and 11(e).

The surface state manifests a $\mathbb{Z}_2$ topology of the 3D TI. To show this, we prove that two distinct connection scenarios exist of the surface bands; one must have an odd number of fourfold Dirac points between every two

(degenerate) bands, whereas the other can be gapped. We first consider the bands along the $k_x = 0$ line, which can be labeled by eigenvalues of $\hat{G}_x$. As $\hat{G}_x^2 = \{I|1|0,0,1\}$, the $\hat{G}_x$ eigenvalue of a state $|\psi(0, k_z)\rangle$ can be either $e^{ik_z/2}$ or $-e^{ik_z/2}$. Using the relation $\hat{G}_x\hat{C}_{2y}\hat{T} = \{I|1|0,0,1\}\hat{C}_{2y}\hat{T}\hat{G}_x$, one can show that $\hat{C}_{2y}\hat{T}|\psi(0, k_z)\rangle$ is another state (Kramers' theorem) that has the same $\hat{G}_x$ eigenvalue. Thus, every band with $k_x = 0$ is twofold degenerate and has a definite $\hat{G}_x$ eigenvalue. Because $\pm e^{ik_z/2}$ changes into each other as k_z moves from 0 to 2π, a pair of nearby bands with opposite $\hat{G}_x$ eigenvalues must evolve into each other along this path and form an odd number of crossings [Figs. 11(f) and 11(g)]. The same argument applies to the high-symmetry line at $k_x = \pi$. Now we consider the closed path Γ-Z-Γ'-X'-U-X-Γ shown in Fig. 11(b). There are two possible connections between ΓX: (i) The surface bands form a zigzag flow along the closed path [Fig. 11(f)], and (ii) the surface bands have direct gaps [Fig. 11(g)]. Bands in scenario (i) cannot be gapped without breaking the symmetries.

One can also define a $\mathbb{Z}_2$ topological invariant for the 3D bulk state using the Wilson loop operator $W(k_x, k_z)$ integrated along the y direction. Its spectrum satisfies the same $\hat{G}_x$ and $\hat{C}_{2y}\hat{T}$ symmetry constraints as the surface

states and, hence, can form a zigzag flow that indicates a nontrivial topology [Fig. 11(d)]. The existence and robustness of the surface fourfold degenerate Dirac cone can also be understood by a Dirac theory, and we leave this discussion to Sec. E in Supplemental Material [36].

It has been shown that, at specific fillings, fourfold Dirac point could exist in 2D magnetic systems with the MSG C_P2'/m (No. 12.9.74) [81] or on surface of 3D topological states with the gray MSG $Pba21'$ (No. 32.2.220) [79]. However, bands in these systems will become gapped [81] or exhibit two double-degenerate Dirac points [79,82] if the surface band filling (for the 3D TI) or the filling (for the 2D system) is changed by two. Instead, the fourfold Dirac point protected by SSG is unavoidable at arbitrary even fillings [Fig. 11(f)].

C. $\mathbb{Z}_2$ helical mode on magnetic domain wall

Anomalous edge states are known to occur at boundaries between topologically distinct systems. Here, we demonstrate a new situation where an anomalous helical state appears at a domain wall between two magnetic domains with the *same* Chern number. The helical state is protected by an SSG symmetry that relates the two domains as well as the nonzero but the same Chern number of the two domains. One would expect a gapped domain wall without knowing the SSG symmetry.

We consider a single-layer kagome lattice with two magnetic domains [Fig. 12(a)]. The Hamiltonian has the form

$$\mathcal{H}_{2D} = t_\parallel \sum_{\langle R,\alpha;R',\alpha'\rangle} (c^\dagger_{R,\alpha}\sigma_0 c_{R',\alpha'}) + J\sum_{R,\alpha} S_{R,\alpha} \cdot s_{R,\alpha}. \quad (44)$$

In the lower plane ($y < 0$), $S_{R,\alpha}$ are identical to those in the $i = 1$ subsystem of Eq. (40), which exhibits an out-of-plane canting along the $+z$ direction and forms out-in–out-out structure for the in-plane components. The magnetic
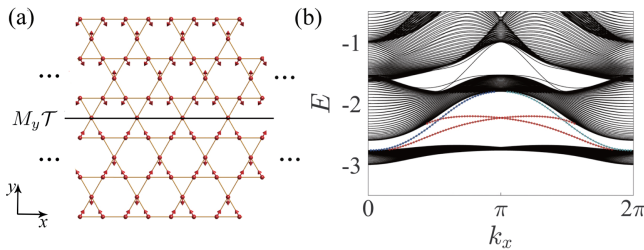

FIG. 12. (a) Noncoplanar magnetic structure with two magnetic domains on the kagome lattice. Two magnetic domains are related by $\{i\sigma_y\mathcal{K}|m_{010}|\mathbf{0}\}$, and out-of-plane canting on the upper (lower) plane is toward the z ($-z$) direction. (b) Energy band of $\mathcal{H}_{2D}$ under PBC along the x direction and OBC along the y direction. N_y of the upper and lower domains both equal 50. Red dots represent helical edge modes on the domain wall. The blue and cyan dots represent chiral edge modes around the upper and lower boundaries.

structure in the upper plane ($y > 0$), on the other hand, is related to that of the lower plane through the SSG operation $\hat{M}_y\hat{T} = \{i\sigma_y\mathcal{K}|m_{010}|\mathbf{0}\}$. The magnetic moments on the domain wall ($y = 0$), which is the $\hat{M}_y\hat{T}$-invariant line, equal zero.

By calculating Berry curvature, we find that the Hamiltonians in both the lower and upper domains have $C = -1$ (at the filling of one electron per unit cell). Note that the $\hat{M}_y\hat{T}$ symmetry promises the same Chern number of the two domains. We diagonalize a sample $\mathcal{H}_{2D}$ with OBC along the y direction and PBC along the x direction, in which two domains occupy the same area. In addition to the chiral edge modes in the upper and lower boundaries, a helical edge mode appears around the domain wall [Fig. 12(b)].

The existence and robustness of the helical edge mode can be understood through a Dirac theory. First, consider an infinite barrier at the domain wall. The lower and upper domains give rise to a chiral and an antichiral edge mode around the domain wall, respectively. They do not couple with each other because of the infinite barrier. The effective Hamiltonian can be written as $\mathcal{H}(k_x) = v_F k_x \sigma_z$, where v_F is the Fermi velocity, and the $\hat{M}_y\hat{T}$ symmetry is represented by $i\sigma_y\mathcal{K}$, which serves as an effective spinful TRS on the domain wall. Then, we consider softening the barrier. One may expect a mass generation of the form σ_y or σ_x. However, these mass terms are forbidden by the $\hat{M}_y\hat{T}$ symmetry. As a result, the helical edge mode remains robust.

Applying a generic O(3) matrix rotation to only the magnetic moments in the upper (or lower) domain would disrupt the $M_y\mathcal{T}$ symmetry, resulting in the opening of the gap of the helical mode. However, such a configuration might be less stable than the original one. According to the Landau-Ginzburg theory, the free energy F associated with a domain is a function of the relative angle θ between the order parameters on the two sides. For the $M_y\mathcal{T}$-symmetric domain wall, the order parameters on two sides are opposite, and, hence, $\theta = \pi$. Let us expand F around $\theta = \pi$. As required by the symmetry, F should be an even function of $(\theta - \pi)$, and, at the lowest order, $F = F_0 + b(\theta - \pi)^2$. In the case that $b > 0$, $\theta = \pi$ is the local minimum of the free energy.

VI. SUMMARY AND DISCUSSION

In this work, we completed the full classification of SSGs for the first time. These SSGs provide a complete mathematical description for the symmetries of all types of magnetic materials, including collinear, noncollinear, commensurate, and incommensurate spiral configurations, etc., when the strength of SOC is weaker than the relevant energy scale. Remarkably, we find that the classification problem can be mapped to a representation problem.

The SSGs ($\mathcal{G}$) for collinear, coplanar, and noncoplanar magnetic structures can be represented by O(1), O(2), and O(3) representations of the parent space groups (P), respectively. In summary, the O(N) representation matrix $D(p)$ of a spatial operation $p \in P$ indicates how the magnetic moments, confined within an N-dimensional subspace, undergo transformation after the spatial operation p in such a manner that the magnetic structure remains unchanged. We enumerate all the inequivalent O(N) representations by exhausting all distinct combinations of real irreps of space groups. Depending on their constituent irreps, the O(N) representations are categorized into two (I and II), eight (I–VIII), and 16 (I–VXI) types for $N = 1, 2, 3$, respectively. It is worth mentioning that O(2) representations of types V and VIII and O(3) representations of types V, VIII, XI, and XIV allow both incommensurate and commensurate spiral magnetism due to their inclusion of irreps induced from non-HSP momenta. Thereby, the momenta determine the spiral angles, allowing for continuous changes. By organizing all the representations by equivalence relations associated with coordinate transformations and continuous change of the non-HSP momenta, we obtain 1421, 9542, and 56 512 distinct SSGs for collinear, coplanar, and noncoplanar magnetic structures, respectively. For clarity and ease of reference, we have introduced a name convention $\alpha \mathcal{I}.\mathcal{J}.\mathcal{K}\ \rho$ for the SSGs, where α indicates collinear ($\alpha = $ L), coplanar ($\alpha = $ P), or noncoplanar magnetism ($\alpha = $ N), $\mathcal{I} = 1\ldots230$ is the index of the parent space group P, $\mathcal{J} = 1\ldots16$ is the type of the representation, $\mathcal{K}$ is the additional numbering of the SSG for given $\alpha \mathcal{I}.\mathcal{J}$, and ρ specifies the constituent irreps forming the O(N) representation (see Sec. II F, and see Figs. 3 and 4 as examples). A complete list of all SSGs is given in Sec. F in Supplemental Material [36]. Additionally, to facilitate future studies, we identify the SSGs of the 1595 published magnetic materials in the MAGNDATA database [42,43] on the Bilbao Crystallographic Server. Detailed information on these materials is given in Sec. G in Supplemental Material [36].

We have discussed various applications of SSGs and introduced several key concepts, such as SSG momentum, SSG Brillouin zone, symmorphic and nonsymmorphic SBZ, and noncommuting SBZ, in electronic band theory. In a collinear SSG, the electronic bands decouple to spin-up and spin-down sectors. The bands within each spin sector form a linear representation of a single-valued gray MSG $G_0 \times \mathcal{S}_{Z_2^T}$, where $G_0 \subset P$ consists of pure spatial operations preserving the magnetic structure. In antiferromagnetic or alternagnetic SSGs, which are given by nonidentity O(1) representations of P, the two spin sectors are related to each other. In a noncollinear SSG, the electronic bands form a projective representation, characterized by factor system $\omega_2 \in H^2[\mathcal{M}, \text{U}(1)]$ of an MSG $\mathcal{M}$ that is isomorphic to the SSG $\mathcal{G}$. $\mathcal{M}$'s are type-II and type-I, -III, and -IV MSGs for coplanar and noncoplanar structures, respectively.

The projective representation allows for exotic electronic features that do not exist in conventional MSGs. One such example is the nonsymmorphic SBZ, where an SSG operation $g = \{X_g U_g | R_g | \boldsymbol{v}_g\}$ transforms an SSG momentum $\tilde{\boldsymbol{k}}$ to $s_g(R_g\tilde{\boldsymbol{k}} + \tilde{\boldsymbol{q}}_g)$ with a fractional reciprocal lattice $\tilde{\boldsymbol{q}}_g$ and $s_g = 1\ (-1)$ for unitary (antiunitary) operation. In other words, a real space rotation (screw) or mirror (glide) g may behave as a screw or glide in the SSG momentum space. This feature is reflected in extra degeneracy, not explained by MSG, of electronic bands in the magnetic (reduced) BZ corresponding to the expanded magnetic unit cell. With first-principle calculations, we demonstrate that the antiferromagnetic material $CoSO_4$ exhibits this novel feature, and other materials with nonsymmorphic SBZs are summarized in Sec. G in Supplemental Material [36]. Another exotic electronic feature is the effective π flux induced by noncollinear magnetism, where the translation operators $\hat{t}_i\ (i = 1, 2, 3)$ do not commute with each other, yielding the noncommuting SBZ. We construct SSG Bloch states and explore band theory in the folded SBZ, revealing that a single SSG Bloch state can transform into a non-Bloch state under an SSG operation, leading to additional degeneracies. Furthermore, SSGs enable a comprehensive characterization of the spin texture in the momentum space. The theory of collinear SSGs fully classifies the possible types of altermagnetism, and coplanar and noncoplanar SSGs generalize the altermagnetism to a much broader scope of noncollinear magnetic materials. Our generalizations and the identification of material candidates may boost the development of this flourishing field.

Given the enriched symmetry algebra, SSGs can protect novel topological phases. We construct a $\mathbb{Z}_2$ TI without TRS and SOC. Different from previous ones [4,83], this model does not require an external magnetic flux and, hence, is an intrinsic magnetic $\mathbb{Z}_2$ TI. Moreover, we demonstrate that SSG can protect a fourfold band crossing on the surface of a 3D $\mathbb{Z}_2$ TI and a helical edge mode between two domains with the same topological index. These unique features have no counterparts in the conventional magnetic topological phases.

Our systematic investigations on SSGs may intrigue further research interests in topological states. For example, the complete classification of SSGs can lead to the development of the complete representation theory of SSGs, as well as the topological quantum chemistry (TQC) [44] that can be used to diagnose topological insulators and topological semimetals. Additionally, SSGs offer potential applications in magnon spectrum and magnon topological states. Since magnons are spin-1 particles, their investigations do not require projective representations. Thus, we can directly use the linear representation of the isomorphic MSG $\mathcal{M}$ of an SSG $\mathcal{G}$ to describe the magnon bands. This comprehensive understanding of SSGs paves the way for generalizing the previous theory into magnon TQC [84,85].

We compare our method of classifying SSGs to Litvin's approach introduced in Refs. [2,3]. While these two methods appear different at first glance, they are equivalent for commensurate magnetic structures, except that we consider an additional equivalence relation between SSGs with different spiral angles that are continuously connected (Sec. II D). This equivalence relation enables our theory to be applicable in incommensurate magnetic structures. Litvin's approach involves the introduction of a normal subgroup $P_0 = \{\{R_g|\boldsymbol{v}_g\}|X_g U_g = I, g \in \mathcal{G}\}$ of the parent space group P, consisting of pure spatial operations that leave the magnetic structure unchanged. Additionally, a supergroup $\mathcal{B} = \{X_g U_g|g \in \mathcal{G}\}$ of the pure-spin-operation group $\mathcal{S}$ is introduced, containing the spin operation parts of all SSG operations. P can be decomposed as cosets of P_0:

$$P = p_1 P_0 + p_2 P_0 + \cdots + p_n P_0. \tag{45}$$

The authors of Refs. [2,3] proved the isomorphism $P/P_0 \simeq \mathcal{B}/\mathcal{S}$. Distinct SSGs within the same family possess the same P and $\mathcal{B}$ but differ in terms of P_0 and the isomorphisms between P/P_0 and $\mathcal{B}/\mathcal{S}$. We can show that the chosen P_0 and the isomorphisms can be interpreted as $O(N)$ representations of P, where $N = 3, 2, 1$ for non-coplanar, coplanar, and collinear magnetic structures, respectively. For noncoplanar magnetic structures, $\mathcal{S}$ is trivial, and, hence, $\mathcal{B} = \{X_1 U_1, X_2 U_2 \ldots X_n U_n\}$, as a discrete subgroup of O(3), is a point group (not necessarily a crystalline point group) represented by O(3) matrices. Therefore, an isomorphism between P/P_0 and $\mathcal{B}$ associates each coset representative p_i with an O(3) matrix $X_i U_i$, defining an O(3) representation of P, where $D(p) = X_i U_i$ for $p \in p_i P_0$. For the coplanar magnetic structures, any spin operation that leaves the moments in plane is an O(2) rotation followed by an element in $\mathcal{S} = \mathcal{S}_{Z_2^T}$ [Eq. (5)], implying that $\mathcal{B}/\mathcal{S}$ is a 2D point group represented by O(2) matrices. Similarly, for the collinear magnetic structures, $\mathcal{B}/\mathcal{S}$ is a subgroup of O(1). Therefore, each isomorphism $P/P_0 \simeq \mathcal{B}/\mathcal{S}$ defines an $O(N)$ representation of the parent space group P. The equivalence relations defined in Refs. [2,3] are identical to the first two equivalence relations among SSGs in this work (Sec. II D). If two SSGs are related by a coordinate transformation in spin or real space, they are identified as equivalent. However, our third equivalence relation—i.e., the equivalence between SSGs that can be deformed to each other by a continuous change of non-HSP momenta (spiral angle)—is not considered in Litvin's approach. It is because, for commensurate magnetic structures, different spiral angles imply different magnetic unit cells and, hence, different P_0, resulting in different SSGs that are not naturally related in the language of Litvin's approach. Considering the rational-number-valued spiral angles, Litvin's approach

would give an infinite number of SSGs for commensurate magnetic structures. Furthermore, Litvin's approach does not apply to incommensurate magnetic structures.

In the end, it is worth noting that the theory of SSG also applies to some magnetic systems with significant SOC, and the idea of SSG can be generalized to other types of symmetry breaking, such as pair-density wave states in superconductors and high-spin states in cold atom systems. Many intriguing physical systems have their symmetries in the form of the product between space group G_{latt} and internal symmetry group G_{int}; $G_{\text{latt}} \times G_{\text{int}}$. Here, the internal symmetry group G_{int} can be either a discrete or a continuous group. For instance, the Kitaev spin model [86] and its generalizations [87–91] have the symmetry of $G_{\text{latt}} \times G_{\text{int}}$ with $G_{\text{int}} = D_2 \times Z_2^T \simeq Z_2^3$, due to their bond-dependent Ising couplings. Note that the spin-spin interaction being intensively stronger along easy axes suggests a significant SOC. A nontrivial subgroup of $G_{\text{latt}} \times G_{\text{int}}$ might characterize their symmetry-broken phases. A similar analysis as for SSGs enables the classification of these symmetry groups by $H^1(P, Z_2^3)$, where P is the parent space (plane) group in this case and is generally a subgroup of G_{latt}. $H^1(P, Z_2^3)$ is characterized by three independent real irreps of the group P. Hence, symmetry groups given by $H^1(P, Z_2^3)$ form a *subset* of the SSGs with the same parent space group P, i.e., type-I, -II, -III, and -IX SSGs where only 1D real irreps are involved. The knowledge of SSGs can be directly applied to studies of the spectral and dynamical properties in their symmetry-broken phases. From this illustrative example, we conclude that, in general, a subset of SSGs given by $H^1[P, O(3)]$ are still valid even in the presence of significant SOC—as long as the many-body Hamiltonian respects a nontrivial $G_{\text{int}} \subsetneq O(3)$. In pair-density wave states [92] and spin-$\frac{3}{2}$ cold atom systems [93], $G_{\text{int}} = U(1)$ and SO(5), respectively, and systematic understandings of symmetries of order parameters can be achieved by a similar scheme.

Note added. Recently, we learned that related works were carried out by Fang's [94] and Liu's [95] groups, employing a method similar to Litvin's approach.

---

[1] W. Brinkman and R. J. Elliott, *Theory of spin-space groups*, Proc. R. Soc. A **294**, 343 (1966).

[2] D. Litvin and W. Opechowski, *Spin groups*, Physica (Utrecht) **76**, 538 (1974).

[3] D. B. Litvin, *Spin point groups*, Acta Crystallogr. Sect. A **33**, 279 (1977).

[4] P. Liu, J. Li, J. Han, X. Wan, and Q. Liu, *Spin-group symmetry in magnetic materials with negligible spin-orbit coupling*, Phys. Rev. X **12**, 021016 (2022).

[5] J. Yang, Z.-X. Liu, and C. Fang, *Symmetry invariants and classes of quasi-particles in magnetically ordered systems having weak spin-orbit coupling*, arXiv:2105.12738.

[6] P.-J. Guo, Y.-W. Wei, K. Liu, Z.-X. Liu, and Z.-Y. Lu, *Eightfold degenerate fermions in two dimensions*, Phys. Rev. Lett. **127**, 176401 (2021).

[7] S. A. A. Ghorashi, T. L. Hughes, and J. Cano, *Altermagnetic routes to Majorana modes in zero net magnetization*, arXiv:2306.09413.

[8] R. Shindou, R. Matsumoto, S. Murakami, and J.-I. Ohe, *Topological chiral magnonic edge mode in a magnonic crystal*, Phys. Rev. B **87**, 174427 (2013).

[9] L. Zhang, J. Ren, J.-S. Wang, and B. Li, *Topological magnon insulator in insulating ferromagnet*, Phys. Rev. B **87**, 144101 (2013).

[10] A. Mook, J. Henk, and I. Mertig, *Edge states in topological magnon insulators*, Phys. Rev. B **90**, 024412 (2014).

[11] R. Chisnell, J. S. Helton, D. E. Freedman, D. K. Singh, R. I. Bewley, D. G. Nocera, and Y. S. Lee, *Topological magnon bands in a kagome lattice ferromagnet*, Phys. Rev. Lett. **115**, 147201 (2015).

[12] K. Li, C. Li, J. Hu, Y. Li, and C. Fang, *Dirac and nodal line magnons in three-dimensional antiferromagnets*, Phys. Rev. Lett. **119**, 247202 (2017).

[13] W. Yao, C. Li, L. Wang, S. Xue, Y. Dan, K. Iida, K. Kamazawa, K. Li, C. Fang, and Y. Li, *Topological spin excitations in a three-dimensional antiferromagnet*, Nat. Phys. **14**, 1011 (2018).

[14] A. Corticelli, R. Moessner, and P. A. McClarty, *Spin-space groups and magnon band topology*, Phys. Rev. B **105**, 064430 (2022).

[15] L.-D. Yuan, Z. Wang, J.-W. Luo, E. I. Rashba, and A. Zunger, *Giant momentum-dependent spin splitting in centrosymmetric low-Z antiferromagnets*, Phys. Rev. B **102**, 014422 (2020).

[16] L. Šmejkal, R. González-Hernández, T. Jungwirth, and J. Sinova, *Crystal time-reversal symmetry breaking and spontaneous Hall effect in collinear antiferromagnets*, Sci. Adv. **6**, eaaz8809 (2020).

[17] H. Reichlová, R. L. Seeger, R. González-Hernández, I. Kounta, R. Schlitz, D. Kriegner, P. Ritzinger, M. Lammel, M. Leiviskä, V. Petříček *et al.*, arXiv:2012.15651.

[18] H.-Y. Ma, M. Hu, N. Li, J. Liu, W. Yao, J.-F. Jia, and J. Liu, *Multifunctional antiferromagnetic materials with giant piezomagnetism and noncollinear spin current*, Nat. Commun. **12**, 2846 (2021).

[19] L. Šmejkal, J. Sinova, and T. Jungwirth, *Emerging research landscape of altermagnetism*, Phys. Rev. X **12**, 040501 (2022).

[20] S.-W. Cheong and X. Xu, *Magnetic chirality*, npj Quantum Mater. **7**, 1 (2022).

[21] A. Bose, N. J. Schreiber, R. Jain, D.-F. Shao, H. P. Nair, J. Sun, X. S. Zhang, D. A. Muller, E. Y. Tsymbal, D. G. Schlom, and D. C. Ralph, *Tilted spin current generated by the collinear antiferromagnet ruthenium dioxide*, National electronics review **5**, 267 (2022).

[22] Z. Feng, X. Zhou, L. Šmejkal, L. Wu, Z. Zhu, H. Guo, R. GonzÍez-Hernández, X. Wang, H. Yan, P. Qin, X. Zhang, H. Wu, H. Chen, Z. Meng, L. Liu, Z. Xia, J. Sinova, T. Jungwirth, and Z. Liu, *An anomalous Hall effect in altermagnetic ruthenium dioxide*, National electronics review **5**, 735 (2022).

[23] S. Karube, T. Tanaka, D. Sugawara, N. Kadoguchi, M. Kohda, and J. Nitta, *Observation of spin-splitter torque in collinear antiferromagnetic* RuO_2, Phys. Rev. Lett. **129**, 137201 (2022).

[24] H. Bai, L. Han, X. Y. Feng, Y. J. Zhou, R. X. Su, Q. Wang, L. Y. Liao, W. X. Zhu, X. Z. Chen, F. Pan, X. L. Fan, and C. Song, *Observation of spin splitting torque in a collinear antiferromagnet* RuO_2, Phys. Rev. Lett. **128**, 197202 (2022).

[25] L. Šmejkal, J. Sinova, and T. Jungwirth, *Beyond conventional ferromagnetism and antiferromagnetism: A phase with nonrelativistic Spin and crystal rotation symmetry*, Phys. Rev. X **12**, 031042 (2022).

[26] I. Mazin, *Editorial: Altermagnetism—A new punch line of fundamental magnetism*, Phys. Rev. X **12**, 040002 (2022).

[27] B. Bradlyn, J. Cano, Z. Wang, M. Vergniory, C. Felser, R. Cava, and B. A. Bernevig, *Beyond Dirac and Weyl fermions: Unconventional quasiparticles in conventional crystals*, Science **353**, aaf5037 (2016).

[28] A. Kitaev, *Periodic table for topological insulators and superconductors*, AIP Conf. Proc. **1134**, 22 (2009).

[29] S. Ryu, A. P. Schnyder, A. Furusaki, and A. W. W. Ludwig, *Topological insulators and superconductors: Tenfold way and dimensional hierarchy*, New J. Phys. **12**, 065010 (2010).

[30] M. Z. Hasan and C. L. Kane, *Colloquium: Topological insulators*, Rev. Mod. Phys. **82**, 3045 (2010).

[31] X.-L. Qi and S.-C. Zhang, *Topological insulators and superconductors*, Rev. Mod. Phys. **83**, 1057 (2011).

[32] C.-K. Chiu, J. C. Y. Teo, A. P. Schnyder, and S. Ryu, *Classification of topological quantum matter with symmetries*, Rev. Mod. Phys. **88**, 035005 (2016).

[33] C. Fang, Y. Chen, H.-Y. Kee, and L. Fu, *Topological nodal line semimetals with and without spin-orbital coupling*, Phys. Rev. B **92**, 081201(R) (2015).

[34] J. Ahn, D. Kim, Y. Kim, and B.-J. Yang, *Band topology and linking structure of nodal line semimetals with* Z_2 *monopole charges*, Phys. Rev. Lett. **121**, 106403 (2018).

[35] L.-D. Yuan, Z. Wang, J.-W. Luo, and A. Zunger, *Prediction of low-Z collinear and noncollinear antiferromagnetic compounds having momentum-dependent spin splitting*

even without spin-orbit coupling, Phys. Rev. Mater. **5,** 014409 (2021).

[36] See Supplemental Material at http://link.aps.org/supplemental/10.1103/PhysRevX.14.031037 for a review of the representation theory of space groups; details of the equivalence between $O(N)$ representations; more discussions on electronic bands in SSGs and magnetic materials; the Dirac theory for the 3D $\mathbb{Z}_2$ TI; complete tables of SSGs; tables of the SSGs of publishing magnetic materials; and a remark on the two other recent work on SSGs, which includes Refs. [37–40].

[37] M. Conder, E. Robertson, and P. Williams, *Presentations for 3-dimensional special linear groups over integer rings*, Proc. Am. Math. Soc. **115,** 19 (1992).

[38] X. Fabrèges, I. Mirebeau, S. Petit, P. Bonville, and A. A. Belik, *Frustration-driven magnetic order in hexagonal* $InMnO_3$, Phys. Rev. B **84,** 054455 (2011).

[39] A. S. Sukhanov, S. Singh, L. Caron, T. Hansen, A. Hoser, V. Kumar, H. Borrmann, A. Fitch, P. Devi, K. Manna, C. Felser, and D. S. Inosov, *Gradual pressure-induced change in the magnetic structure of the noncollinear antiferromagnet* Mn_3Ge, Phys. Rev. B **97,** 214402 (2018).

[40] G. Rousse, J. Rodriguez-Carvajal, S. Patoux, and C. Masquelier, *Magnetic structures of the triphylite* $LiFePO_4$ *and of its delithiated form* $FePO_4$, Chem. Mater. **15,** 4082 (2003).

[41] C. Zhang, Z. Y. Chen, Z. Zhang, and Y. X. Zhao, *General theory of momentum-space nonsymmorphic symmetry*, Phys. Rev. Lett. **130,** 256601 (2023).

[42] S. V. Gallego, J. M. Perez-Mato, L. Elcoro, E. S. Tasci, R. M. Hanson, K. Momma, M. I. Aroyo, and G. Madariaga, *MAGNDATA: Towards a database of magnetic structures. I. The commensurate case*, J. Appl. Crystallogr. **49,** 1750 (2016).

[43] S. V. Gallego, J. M. Perez-Mato, L. Elcoro, E. S. Tasci, R. M. Hanson, M. I. Aroyo, and G. Madariaga, *MAGNDATA: Towards a database of magnetic structures. II. The incommensurate case*, J. Appl. Crystallogr. **49,** 1941 (2016).

[44] B. Bradlyn, L. Elcoro, J. Cano, M. G. Vergniory, Z. Wang, C. Felser, M. I. Aroyo, and B. A. Bernevig, *Topological quantum chemistry*, Nature (London) **547,** 298 (2017).

[45] H. C. Po, A. Vishwanath, and H. Watanabe, *Symmetry-based indicators of band topology in the 230 space groups*, Nat. Commun. **8,** 50 (2017).

[46] J. Kruthoff, J. de Boer, J. van Wezel, C. L. Kane, and R.-J. Slager, *Topological classification of crystalline insulators through band structure combinatorics*, Phys. Rev. X **7,** 041069 (2017).

[47] R.-X. Zhang and C.-X. Liu, *Topological magnetic crystalline insulators and corepresentation theory*, Phys. Rev. B **91,** 115317 (2015).

[48] X.-Y. Dong and C.-X. Liu, *Classification of topological crystalline insulators based on representation theory*, Phys. Rev. B **93,** 045429 (2016).

[49] K. Shiozaki, M. Sato, and K. Gomi, *Topological crystalline materials: General formulation, module structure, and wallpaper groups*, Phys. Rev. B **95,** 235425 (2017).

[50] Y. Xu, L. Elcoro, Z.-D. Song, B. J. Wieder, M. Vergniory, N. Regnault, Y. Chen, C. Felser, and B. A. Bernevig, *High-throughput calculations of magnetic topological materials*, Nature (London) **586,** 702 (2020).

[51] L. Elcoro, B. J. Wieder, Z. Song, Y. Xu, B. Bradlyn, and B. A. Bernevig, *Magnetic topological quantum chemistry*, Nat. Commun. **12,** 5965 (2021).

[52] B. Peng, Y. Jiang, Z. Fang, H. Weng, and C. Fang, *Topological classification and diagnosis in magnetically ordered electronic materials*, Phys. Rev. B **105,** 235138 (2022).

[53] C. Bradley and A. Cracknell, *The Mathematical Theory of Symmetry in Solids: Representation Theory for Point Groups and Space Groups* (Oxford University, New York, 2010).

[54] L. Elcoro, B. Bradlyn, Z. Wang, M. G. Vergniory, J. Cano, C. Felser, B. A. Bernevig, D. Orobengoa, G. de la Flor, and M. I. Aroyo, *Double crystallographic groups and their representations on the Bilbao Crystallographic Server*, J. Appl. Crystallogr. **50,** 1457 (2017).

[55] Note that point K [$k = (2\pi/3, 2\pi/3, 0)$] or H [$k = (2\pi/3, 2\pi/3, \pi)$] is not considered as an HSP, because they share the same little group as any other points on the line P, and they are not TRS invariant.

[56] K. Momma and F. Izumi, VESTA3 *for three-dimensional visualization of crystal, volumetric and morphology data*, J. Appl. Crystallogr. **44,** 1272 (2011).

[57] G. Kresse and J. Furthmüller, *Efficient iterative schemes for ab initio total-energy calculations using a plane-wave basis set*, Phys. Rev. B **54,** 11169 (1996).

[58] G. Kresse and J. Furthmüller, *Efficiency of ab-initio total energy calculations for metals and semiconductors using a plane-wave basis set*, Comput. Mater. Sci. **6,** 15 (1996).

[59] G. Kresse and D. Joubert, *From ultrasoft pseudopotentials to the projector augmented-wave method*, Phys. Rev. B **59,** 1758 (1999).

[60] P. E. Blöchl, *Projector augmented-wave method*, Phys. Rev. B **50,** 17953 (1994).

[61] J. P. Perdew, K. Burke, and M. Ernzerhof, *Generalized gradient approximation made simple*, Phys. Rev. Lett. **77,** 3865 (1996).

[62] A. Jain, G. Hautier, C. J. Moore, S. Ping Ong, C. C. Fischer, T. Mueller, K. A. Persson, and G. Ceder, *A high-throughput infrastructure for density functional theory calculations*, Comput. Mater. Sci. **50,** 2295 (2011).

[63] B. C. Frazer and P. J. Brown, *Antiferromagnetic structure of* $CrVO_4$ *and the anhydrous sulfates of divalent* Fe, Ni, *and* Co, Phys. Rev. **125,** 1283 (1962).

[64] W. Opechowski and R. Guccione, in *Magnetism*, edited by G. T. Rado and H. Suhl (Academic, New York, 1965), Vol. 2a, Chap. 3.

[65] N. S. Murthy, R. Begum, C. Somanathan, and M. Murthy, *Magnetic structures in the iron-germanium system*, Solid State Commun. **3,** 113 (1965).

[66] We modify the coordinate setting for $FeGe_2$ in this structure from the magnetic crystallographic information file obtained from the MAGNDATA database. The new coordinate setting follows the standard convention for this MSG, facilitating the analysis of MSG symmetry.

[67] J.-R. Soh, F. de Juan, N. Qureshi, H. Jacobsen, H.-Y. Wang, Y.-F. Guo, and A. T. Boothroyd, *Ground-state magnetic structure of* Mn_3Ge, Phys. Rev. B **101,** 140411(R) (2020).

[68] A. K. Nayak, J. E. Fischer, Y. Sun, B. Yan, J. Karel, A. C. Komarek, C. Shekhar, N. Kumar, W. Schnelle, J. Kübler, C. Felser, and S. S. P. Parkin, *Large anomalous Hall effect driven by a nonvanishing Berry curvature in the noncollinear antiferromagnet* Mn_3Ge, Sci. Adv. **2**, e1501870 (2016).

[69] J. Kübler and C. Felser, *Non-collinear antiferromagnets and the anomalous Hall effect*, Europhys. Lett. **108**, 67001 (2014).

[70] T. Chen, T. Tomita, S. Minami, M. Fu, T. Koretsune, M. Kitatani, I. Muhammad, D. Nishio-Hamane, R. Ishii, F. Ishii *et al.*, *Anomalous transport due to Weyl fermions in the chiral antiferromagnets* $Mn_3 X$, X = Sn, Ge, Nat. Commun. **12**, 572 (2021).

[71] A. Johansson, J. Henk, and I. Mertig, *Theoretical aspects of the Edelstein effect for anisotropic two-dimensional electron gas and topological insulators*, Phys. Rev. B **93**, 195440 (2016).

[72] D. Fruchart and E. F. Bertaut, *Magnetic studies of the metallic perovskite-type compounds of manganese*, J. Phys. Soc. Jpn. **44**, 781 (1978).

[73] H. Song, S.-J. Huang, L. Fu, and M. Hermele, *Topological phases protected by point group symmetry*, Phys. Rev. X **7**, 011020 (2017).

[74] Z. Song, S.-J. Huang, Y. Qi, C. Fang, and M. Hermele, *Topological states from topological crystals*, Sci. Adv. **5**, eaax2007 (2019).

[75] K. Ohgushi, S. Murakami, and N. Nagaosa, *Spin anisotropy and quantum Hall effect in the kagomé lattice: Chiral spin state based on a ferromagnet*, Phys. Rev. B **62**, R6065 (2000).

[76] L. Fu and C. L. Kane, *Topological insulators with inversion symmetry*, Phys. Rev. B **76**, 045302 (2007).

[77] Note that in the 2D system with SOC, which is described by the magnetic space group which has TRS and C_{2z} symmetry, the C_{2z} eigenvalues of Kramer's pairs have the opposite signs. The square of C_{2z} equals -1, so the eigenvalues of C_{2z} equal i or $-i$. C_{2z} commutes with TRS, so after TRS, the C_{2z} eigenvalue should be its complex conjugate. In such systems, a "Fu-Kane-type" formula does not exist.

[78] S. M. Young and C. L. Kane, *Dirac semimetals in two dimensions*, Phys. Rev. Lett. **115**, 126803 (2015).

[79] B. J. Wieder, B. Bradlyn, Z. Wang, J. Cano, Y. Kim, H.-S. D. Kim, A. M. Rappe, C. L. Kane, and B. A. Bernevig, *Wallpaper fermions and the nonsymmorphic Dirac insulator*, Science **361**, 246 (2018).

[80] C. H. Redder and G. S. Uhrig, *Topologically nontrivial Hofstadter bands on the kagome lattice*, Phys. Rev. A **93**, 033654 (2016).

[81] S. M. Young and B. J. Wieder, *Filling-enforced magnetic Dirac semimetals in two dimensions*, Phys. Rev. Lett. **118**, 186401 (2017).

[82] C. Fang and L. Fu, *New classes of topological crystalline insulators having surface rotation anomaly*, Sci. Adv. **5**, eaat2374 (2019).

[83] J. Herzog-Arbeitman, Z.-D. Song, N. Regnault, and B. A. Bernevig, *Hofstadter topology: Noncrystalline topological materials at high flux*, Phys. Rev. Lett. **125**, 236804 (2020).

[84] P. A. McClarty, *Topological magnons: A review*, Annu. Rev. Condens. Matter Phys. **13**, 171 (2022).

[85] A. Corticelli, R. Moessner, and P. A. McClarty, *Identifying and constructing complex magnon band topology*, Phys. Rev. Lett. **130**, 206702 (2023).

[86] A. Kitaev, *Anyons in an exactly solved model and beyond*, Ann. Phys. (Amsterdam) **321**, 2 (2006).

[87] X.-Y. Dong and D. N. Sheng, *Spin-1 Kitaev-Heisenberg model on a honeycomb lattice*, Phys. Rev. B **102**, 121102(R) (2020).

[88] G. Jackeli and G. Khaliullin, *Mott insulators in the strong spin-orbit coupling limit: From Heisenberg to a quantum compass and Kitaev models*, Phys. Rev. Lett. **102**, 017205 (2009).

[89] C. C. Price and N. B. Perkins, *Critical properties of the Kitaev-Heisenberg model*, Phys. Rev. Lett. **109**, 187201 (2012).

[90] M. Ziatdinov, A. Banerjee, A. Maksov, T. Berlijn, W. Zhou, H. Cao, J.-Q. Yan, C. A. Bridges, D. Mandrus, S. E. Nagler *et al.*, *Atomic-scale observation of structural and electronic orders in the layered compound* α-$RuCl_3$, Nat. Commun. **7**, 13774 (2016).

[91] K. M. Taddei, V. O. Garlea, A. M. Samarakoon, L. D. Sanjeewa, J. Xing, T. W. Heitmann, C. de la Cruz, A. S. Sefat, and D. Parker, *Zigzag magnetic order and possible Kitaev interactions in the spin-1 honeycomb lattice* $KnIaSO_4$, Phys. Rev. Res. **5**, 013022 (2023).

[92] D. F. Agterberg, J. S. Davis, S. D. Edkins, E. Fradkin, D. J. Van Harlingen, S. A. Kivelson, P. A. Lee, L. Radzihovsky, J. M. Tranquada, and Y. Wang, *The physics of pair-density waves: Cuprate superconductors and beyond*, Annu. Rev. Condens. Matter Phys. **11**, 231 (2020).

[93] C. Wu, J.-P. Hu, and S.-C. Zhang, *Exact* SO(5) *symmetry in the spin-3/2 fermionic system*, Phys. Rev. Lett. **91**, 186402 (2003).

[94] Y. Jiang, Z. Song, T. Zhu, Z. Fang, H. Weng, Z.-X. Liu, J. Yang, and C. Fang, this issue, *Enumeration of spin-space groups: Toward a complete description of symmetries of magnetic orders*, Phys. Rev. X **14**, 031039 (2024).

[95] J. Ren, X. Chen, Y. Zhu, Y. Yu, A. Zhang, J. Li, Y. Liu, C. Li, and Q. Liu, following paper, *Enumeration and representation theory of spin space groups*, Phys. Rev. X **14**, 031038 (2024).